Dynamics of High Barrier Gas-surface Reactions studied by Laser Assisted Associative Desorption

Diekhöner, Lars

Publication date:
2000

Document Version
Publisher's PDF, also known as Version of record

Dynamics of High Barrier Gas-Surface Reactions
studied by
Laser Assisted Associative Desorption

Ph.D. Thesis

Lars Diekhöner

Fysisk Institut
Syddansk Universitet
Odense Universitet
April 2000

Preface

This thesis is submitted to the Faculty of Science and Engineering, University of Southern Denmark, Odense University to fulfill the requirements for the Ph.D. degree in physics. The experimental research presented in this thesis has been carried out at the Physics Department of Odense University during the last four years. The main results have been published in the articles listed below and appended in full at the end of the thesis.

List of publications

[1]   L. Diekhöner, D.A. Butler, A. Baurichter and A.C. Luntz
       Parallel pathways in methanol decomposition on Pt(111)
       Surface Science, **409**: 384, (1998).

[2]   L. Diekhöner, A. Baurichter, H. Mortensen and A.C. Luntz
       Observation of metastable atomic nitrogen adsorbed on Ru(0001)
       Journal of Chemical Physics, **112**: 2507, (2000).

[3]   L. Diekhöner, H. Mortensen, A. Baurichter and A.C. Luntz
       Coverage dependence of activation barriers: Nitrogen on Ru(0001)
       Journal of Vacuum Science and Technology A, **18**(4): in press, (2000).

[4]   L. Diekhöner, H. Mortensen, A. Baurichter, A.C. Luntz and B. Hammer
       Dynamics of high barrier surface reactions: Laser Assisted Associative Desorption of N_2 from Ru(0001)
       Physical Review Letters, **84**: 4906, (2000).

<div align="right">

Lars Diekhöner
Odense, April 25, 2000

</div>

Content

1 Introduction

Surface science has in the recent decades become a very important discipline in its own right. The field is in general concerned with the physical and chemical properties of surfaces and the interaction between surfaces and gases or electromagnetic radiation. It is of fundamental scientific interest to understand these issues in detail. Furthermore, surface science is motivated by a number of applications. Take the growth of nano-technology as an example - the smaller structures get, the more important are the surface properties. Microelectronics, catalysis, corrosion and tribology are some of the important applied fields where detailed knowledge of the interaction with the surface is necessary. This thesis is concentrated on the dynamics of gas-surface interactions, with a special emphasis on dissociative chemisorption and associative desorption. These are fundamental steps of gas-surface chemical reactions motivated partly because of its importance to heterogeneous catalysis.

What happens when a molecule interacts with a surface? Is a molecule incident on a surface simply scattered elastically from the surface, or is energy transferred between the molecule and the surface, and how does this depend on the initial state of the molecule and the surface? Much can be learned by studying gas-surface scattering [5]. If now the molecule looses sufficient energy and momentum in the collision, it may adsorb on the surface. It can diffuse around, dissociate, react with other adsorbates or acquire sufficient thermal energy to desorb back into the gas phase again.

Some reactions that only occur in the gas phase under extreme conditions, if at all, are possible if a surface is involved catalytically. Molecular bonds are easier broken and reactants are brought together in close contact at the surface. Lowering of the overall activation energy of the reaction and improved selectivity in forming the desired product is the heart of heterogeneous catalysis. Although the complete reaction involves many elementary steps, the rate-limiting step in the overall catalytic reaction on a surface is often the dissociative chemisorption of one of the reactants. This key step is therefore very important to understand in detail.

1.1 Dissociative adsorption dynamics

In 1932 Lennard-Jones described the dissociation of a diatomic molecule (A_2) on a metal surface (M) in terms of a one-dimensional potential energy surface (PES) shown in the figure below where the only variable is the molecule-surface distance (z) [6].
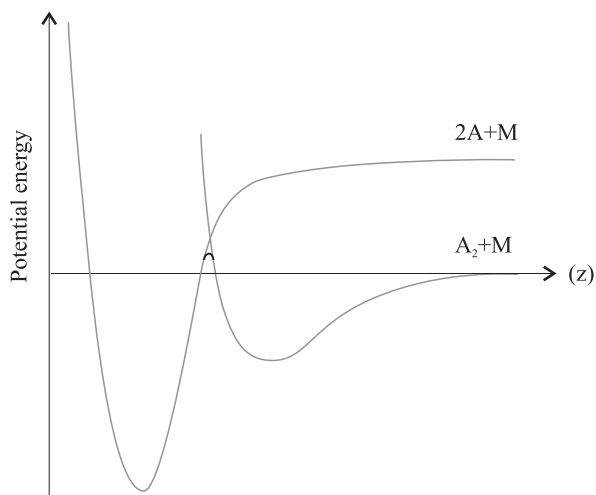
Figure 1. Potential energy (gray curves) of the molecular state (A_2+M) and the dissociated atomic state (2A+M). The "avoided crossing" between the two curves is indicated in black.

First we follow the molecular potential (A_2+M). At some distance from the surface the molecule finds a minimum and binds in a physisorbed state through the weak van der Waals interaction, or in a stronger molecular chemisorbed state. Approaching closer to the surface leads to an increasing repulsion, due to overlap between the electronic wave functions of the molecule and the solid. The bonding between the atoms and the surface is much stronger and the atomic PES (2A+M) experiences therefore a deeper minimum at a closer distance. In the electronically adiabatic approximation, the nuclei follow the ground state potential energy surface. Crossing between the two curves is avoided and the molecule dissociates. If the avoided crossing point is positioned above zero in energy (relative to the infinitely separated molecule-surface asymptote), the dissociation process is said to have an activation barrier. Note that this value is much lower than the molecular bond energy, i.e. the energy needed to dissociate the molecule in the gas phase, which is equal to the lateral separation of the two curves (2A+M) and (A_2+M) at large z. If, on the other hand, the avoided crossing point is below zero, no barrier is present and the molecule readily dissociates on the surface. Mainly activated processes will be discussed here.

The schematic 1-dim PES of Figure 1 rationalizes two generic pathways to dissociation. First, a precursor-mediated process, where a molecule adsorbs intact on the surface in the molecular state and gets thermally equilibrated. By further thermal activation the molecule can now either desorb back into the gas phase or dissociate. The molecular state can thereby act as a precursor prior to dissociation. The other possibility is the so-called direct process, where the molecule dissociates directly upon impact with the surface. Experimentally we can distinguish between these two pathways by measuring the dissociative sticking probability as a function of incident translational energy and surface temperature. If dissociation occurs via the precursor, the molecule first has to lose its incoming translational energy and momentum to get trapped in the molecular well. The probability of getting trapped decreases with translational energy, since the molecule then has to lose more energy. Once trapped in the precursor state, there will be competition between desorption back into the gas phase or dissociation. The activation energies for these two processes will most likely be different, and there will be a temperature dependent branching ratio for the rate of each process. In other words, the dissociation probability will be strongly surface

temperature dependent. If dissociation occurs via the direct process only, the dissociation probability will increase with incoming energy, necessary to surmount the barrier. Judging from Figure 1 one would say that if the translational energy is below the barrier between the molecular and dissociated state no dissociation takes places and if above the barrier dissociation occurs with unity probability. Since dissociation occurs before the molecule is thermally equilibrated, the surface temperature is expected to play only a minor role, if any at all.

It is certainly possible that both dissociation mechanisms can contribute in a given molecule-surface interaction. Experimentally one would observe initially a decrease in the dissociation probability with energy, evident of a trapping into a precursor and at higher energy an increase due to direct dissociation. A few examples are N_2 on W(100) [7,8], CH_4 on Ir(110) [9,10] and Ir(111) [11], NH_3 on Ru(0001) [12] and CH_3OH on Pt(111) [1]. In the latter two it was shown that the direct process occurred on the terrace sites and the precursor-mediated occurred at defects. For methanol on Pt(111), this will be discussed in detail in chapter 3.

Clearly many more degrees of freedom than the molecule-surface distance are anticipated to play a role. For example the step-like behavior of direct dissociation described above within the 1-dim model is not observed. Instead a more smooth increase without a sharp threshold is seen, where the dissociation probability often follows an "S-shaped" curve as a function of translational energy. This broadening is evident for the multi-dimensionality of the process, like e.g. barriers depending on, where on the surface the molecule hits, how the molecule is oriented etc.

Also the internal energy of the molecule has to be considered. In some cases vibrationally and rotationally excited molecules can have a different threshold for translational activation. Numerous experiments and theoretical calculations have pointed out that a complete PES is multi-dimensional: $V(z,d,x,y,\gamma,\{u_i\})$ where z is the distance to the surface, d the molecular internuclear separation, (x,y) is the position on the surface, or unit cell, γ is the orientation of the molecule to the surface normal and $\{u_i\}$ are the lattice coordinates. The introduction of these extra coordinates enables us to describe phenomena like distribution of barriers ("impact parameter" dependence (x,y)), steric effects (γ), vibrational effects (d), interaction with phonons ($\{u_i\}$) etc. For poly-atomic molecules even more coordinates have to be included. It is impossible to visualize graphically a multi-dimensional PES. Including one more coordinate, such as the inter-nuclear distance of the molecule, already enhances the understanding substantially.

A two-dimensional PES is often visualized by drawing contours of constant potential energy as a function of the two coordinates. For a di-atomic molecule, the obvious coordinate to include is the inter-nuclear distance of the molecule, i.e. the bond separation d, as well as the distance from the surface z. Below are shown models of 2-dim PES's. The entrance channel in the upper left part of the PES, represents the unperturbed molecule far away from the surface at large z where the PES along d is like for the free molecule (a Morse potential). In the exit channel at large d (lower right part of the PES) the molecule is broken up and the PES is the one described by the atom-surface interaction. The two extremes of the potential can be determined separately by different gas-phase and surface spectroscopic or theoretical methods. The interesting and difficult part is the reaction zone, where the dissociation or transition

from molecule to adsorbed atoms takes place. As already emphasized, the dissociation may be activated. The detailed shape of this 2-dim PES determines the dynamics of dissociative adsorption as well as associative desorption, with respect to the two coordinates involved, where the location of the barrier plays a major role [13]. We can thus discuss the role of translational vs. vibrational energy in promoting dissociation and for associative desorption the energy released in translation and vibration respectively, by looking closer at the 2-dim PES.
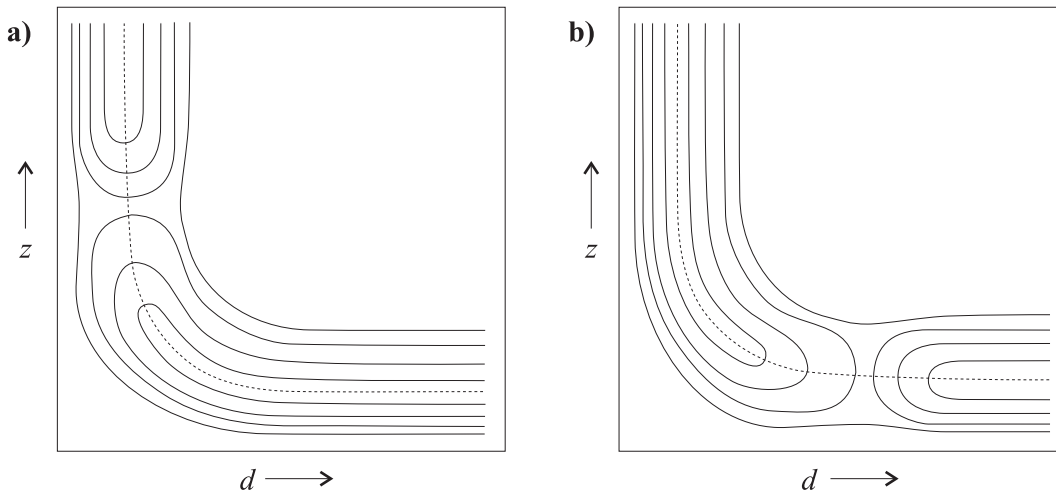
Figure 2. Model PES for dissociation of a molecule on a surface, where z is the molecule-surface distance and d is the inter-nuclear distance (or bond length) of the molecule. **a)** a so-called early barrier and **b)** a so-called late barrier. The equipotential curves are shown as solid lines and the minimum energy pathway is shown as a dashed line.

Motion across the barrier, i.e. along the minimum energy pathway, is needed to induce dissociation. Figure 2a shows a system characterized by a so-called early barrier, i.e. the barrier is located in the entrance channel to adsorption. Sufficient motion in the z-direction, i.e. translational energy, will promote dissociation. Increasing the vibrational energy of the molecule will not increase the dissociation probability. In Figure 2b is shown a system characterized by a so-called late barrier, i.e. the barrier is located in the exit channel. The transition state is located at an extended molecular bond length, and energy has to be placed in the d-coordinate to surmount the barrier. Thus, vibrational excitation increases the dissociation probability at given incident translational energy. In other words, the location of the barrier determines how effective vibrational energy is in promoting dissociation and by how much the translational threshold is shifted down with vibrational excitation. Introducing these 2-dim PES's, the effect of vibrational as well as translational activation can be rationalized.

The classical example of vibrational activation is hydrogen dissociation on copper surfaces, where increasing the vibrational energy of the incident D_2 shifted down the translational threshold. This was shown experimentally [14] as well as theoretically [13,15]. Now, other degrees of freedom could very well affect the dissociation process. To map out the dependence of other internal coordinates one would like to prepare the incoming molecules in specific quantum states and measure the dissociation

probability. This can in principle be done using laser excitation techniques [16], but it is very difficult in practice.

1.2 Associative desorption dynamics

Another approach is to realize that dissociative adsorption and associative desorption are time-reversed processes, described by the same PES if their pathways are the same. A desorption experiment will therefore probe the same PES as an adsorption experiment. The desorbing molecules can be detected quantum state-resolved using sensitive laser spectroscopic techniques like laser induced florescence (LIF) and resonance enhanced multi-photon ionization (REMPI). In this way all the molecular degrees of freedom, translation, rotation and vibration, can be determined. If now we apply detailed balance, full state-resolved information from the desorption experiment can be transferred to the adsorption process [17]. According to the principle of detailed balance the state-resolved desorption and adsorption fluxes are equal under thermal equilibrium, i.e. $f_{des}(E,\alpha,T)dE = f_{ads}(E,\alpha,T)dE$, where E is the translational energy, T the temperature and α indicates the quantum numbers for internal degrees of freedom. The adsorption flux can be written as the product of the energy distribution of the gas (at thermal equilibrium) impinging on the surface, i.e. a Maxwell Boltzmann distribution $F_{MB}(E,\alpha,T)$, and the energy dependent adsorption probability $S(E,\alpha)$. We find $f_{ads}(E,\alpha,T) \propto F_{MB}(E,\alpha,T)S(E,\alpha)$ and can then write $f_{des}(E,\alpha,T) \propto E\,exp(-E/k_BT)exp(-E_\alpha/k_BT)S(E,\alpha)$, where E_α is indicating the energy of the internal degrees of freedom of the molecule. Measuring $S(E,\alpha)$ in a supersonic molecular beam experiment allows us to determine the desorption flux, and on the contrary measuring the desorption flux enables us to determine $S(E,\alpha)$.

Even though experiments often are performed far from thermal equilibrium (e.g. the gas in a supersonic beam is not at the same temperature as the surface etc.) it has been shown that detailed balance is applicable to relate a number of adsorption/desorption processes [18,19]. It was mentioned earlier that the dissociative sticking of H_2 on copper was vibrationally activated. Application of detailed balance would predict that associative desorbing hydrogen is formed with high vibrational population. This is indeed observed experimentally [20-22]. Looking at the model PES (Figure 2b), we can see that the molecule is formed on the surface with the transition state at an extended bond length, resulting in the large vibrational excitation of the desorbed molecules. Dynamical calculations on these PES's have shown the effects theoretically [13,23].

1.3 Applications to N$_2$/Ru(0001)

It is well recognized that the activated dissociation of simple gas phase molecules at metal surfaces is often the rate-limiting step in many industrially important catalytic processes. This recognition has stimulated much experimental and theoretical work over the past several decades in the kinetics and dynamics of activated dissociative chemisorption.

As discussed above, there are many ways to study dissociative adsorption. Let us turn to a specific example, nitrogen on Ru(0001), that has attracted much attention recently due to the possible role of supported Ru as an end catalyst for NH_3 synthesis. The rate-limiting step in the overall reaction is believed to be dissociative chemisorption of N_2. The N-N bond energy in the gas phase is ~10 eV, breaking the bond at the Ru surface lowers the energy cost substantially, but there is still a large barrier. Such a high barrier surface reaction is very difficult to study, evident from the many experimental contributions presented below.

Early experiments involved extensive dosing with N_2 measuring the dissociation probability S_0. A value of $S_0=10^{-6}$ at room temperature was found [24]. Later experiments showed that this "high" value was due to a hot ion gauge filament. Turning this off resulted in $S_0=10^{-12}$ [25]. The effect of the hot filament could be to create molecules in electronically or vibrationally excited states or atoms, increasing the measured S_0. The thermal dependence of the rate of N_2 dissociation at high pressures gave an activation barrier of only 0.4 eV [26]. However, if the (low density) natural steps on the surface were poisoned by coadsorption of gold, a much higher barrier of 1.3 eV was obtained. The authors suggested that the dissociation rate is strongly influenced by steps/defects [26]. A molecular beam experiment, by Romm *et al*, showed that vibrational as well as translational activation was occurring and a barrier of ~2 eV was suggested [27]. But the experimental data in this work are not consistent with several newer molecular beam experiments made by Kleyn and coworkers [28], Egeberg *et al*. [29] as well as a preliminary beam experiment by us [30]. Thus, it is uncertain as how to evaluate their experiment and conclusion. The newer beam experiments only covered a narrow translational energy range and no attempt was made to estimate the barrier height, although all molecular beam experiments suggest a very high barrier. Recent measurements of N_2 formed by associative desorption from Ru(0001) [31] present a puzzling picture for the barrier since the energy dependence of the desorption flux peaks at low translational energies (consistent with a low barrier) but tails to high translational energies (consistent with a high barrier).

The first density functional theory (DFT) calculation showed that dissociation took place over a substantial barrier of 1.36 eV [32]. Improved DFT calculations determined the barrier to be 2 eV [4,26,31]. It was also calculated that the barrier decreased strongly for dissociation at step sites [26].

In conclusion, experimental determination of the barrier to dissociation of N_2 on Ru(0001) seems to be a difficult task. There is no doubt that the barrier is very high, and that special sites on the surface with lower barriers seem to dominate the reaction in most experiments.

This thesis describes a new technique to study the dynamics of high barrier surface reactions which we term laser assisted associative desorption (LAAD). We have applied this technique to study associative desorption of N_2 from Ru(0001). The translational energy distribution of N_2 formed by associative desorption is measured with time-of-flight techniques following a short laser induced temperature jump. It will be shown that presence of defects does not affect the results significantly. We have determined the barrier not only at low coverage like in other experiments but also at higher coverages. These higher coverage states have not been observed before. We

will show that the barrier increases with coverage. LAAD also gives information on the vibrational state distribution, *without* using state-resolved detection. We find that desorbing N_2 are formed in high vibrational states.

1.4 Outline of the thesis

First an overview of the experimental equipment will be presented in chapter 2. A molecular beam study of methanol dissociation on Pt(111) is presented in chapter 3. In chapter 4 adsorption-induced desorption will be discussed. It will be shown that N_2 is desorbed promptly upon adsorption of D or H atoms. The nitrogen/Ru(0001) system will be introduced in chapter 5. We have shown that high N coverages on a Ru(0001) surface can be produced by N atom dosing. These experiments will be discussed in chapter 6. The general physics of laser assisted associative desorption will be presented in chapter 7. In chapter 8 and 9, LAAD will be applied to study N_2 and CO associative desorption from Ru(0001). Chapter 10 gives a summary of the findings as well as a summary in danish. References are given in chapter 11.

2 Overview of experimental equipment

The experimental equipment will be introduced here. Also a description of time-of-flight measurements is given.

2.1 Vacuum system

The experiments were performed in a turbo pumped (550 l/s) ultra-high vacuum (UHV) system, having a base pressure of 1×10^{-10} Torr. A Ti-sublimation pump was occasionally used to lower the background at high gas load and further reduced the base pressure to 5×10^{-11} Torr. The system consists of a sample manipulator with x-y-z and rotational motion, a triply differentially pumped supersonic molecular beam and several gas inlets for background dosing with a number of gases. Part of this system has been described previously [33]. Atom dosing of the sample was accomplished via an active "beam" produced with a microwave discharge atom source described in detail in section 6.2. A number of "analytical tools" were attached: A differentially pumped quadrupole mass spectrometer (QMS) with an orifice of 5 mm in diameter placed 2 mm from the sample. In this way we ensure that only species desorbing from the front surface are detected by the QMS. This enables us to do careful temperature programmed desorption (TPD). The system also included standard surface preparation and analytical equipment such as an ion gun for sputter cleaning of the sample, Auger electron spectroscopy (AES) with a single pass cylindrical mirror analyzer to determine chemical impurities in the surface region and measure adsorbate coverages and a low energy electron diffraction (LEED) apparatus, to investigate the ordered structure of surface and adlayers. An additional QMS measured the background gas in the chamber. A rotatable differentially pumped mass spectrometer was used to detect desorbing molecules from the surface in LAAD experiments and to measure time-of-flight (TOF) distributions. This QMS was also used to characterize the molecular beam. The UHV chamber is equipped with a number of windows to allow entrance of laser beams at various angles of incidence to the surface. Details about crystal cleaning can be found in section 3.2 for Pt(111) and 6.2 for Ru(0001).

2.2 Molecular beams

Apart from producing molecules at high energy (up to several eV), supersonic molecular beams have the advantage of low divergence and a well-defined direction, achieved by selecting only the central part of the beam by use of skimmers and apertures in a number of stages of differential pumping. The beam entering the main UHV chamber is therefore collimated to a few mm in diameter, allowing control of the angle of incidence at the sample, and ensuring that the beam only impinges on the sample.
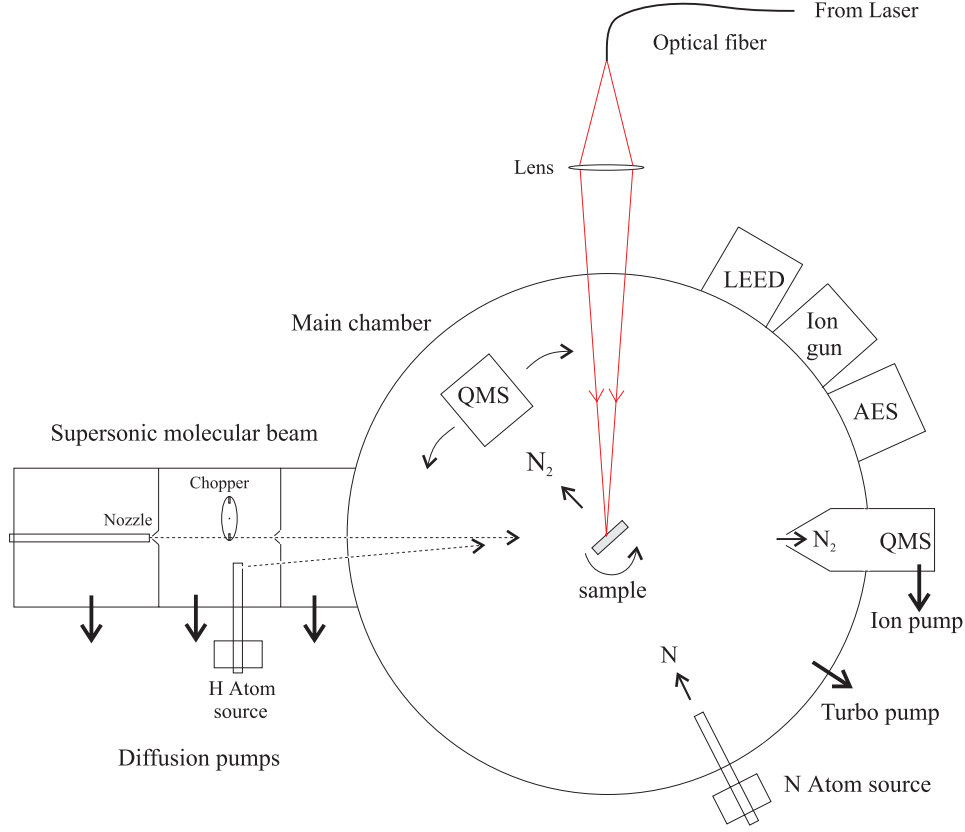
Figure 3. Schematic (top) view of the apparatus.

Consider first a thermal beam where a gas at low pressure effuses out of a chamber through a small orifice. This is a so-called Knudsen source. The mean free path λ of the gas is much greater than the smallest dimension of the source orifice (its diameter *d*). This means, that only a few collisions between molecules are taking place in the effusive beam while exiting the source. The temperature of the source, T_{source}, characterizes all degrees of freedom. The velocity distribution for the flux along the beam axis is given by a Maxwell-Boltzmann distribution

$$I(v) \propto v^3 \, exp\left(- \frac{mv^2}{2k_B T_{source}} \right) \tag{2.1}$$

The velocity distribution of the atom beam mentioned above was described by this equation. Unfortunately, for some purposes, the spread in velocities is large. To study the dependence of e.g. dissociation on energy a more mono-energetic beam source can be achieved with the supersonic nozzle beam. This source operates at high pressures, where gas expands from a high- into a low-pressure region through a very small orifice. A large number of inter-molecular collisions are taking place as the gas exits the source ($\lambda << d$) which leads to substantial cooling of the gas with respect to a reference frame moving with the gas at the flow velocity v_0. The average velocity is thus given by v_0 and the velocity distribution in the moving frame will again be a Maxwell-Boltzmann distribution, now characterized by a low temperature $T_{\parallel}$ and

thereby a small spread in velocity: $\Delta v = \sqrt{2k_B T_{\parallel} / m}$. An observer in the "laboratory frame", will measure the following flux-weighted distribution:

$$I(v) \propto v^3 \exp\left(-\frac{m}{2k_B T_{\parallel}} (v - v_0)^2 \right) \qquad (2.2)$$

The velocity distribution of the beam was measured via time of flight (TOF) from a mechanical chopper to a mass spectrometer in the main chamber. Most beams were characterized by $\Delta v / v_0 < 0.07$, corresponding to a spread in translational energy of $\Delta E / E_0 < 0.14$. The values for the effusive beam are $\Delta v / v_0 \approx 0.8$ and $\Delta E / E_0 \approx 1.8$.

Thermal energy is converted to directed translational energy, and the velocity of the supersonic beam can be controlled by varying the temperature of the gas before the isentropic expansion, i.e. the nozzle temperature. Furthermore with use of seeding techniques, supersonic beams with translational energies over a wide range can be produced. When an expanding light gas (the "carrier gas") contains a small fraction of heavier gas (the "seed gas"), the heavy molecules will reach nearly the same flow velocity as the light molecules. They are accelerated via the collisions in the nozzle. Since they are heavier a corresponding increase in translational energy is achieved. By controlling the mixing ratio and nozzle temperature, one can vary the translational energy from thermal energies to several eV.

Concerning internal degrees of freedom, the rotational temperature is low due to the many collisions, whereas not enough collisions are taking place to cool vibrations significantly. The vibrational temperature is therefore very close to the nozzle temperature (T_n). Using seeding (and/or "anti-seeding" where the carrier gas is heaviest resulting in a deceleration of the seed gas), beams with the same translational energy but different vibrational energies can be produced. For example, N_2 beams made by seeding N_2 in He at low T_n and using only N_2 (unseeded) at high T_n can give different vibrational temperatures of the N_2 while the translational energy is unchanged. This can be used to investigate dependencies of these two particular degrees of freedom on dissociation separately, to some extent.

More details about supersonic beams can be found in the review by Scoles [34].

2.3 Laser

For the laser assisted associative desorption (LAAD) experiments we use a pulsed alexandrite laser from Light Age Inc. (Model 101 PAL^{TM}). The laser is a flash lamp pumped solid-state laser where the active medium is an alexandrite rod (Cr^{3+}: $BeAl_2O_4$). Part of the energy in the optically active Cr^{3+} ion is released into lattice phonons. There is a possibility of tuning the lasing wavelength over a range from 720-800 nm, due to the vibronic coupling of the lower level of the laser transition. Also the pulse length can be varied between 60-150 ns, depending on wavelength and pump power. The optimal output of the laser is reached at elevated temperatures (200° C).

Due to the ease of using flowing water to stabilize the rod temperature, the laser is operated at 80º C. The optical resonator is designed to give lasing in multiple spatial modes, resulting in a nearly flat top spatial profile without "hot spots" as verified with burn paper. A Pöckels cell is used to Q-switch the laser. We achieved pulse energies of ca 200-300 mJ/pulse in long pulse mode (non Q-switched) and 400 mJ/pulse when Q-switched. Pulse energies of 150-200 mJ/pulse (Q-switched) were normally used in the experiments, giving a temporal pulselength of 100-130 ns (two different laser rods). The wavelength is ca. 750 nm. The output is linearly polarized and the use of a polarizer allowed easy control of the intensity. The laser was operated at a repetition rate of 10 Hz. General information about alexandrite lasers can be found in ref. [35]

The Alexandrite laser was running with several modes (ca 5), causing some spatial inhomogeneity in the beam intensity profile. Because of mode beating there is some of shot to shot fluctuation in the spatial pattern of beam. Since inhomogeneities in the beam could emphasize laser damage problems the laser beam was homogenized prior to striking the surface by propagating the light through a long coiled multimode silica clad fiber of 400 µm core diameter. Because many modes of the fiber are excited, the net result is that shot to shot spatial fluctuations of the laser beam are minimized, as well as minimizing any small-scale spatial structure in the beam. In addition, an unpolarized beam (averaged over a reasonably small spatial scale) is also obtained. The light output from the end of the fiber (0.4 mm in diameter) is geometrically imaged onto the surface with 3X magnification using a single lens (see Figure 3). Assuming perfect geometrical optics imaging from the fiber tip onto the surface, the net result is that the surface is illuminated with a 1.2 mm diameter highly reproducible and smooth spatial laser pulse with a nearly Gaussian spatial distribution as measured by a scanning small aperture. The main purpose of sending the light through a fiber was to minimize laser-induced damage of the surface. This issue will be discussed later in section 7.4. The temporal profile of the laser pulse is Gaussian, as detected with a fast photodiode and seen on an oscilloscope.

2.4 Time-of-flight

Many of the data presented in this thesis are recorded with time-of-flight (TOF) techniques, i.e. measuring the flight time for a known distance. Determination of the translational energy of the molecular beam has been done by measuring the TOF from a mechanical chopper, placed in the beam line in the second beam chamber, to a detector, the rotatable QMS. The chopper is a fast rotating (100 Hz) disc with two diagonally placed narrow slits. The beam is blocked by the disk, except when the slit is in the beam line. A short pulse of gas is allowed to move down the beam line and enter the main chamber, where it is detected with the QMS and the TOF recorded in a multichannel scaler. The opposite slit is used to trigger the "clock" via a light emitting diode and a photo transistor. The rotation frequency and the slit-width of the chopper is chosen to ensure that the temporal width of the pulse from the chopper is much smaller than the total flight time from chopper to the ionizer of the QMS. The travelling distance is in principle given by the mechanical dimensions of the vacuum-system. The transmission time τ_{QMS} through the QMS, i.e. the time it takes to move from the ionizer to the channeltron were the ions are detected, depends on the particle mass, but is independent of initial (beam) velocity since the ionized particles are accelerated by a strong electric field.

We can calibrate the distance by measuring TOF's of supersonic beams of gases like He and Ar at various nozzle temperatures and comparing with the theoretical velocity distributions [34]. τ_{QMS} can be found by using a beam of polyatomic molecules like CO_2 or N_2. The energetic electrons in the ionizer region crack a fraction of the molecules. These parts, e.g. C, CO and CO_2, will have different masses and thus different τ_{QMS}, while the TOF from chopper to ionizer is the same. It was found that the mass dependence of the transmission time (in µs) was given by $\tau_{QMS} \approx 5 \cdot \sqrt{m/q}$, where m/q is the particle mass to charge ratio inserted in amu/e. Details about calibration of the TOF will be given elsewhere [36].

In the LAAD experiments, molecules are desorbed from the surface by a laser induced temperature jump. Desorption occurs only over a time that is much smaller than the flight time and TOF techniques can thus be used to measure translational energy distributions. The flight distance has been determined as follows.
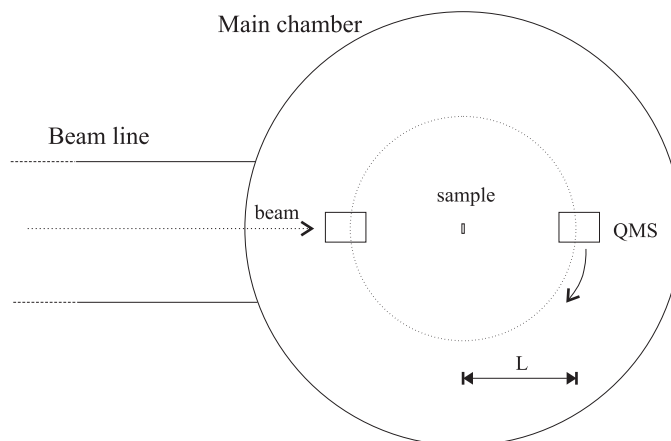
Figure 4. Schematic view of the determination of distance from surface to ionizer. The sample is lifted out of the way during these measurements.

The sample is placed at the center of the chamber. The differentially pumped rotatable QMS rotates about this center on a circle with radius L (see Figure 4). This QMS is constructed such that after the molecules are ionized, an electric field bends the ions 90° down and leads them through the quadropole field. There is an opening on the backside of the differentially pumped housing, to allow molecules that are not ionized to leave the QMS region. This reduces the background significantly. The distance from surface to ionizer (L) was determined by measuring the TOF for a He supersonic beam with the QMS placed with the front to the beam, and then after a rotation of 180°, with the backside placed to the beam. Since the average velocity of the He beam is known, we can calculate the difference in distance equal to 2L. Half of that is the distance from the sample to the ionizer. The distance found, L=97 mm, agreed with the geometric measurements within 2 mm. The uncertainty in the distance is thus <2 %, introducing an uncertainty of <4 % in the translational energy measured in LAAD. The laser spot on the surface, from where desorption takes place is only ~1 mm in diameter and the solid angle viewed by the differentially pumped QMS (ionizer) is only 8×10^{-4} sr, defined by an aperture of 2.25 mm placed 71 mm from the surface. The main instrumental broadening is thus due to the finite ionizer length. The TOF distributions

measured in LAAD where averaged over the length of the ionizer which was approximately 5 mm.

2.5 Small vacuum system

A small UHV system was designed to pre-clean the Ru crystal off-line by many oxidation-anneal cycles and to perform first LAAD test experiments. The small UHV system is pumped by a turbo pump (180 l/s). The sample is mounted on a x-y-z manipulator and can be rotated through a differentially pumped rotation stage. A gas manifold connected to a variable leak valve allows inlet of various gases to the chamber. The system is equipped with a number of windows for sending laser light into and out of the chamber. The microwave discharge atom source was initially installed here and the first experiments with N atom dosing of a Ru(0001) surface were performed. The only diagnostic tool was the differentially pumped QMS described earlier. These experiments revealed that it was possible to achieve very high coverages of adsorbed N with atom dosing. These high coverage N-states could be characterized only by TPD, though, and other diagnostic tools such as AES and LEED became necessary. Therefore the experiments were continued in the main UHV system. The small system is now successfully used to test various experimental setups.

3 Parallel pathways in methanol decomposition on Pt(111)

3.1 Introduction

Surface dynamics studies on well-defined metal single crystals have identified two fundamental classes of bond-breaking reactions at surfaces: direct dissociation of the molecule upon impact, and indirect dissociation via an adsorbed 'precursor' state. These are typically characterized by different dependencies on the translational energy of the molecules and the surface temperature. Results of a system where both dissociation mechanisms occur in parallel will be presented here. It will be shown that a non-activated indirect channel can exist alongside a direct channel with a large activation barrier (~0.5 eV). This occurs through a surface site dependence and modification of the surface allows us to control one of the channels. The non-activated, precursor mediated channel occurs at minority defect sites, while the activated, direct channel occurs at the majority terrace sites. Finally, from the dissociation dynamics, it is possible to make estimates for the associative desorption rate, the final step in the catalytic synthesis of CH_3OH. The importance of surface defects in determining the branching ratio between thermal and hyper-thermal products of this reaction is discussed.
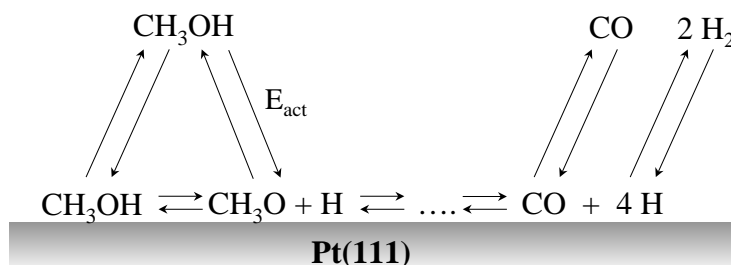
Figure 5. Schematic description of the methanol decomposition (synthesis) over a transition metal surface. The first step is the breaking of the O-H bond, either via an adsorbed methanol precursor state, or directly over an activation barrier. The methoxy species then rapidly decomposes to $CO_{(ads)}$ and $H_{(ads)}$, which then desorb at sufficiently high surface temperatures.

The dissociation of methanol on a Pt(111) surface was chosen as it represents an ideal model for the reaction of small organic molecules at surfaces. Due to its industrial importance, the synthesis and reaction of methanol have been studied on a range of transition metal surfaces. On Pt(111), methanol is adsorbed intact at 100 K and it is generally believed that it decomposes to $H_{(ads)}$ and $CO_{(ads)}$ above 140 K [37,38]. In common with other methanol decomposition systems, discussed by Davis and Barteu [39], it is believed that the initial step in this reaction is the cleavage of the O-H bond to produce surface methoxy and hydrogen. While methoxy is stable on other metal surfaces, on Pt(111) it undergoes rapid and complete decomposition [37]. This means that the rate limiting step of the complete reaction, i.e. producing gas phase CO and

H$_2$, is the dissociative chemisorption of CH$_3$OH, breaking the O-H bond and forming adsorbed methoxy and hydrogen (see Figure 5 and Figure 9). Since this is the interaction of a gas phase species with a surface, it is open to direct study with supersonic molecular beam techniques. Other authors claim that CH$_3$OH partially decomposes by C-O bond scission on Pt(111) and other metals [40], although the observation of this channel is apparently very dependent upon details of the surface structure. We find no evidence for any C-O bond scission on our sample, as discussed later.

3.2 Experimental

The experiments were performed in the UHV system previously described (chapter 2). A seeded methanol beam was formed by bubbling a high purity carrier gas, (He, H$_2$, Ar or N$_2$,) through a flask of spectroscopic grade methanol. The kinetic energy of the methanol molecules could be varied between 0.10 and 1.02 eV by changing the carrier gas and nozzle temperature, and was measured by their time-of-flight from a mechanical chopper to a quadrupole mass spectrometer (QMS) in the scattering chamber. The beam was always at normal incidence to the surface.

The Pt(111) crystal had been characterized in a number of previous studies [33] and was cleaned by cycles of Ar$^+$ ion bombardment, oxidation (1x10^{-7} Torr, 700 K) and vacuum annealing (1150 K). The crystal was heated by electron bombardment of the backside. The cleanliness was checked by Auger electron spectroscopy (AES) and the defect density was monitored by the well characterized CO temperature programmed desorption (TPD) peak shape [41,42] and by specular helium scattering, which is an extremely sensitive probe of surface defects.

Sexton investigated the interaction of methanol with Pt(111) using electron energy loss spectroscopy (EELS) and TPD. He found that the decomposition of methanol on Pt(111) yields only CO$_{(ads)}$ and H$_{(ads)}$. A TPD of a methanol covered surface resulted in the desorption of only methanol, H$_2$ and CO. No dehydrogenated intermediate species such as methoxy have ever been observed on this surface with EELS, indicating the rapid and exclusive generation of stoichiometric amounts of CO and H$_2$ [37]. This was further verified in the present studies by looking for other desorbing reaction products such as water, CO$_2$ and CH$_4$ during molecular beam dosing. No such species were ever detected. Such species, if present, were at least 100 times smaller than the dominant CO and H$_2$ desorption products and indicate that C-O bond scission was not a significant decomposition channel on our sample.

The rate of decomposition can thus be measured either by following the removal of methanol from the beam by the King & Wells method [43], or the production of H$_2$ or CO which desorb from the surface at 360 and 470 K respectively. The CO and H$_2$ productions were linearly proportional to each other, but in practice we found that we were more sensitive to the production of H$_2$. By measuring the H$_2$ signal with a non line-of-sight QMS and normalizing to the incident flux of methanol, we were able to obtain a relative decomposition probability. Due to the uncalibrated sensitivity of the QMS to methanol and hydrogen this data is in arbitrary units. The absolute reaction probability of methanol was also measured by the method of King and Wells [43]. Under the conditions of maximum decomposition shown in Figure 6 we were just able

to resolve the uptake of methanol by the reaction, placing the maximum probability at approximately 1 %. We have scaled the arbitrary units of the relative signal to this value, so that to a first approximation the relative scale can be read as a % dissociation probability per collision.

In measurements taken below 500 K some poisoning of the reaction was observed as a function of time due to the slow build up of $CO_{(ads)}$. All the data presented here were taken in the zero coverage limit where this poisoning was insignificant.

3.3 Results and discussion

3.3.1 The decomposition mechanism

The relative decomposition probability was measured at surface temperatures between 400 and 1000 K and with incidence beam energies between 0.10 and 1.02 eV. The results are shown as a 3D plot in Figure 6a and as cuts through this plot in Figure 6b and Figure 6c. There are two distinct regions of high decomposition probability. At incidence beam energies below 0.5 eV the probability rises sharply with *decreasing* beam energy and surface temperature. At incidence beam energies above 0.5 eV the decomposition probability rises with *increasing* beam energy, and is almost independent of the surface temperature. These two types of behavior are typical of dissociation mechanisms characterized in studies of many other molecules at surfaces.

The dependence on both incident energy *and* surface temperature for the low incidence energy pathway is exactly the behavior anticipated for a molecular precursor. The mechanism in this regime is thus assigned to an indirect mechanism, mediated by an adsorbed molecular methanol precursor. Under these conditions the rate of dissociation is limited by the population of the methanol precursor. Decreasing the kinetic energy of the molecules increases the probability of trapping into this weakly bound state, and decreasing the surface temperature increases the ratio of dissociation over the more activated desorption of the adsorbed methanol precursor. Thermal desorption studies [37] indicate that the molecular methanol well depth on Pt(111) is approximately 0.5 eV. This is consistent with a high probability of trapping into this well over the approximate incidence energy range 0 - 0.5 eV, as is well known from soft cube models of sticking [44].

The high incidence energy regime behaves as a direct dissociation mechanism involving a considerable energetic barrier. The threshold for dissociation via this mechanism is seen at approximately 0.5 eV in Figure 6. Since thresholds in molecular beam translational excitation experiments are roughly equivalent to thermal activation barriers, we infer that the thermal barrier is roughly of this magnitude. Clearly the dissociation increases slowly with incidence energy above this threshold, indicative of a distribution of barriers characteristic of any multidimensional dynamic process. No such direct channel was observed by Gibson and Dubois in earlier beam studies [38]. However, they were limited to kinetic energies below 0.25 eV and in this energy regime their conclusion that dissociation is dominated by an indirect mechanism is fully in agreement with our observations.
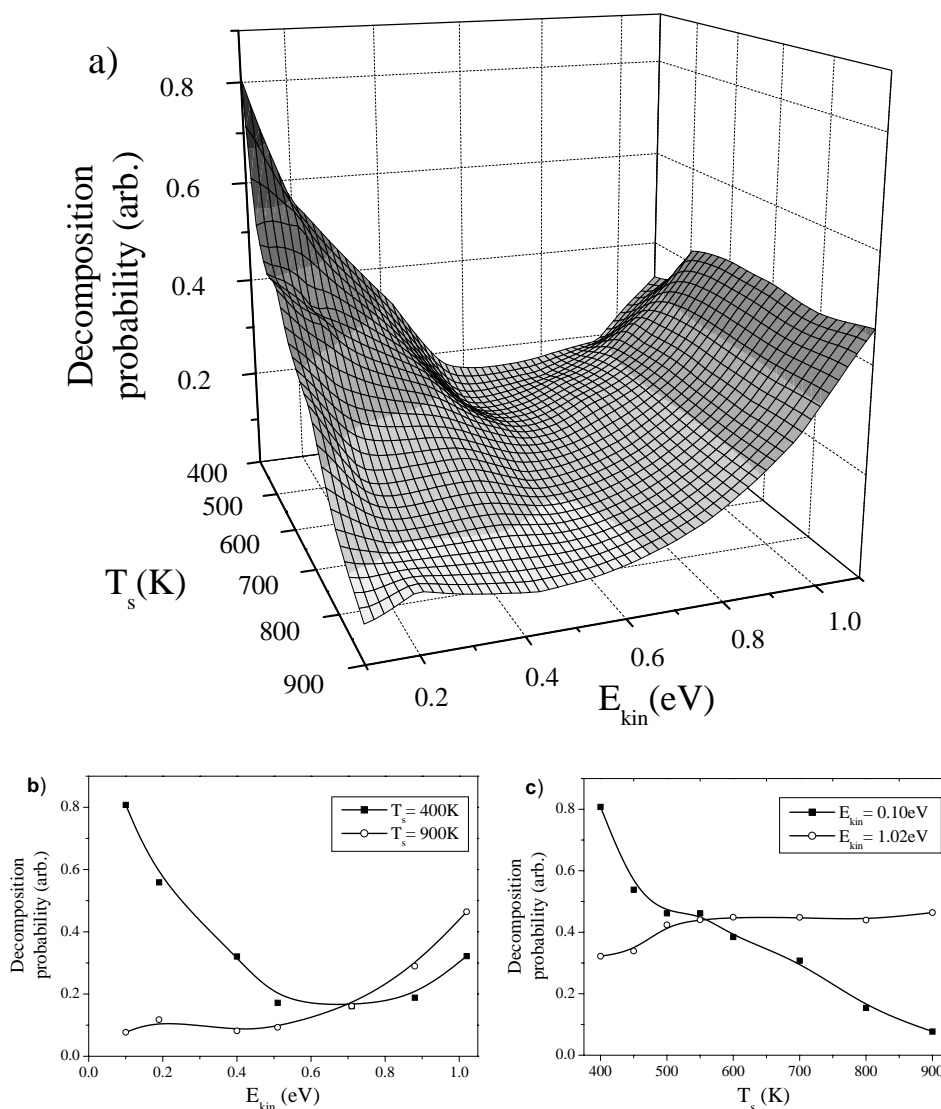
Figure 6. a) Relative methanol decomposition probability (arbitrary units ≈ dissociation probability per collision (%)) as a function of surface temperature (T_s) and incidence beam energy (E_{kin}). **b)** Same data as a function of incidence energy, T_s=400 and 900 K. **c)** Same data as a function of surface temperature, E_{kin}=0.10 and 1.02 eV.

Since molecules dissociating directly upon collision with the surface do not equilibrate to the surface temperature this channel might be expected to be surface temperature independent. While this is generally true above 500 K, a small dependence is observed in the form of a 'step' below 500 K. A possible explanation for this lie in the kinetics of the subsequent decomposition on the surface.

Looking for an isotope effect confirmed that the rate-limiting step is the breaking of the O-H bond. The decomposition probability for deuterated methanol, CH_3OD, was determined by measuring the rate of CO desorption. We found that dissociation through the direct channel, E_{kin}=0.81 eV and T_s=1000 K, was decreased by approximately 20 %, and by 12 % through the indirect channel, E_{kin}=0.075 eV and T_s=550 K.

3.3.2 Role of surface treatment

We would like to explain the simultaneous presence of a non-activated, precursor mediated dissociation channel on a surface that also presents a high barrier to the direct dissociation of molecules approaching from the gas phase. Common arguments for such coexistence invoke a highly restricted phase space at the low energy barrier, but it is difficult to reconcile the simultaneous existence of both a low and high barrier at the same site on the surface.

We have found that we were able to modify the activity of the surface to methanol dissociation substantially for the precursor channel by exposing the surface to O_2 followed by a flash to high temperatures. A surface treatment similar to this was commonly employed by us to ensure that all surface carbon contaminant was removed. This treatment consists of exposure to ca. 50 L of oxygen at room temperature followed by five brief flashes to 1150 K in UHV. Figure 7 shows a series of measurements made on a clean surface, and the same surface following oxygen/flash treatments. Such a treatment significantly reduces the methanol decomposition probability at low surface temperatures, where the precursor channel is dominant, while at high surface temperatures, where the direct channel is dominant, the decomposition is unaffected.
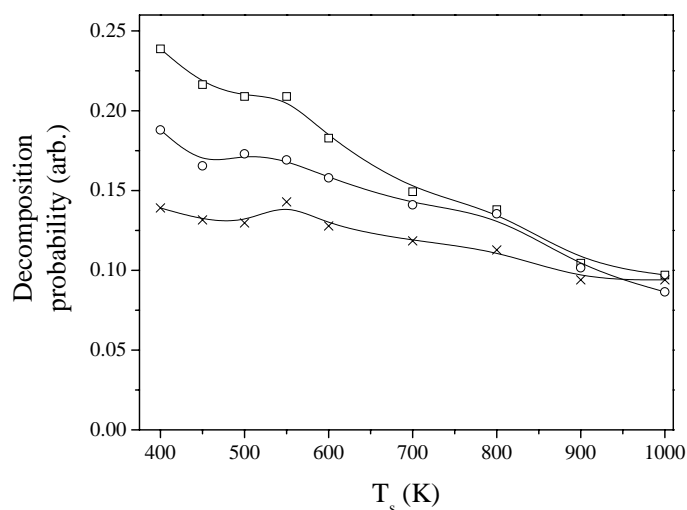
Figure 7. Methanol decomposition probability as a function of the surface temperature on a clean surface (squares) and following one (circles) and two (crosses) oxidation/ flash treatments. E_{kin}=0.45 eV.

This is confirmed in Figure 8 where the same experiment has been performed as a function of the incidence methanol energy at two surface temperatures. At low energies and low surface temperatures the indirect channel is strongly suppressed by the oxygen treatment, while at high surface temperatures, where the direct pathway is dominant, the decomposition probability is unaffected. A second such oxygen/ flash treatment quenches the precursor channel even more, but additional oxygen/ flash treatments have no further effect on activity. After the oxygen/ flash cycles have

quenched the activity of the precursor channel, extended periods of annealing (20 min. at 1150 K) did restore the original activity of the surface to the precursor channel.
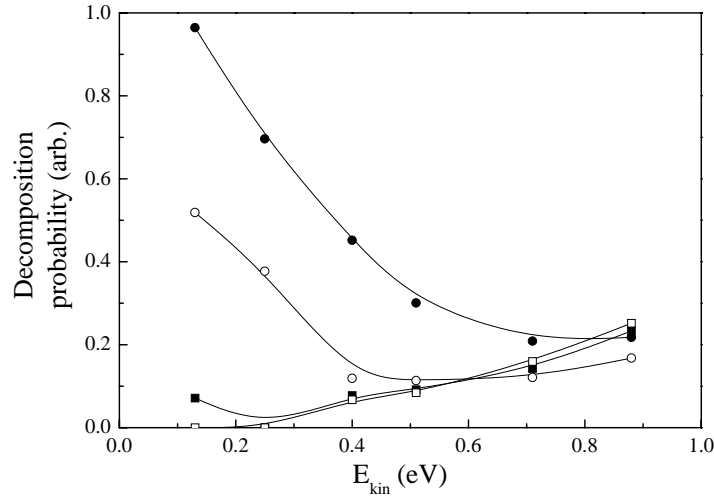
Figure 8. Methanol decomposition probability as a function of incidence energy on a clean surface (solid points) and following one oxidation/ flash treatment. T_s=400 K (circles) and 1000 K (squares).

Oxygen desorbs from Pt(111) at a temperature of 750 K [33,45], and should be completely removed in a single flash to 1150 K. This was confirmed to levels below 1 % by the absence of an oxygen AES peak. Such oxygen/ flash cycles are generally accepted procedures for cleaning residual carbon from the Pt(111) surface, and have been proven quite effective for this purpose on our sample as well. No changes (other than the removal of residual surface carbon) were detectable by Auger spectroscopy in the chemical structure of the surface by the oxygen/ flash treatment. For most species, the sensitivity limits mean that all such chemical changes are typically less than 1 % of a monolayer. In addition, there was no change in the CO thermal desorption peak shape. This TPD peak shape shows a small shoulder to the high temperature side characteristic of ca. 2.5 % defects (believed to be steps due to a slight miscut of the crystal). This also suggests that there was no detectable change in the overall defect density due to the oxygen/ flash cycles. In order to further characterize whether such an oxidation/ flash procedure had any measurable changes in the defect density, specular He atom scattering was employed since the intensity of this is well known to be extremely sensitive to defects/ residual impurities. No changes were observed following the oxidation/ flash treatment in the specular scattering of a 63 meV supersonic nozzle He atom beam detected with a rotatable QMS with 1.5° angular aperture. Again, this infers that there was no substantial change in the dominant defect density (presumably steps) nor in their spatial distribution following the oxidation/ flash.

Even though the oxygen/flash treatment had a strong effect on the precursor channel, we were unable to detect any differences of the surface. This leads us to conclude that the density of sites affected by the oxygen/flash treatment, and responsible for the indirect dissociation, is an extremely small minority site on the surface, certainly less than 1 % of all sites. The most obvious candidate for such a reactive, low density site is some type of surface defect, consistent with the findings of ref. [38]. This leads us to

speculate that oxygen may selectively block these sites, as suggested below, without any measurable effect on the direct dissociation channel. It is likely that the flat (111) terraces remain unaffected by the oxygen/anneal treatment, and it is thus suggested that the direct dissociation occur on the (111) terraces.

We can only speculate as to the identity of the minority defect site responsible for the precursor channel since it is not directly observed. It is unlikely to be the dominant defect sites, e. g. steps, since there were no observable changes via oxidation/ flash in the CO TPD or specular He scattering. Other possibilities are kink sites, minority chemical defects, etc. We note, however, that while a single flash to 1150 K was insufficient to regenerate the activity of the indirect channel, extended periods of annealing did restore the surface to its original activity. The poisoning of the surface activity by oxidation and slow regeneration of this activity is quite reminiscent of the formation and decomposition of silicon oxides on the Pt(111) surfaces. While silicon is thermodynamically unstable at the surface under vacuum, in the presence of surface oxygen it is suggested to form stable Pt-Si-O oxides [46]. These were seen to form rapidly and slowly decompose above 1100 K in vacuum [47]. Although we were unable to observe these oxides by Auger electron spectroscopy, this simply implies that any such oxides were present at coverages below 1 % of a monolayer, and confirms the low Si bulk content of our crystal. One possible scenario for the poisoning of the precursor dissociation via oxidation and subsequent reactivation by extended anneal is that the oxidation causes Pt-Si-O oxides to form or diffuse to these specific active defect sites, thereby decorating them, while the extended anneal dissociates these oxides and reforms the active defect site.

We also consider the contrary hypothesis, i.e. that the extended annealing causes bulk defects/ impurities to diffuse to the surface, while the oxygen/ flash treatment removes these defects/ impurities. However, within the limits of Auger sensitivity, the extended anneal caused no chemical impurities to build up on the surface. Nor did the CO TPD or specular He scattering show any increase in defect concentration with the extended anneal. We therefore consider this possibility less likely.

3.3.3 Surface kinetics

It is impossible from this study to model fully the decomposition kinetics on the surface following the initial O-H bond dissociation. However, the parameters obtained for the dissociation step can be used to provide information on the kinetics of the reverse process, methoxy plus hydrogen associative desorption, the final step in the methanol synthesis reaction (on single crystal surfaces).
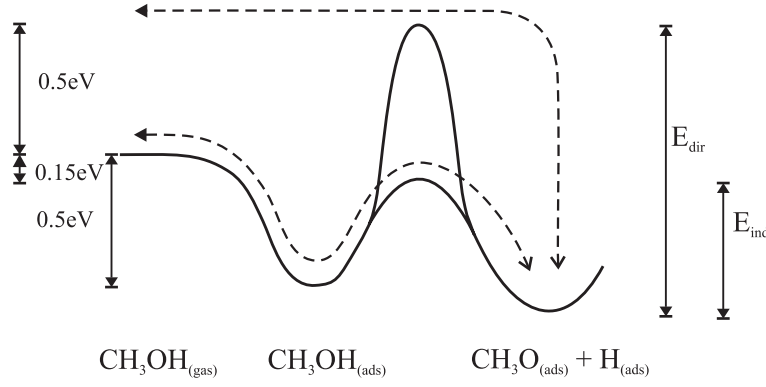
Figure 9. Schematic potential energy diagram for methanol dissociation (associative desorption) on Pt(111). Energy levels are based on results presented here and estimates taken from previous studies.

By microscopic reversibility, the same direct and precursor mediated channels can operate for desorption as in adsorption (Figure 9). Under conditions of thermal equilibrium, the branching ratio of recombination through the direct and indirect channels is then given by eq. (3.1). If we assume that the rate limiting step for desorption through the indirect channel is the recombination of methoxy and hydrogen on the surface, eq. (3.1) will also express the branching ratio of desorption through the two channels.

$$R_{dir/ind} = \frac{\nu_{dir}.exp(-E_{dir}/k_BT_s)}{\nu_{ind}.exp(-E_{ind}/k_BT_s)} \tag{3.1}$$

where E and ν are the activation barriers and the prefactors for recombination through the direct (dir) and indirect (ind) channels (see Figure 9) If we take the simplest approximation, that the prefactor through the indirect channel is the same as the direct channel modified by the relative defect density, $\nu_{ind} = \nu_{dir}.\rho_{def}$, then this simplifies to eq. (3.2),

$$R_{dir/ind} = \frac{exp(-(E_{dir}-E_{ind})/k_BT_s)}{\rho_{def}} \tag{3.2}$$

Assuming detailed balance, i. e. that the desorption experiment averages over the same phase space as the molecular beam sticking experiment, then the difference in barriers is obtained directly from our molecular beam studies. While this assumption is in no way guaranteed, there are only a few documented exceptions where detailed balance is not a "good" approximation [48]. The threshold to the direct channel shows that E_{dir} lies ~0.5 eV above the zero point energy of the gas phase molecule. A fit of standard precursor kinetics to the temperature dependence of the low energy, indirect channel data shows that E_{ind} lies 0.15 eV *below* the zero point energy of the gas phase molecule, hence $E_{dir}-E_{ind} = 0.65$ eV (Figure 9). $R_{dir/ind}$ then varies from $1x10^{-9}$ on a cool surface (300 K) with a relatively high defect concentration (1 %), to 0.8 on a surface with very few defects (0.01 %) at 800 K. Indeed, under most conditions $R_{dir/ind}$ will be significantly less than 1, indicating that the precursor mediated channel will dominate the desorption process. Thus, the low energy pathway not surprisingly is anticipated to dominate desorption kinetics for most realistic surfaces.

Note that several small temperature dependent features are seen in the results, for instance at 550 K in Figure 7. While the relative strength of these features varied somewhat depending on exact surface treatment, they were always present as shown in Figure 7, and were very reproducible for a given surface treatment. Although these features were principally observed for the precursor mediated dissociation channels, we suspect they reflect some competition in the subsequent decomposition kinetics.

3.4 Conclusion

This molecular beam study of methanol decomposition on Pt(111) has shown two different pathways to dissociation of the molecule on the surface. A non-activated channel that goes via a molecular precursor and an activated channel, where the molecule dissociates directly upon impact over a barrier of ~0.5 eV. We found that the precursor channel was strongly affected by the preparation of the surface, where oxygen/flash treatments decreased the decomposition probability. We suggest that the effect of the oxygen/flash treatment is due to the formation of a Pt-Si-O compound at minority defect sites where the precursor channel occurs, and thereby hinders the decomposition. The direct channel was unaffected by this, and is therefore suggested to occur on the (111) terraces.

4 Dynamic displacement of N_2 from Ru(0001) by incident D and H atoms

4.1 Introduction

The catalytic synthesis of ammonia on a Ru surface is believed to occur via a reaction mechanism where N_2 and H_2 dissociates on the surface followed by hydrogenation of N finally producing NH_3, which then desorbs back into the gas phase. The rate-limiting step is believed to be the dissociative chemisorption of N_2 [49].

Experiments in 1998 by Dahl *et al* showed that the overall activation energy for the catalytic synthesis of ammonia was ~101 kJ/mole on a Ru(0001) surface [50]. This sets an upper limit to the activation energy for N_2 dissociation, since additional energy is needed under synthesis conditions to create free sites [50]. Initial DFT calculations by Mortensen *et al.* showed that the barrier for N_2 dissociation on Ru(0001) is 131 kJ/mole eV, with the newest DFT calculations showing an even higher barrier of 190 kJ/mole (2 eV) [4,26,31]. This is much too high to agree with the experiment by Dahl *et al*. The discrepancy has recently been explained by the effect of defects. It was shown, both experimentally and theoretically, that the (natural) presence of defects strongly influenced the dissociation rate of N_2 explained by a much lower barrier at defects than at terrace sites [26].

Before this knowledge was available, Nørskov proposed an alternative mechanism for catalytic ammonia production as an answer to this discrepancy based on the biological process in nature of initially adding an atomic H to molecular N_2. An enzyme (nitrogenase) catalyzes the biological ammonia synthesis. The active part of the enzyme where nitrogen bonds and reacts is believed to be a metal-sulfide-cluster ($MoFe_6S_9$) (see refs. in [51]). DFT calculations have shown that the ammonia synthesis on $MoFe_6S_9$ occurs by adding H-atoms, one by one, to an intact N_2 molecule. After the fifth H is attached, the N_2 molecule breaks apart [51]. A somewhat similar mechanism was suggested for ammonia synthesis on a Ru surface, where the high-pressure reaction of $H_2/N_2/Ru$ could lead to formation of ammonia by initially dissociating H_2 and adding H to molecular N_2 [52,53]. Recent DFT calculations showed that this actually is a rather low-energy pathway with an overall activation energy of 90 kJ/mole [54], compared to the 101 kJ/mole for the mechanism believed to occur via initial N_2 dissociation on the Ru surface [50].

Inspired by these suggestions and findings we believed that exposing N_2 molecules adsorbed on a Ru(0001) surface to an H-atom beam could test this hypothesis. A somewhat similar reaction between an adsorbed molecule and atoms from the gas phase has been observed for hydrogenation of the isoelectronic CO. It was found that H-atoms reacted directly with CO adsorbed on Ru(0001) to form formyl (HCO) and formaldehyde (HCHO) [55]. The reaction was found to occur via an Eley-Rideal mechanism, where the incident H atom is not adsorbed and equilibrated at the surface before reaction with CO.

We performed experiments exposing a N_2 covered Ru(0001) surface at $T_s\sim90$ K to H atoms, produced in a microwave discharge, while looking for produced ammonia during H-dosing. Using a mass spectrometer it was found that no ammonia was desorbed into the gas phase during H-dosing. A TPD experiment following the dosing also showed no ammonia desorbing. In addition, we looked for a product of eventual ammonia decomposition, i.e. atomic nitrogen. Desorption of molecular nitrogen is completed at 140 K, whereas associative desorption of N_2 (at coverages below 0.25 ML) occurs at ~800 K. The associative desorption feature was not observed, showing that no atomic nitrogen was present on the surface.

In conclusion, no ammonia is formed when exposing a N_2 covered Ru(0001) surface to a thermal beam of H-atoms. Instead of this reaction it was found that N_2 molecules desorbed readily upon H-adsorption. The cross section for H displacing N_2 was found to be very high and in short time the surface would be emptied of N_2. However, from these experiments it can not be ruled out that the mechanism for ammonia formation can proceed via attachment of H-atoms to the N_2 molecule. The cross section for attachment of an H-atom may just be negligible and below our detection limit, especially with the strongly competing displacement reaction, which is removing one of the reactants. This displacement will be discussed in the following.

4.2 Adsorption-induced desorption

There are several mechanisms for desorption induced by incident species. One is the so-called collision-induced desorption (CID), where the incoming species transfers enough energy to an adsorbate in a direct collision to overcome the binding to the surface. The process is illustrated in Figure 10a. Some examples are CID of O_2 from Pt(111) by incident high energy ($E_{trans}>1.1$ eV) Xe [56,57] and CID of N_2 from Ru(0001) by incident high energy Ar or Kr ($E_{trans}>0.5$ eV) [58]. Also another mechanism has been identified, where the incoming species chemisorbs and part of the adsorption energy is transferred to an adsorbate, which then desorbs. This process is called dynamic displacement and is pictured in Figure 10b. Rettner and Lee found that exposure of a O_2-covered Pt(111) surface to atomic O, N or H leads to prompt desorption of the O_2, which leaves the surface in a bimodal velocity distribution [59]. Thus, not only is the bond to the surface broken but some of the O_2 molecules gain further energy. The translational energy of the incident atom beam was ~thermal (0.05 eV) and it was argued that even further acceleration in the atom/surface potential well could not lead to CID due to the large mass difference (H vs. O_2) and thereby low mechanical energy transfer in a direct collision. This was further confirmed by the work of Wheeler, Seets and Mullins, who found that the displacement probability was independent of the incident O-atom translational energy, although only a rather narrow range from 0.2-0.45 eV was studied [60]. In another study Rettner and Auerbach found that CO displaced from Cu(111) by incident H atoms, leave the surface vibrationally and rotationally hot, relative to the surface temperature [61]. For both $H/O_2/Pt(111)$ and $H/CO/Cu(111)$ it was believed that the desorption was induced by changes in the local electronic structure of the surface associated with adsorption of the incident atom.
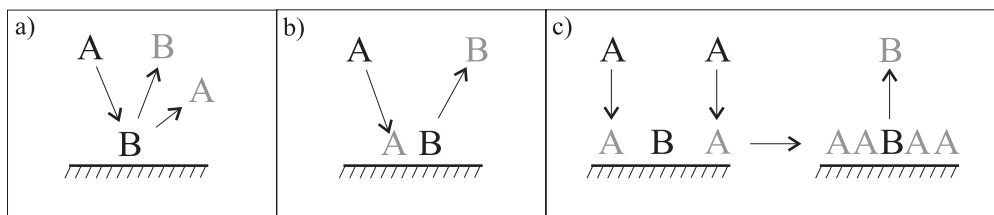
Figure 10. Three mechanisms for adsorption-induced desorption: **a)** Collision-induced desorption, **b)** Dynamic displacement, **c)** Thermodynamic displacement. A is the incident particle and B is the pre-adsorbed species. Black letters refer to before and gray letters refer to after "reaction".

A third mechanism for desorption induced by an adsorbate is what we could call thermodynamic displacement. This adsorption driven displacement can occur when the new adsorbate has a higher binding energy, where lateral interactions between adsorbates lead to desorption of the weakest bound as shown in Figure 10c. It is thus energetically more favorable to have the stronger bound adsorbate on the surface and let the less stable adsorbate desorb into the gas phase. Some examples: Kimmel, Stevenson and Kay showed that physisorbed N_2 is displaced from Pt(111) upon adsorption of CH_4, Kr or H_2O, which all have larger binding energies to Pt(111) than N_2 [62]. Mortensen and Åkerlund showed that Xe was displaced from Pt(111) upon adsorption of the stronger bound CO [63]. All these experiments showed that for an initially partially covered surface desorption did not occur instantaneously upon adsorption, but some time after the dosing was started. It was necessary to build up sufficient coverage of the new adsorbate before desorption of the original adsorbate was initiated. This delay is dependent on the initial coverage.

4.3 Thermodynamic displacement of Xe from Pt(111) by CO

The CO/Xe/Pt(111) will be summarized briefly here. Xe is adsorbed on a Pt(111) surface (0.17 ML, i.e. half of saturation coverage) at T_s=90 K followed by exposure to a supersonic molecular beam of CO with translational energy of 0.44 eV. Figure 11 shows the CO and Xe mass spectrometer signals measured in the background. Initially (at time t_0) CO is hitting an inert quartzflag. Removing the flag (at t_1) exposes the Xe-covered Pt(111) surface to the CO beam. The initial sticking probability of CO is S_0=0.43, as seen from the decrease in CO partial pressure [43]. CO dosing continues for 18 s before Xe desorption sets in (at t_2).
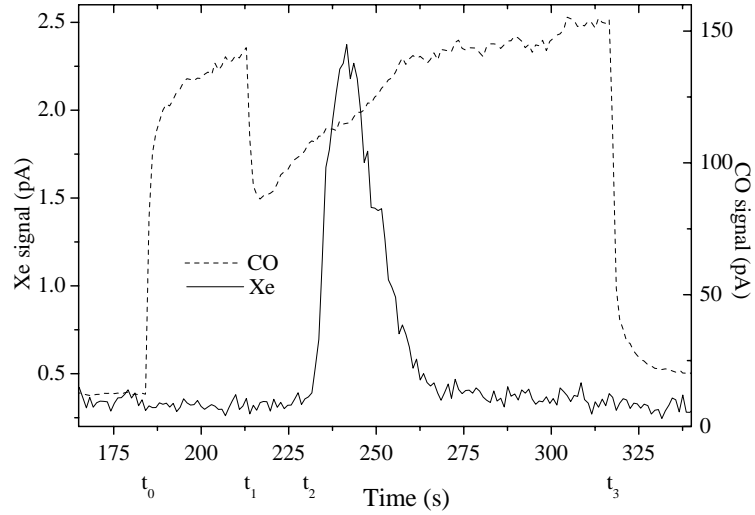
Figure 11. CO and Xe mass spectrometer signals as a function of time. At time t_0 the CO beam hits an inert quartzflag, at t_1 the flag s removed and the CO beam strikes the surface, at t_2 Xe desorption sets in and at t_3 the CO beam is shut off. (Figure from ref. [63])

The above experiment has been repeated for different initial Xe coverages showing that the delay (t_2-t_1) depends on the initial Xe-coverage. In Figure 12 is plotted the CO coverage, at the time where Xe desorption sets in, as a function of initial Xe coverage. The CO coverage was determined by integrating the CO sticking trace, and the Xe coverage was determined by the integrated TPD signal for an equivalent Xe dose. It is seen that the more Xe adsorbed, the more CO is needed to initiate Xe desorption. It is thus necessary to build up a sufficient total coverage of CO and Xe before the weaker bound Xe is pushed off.
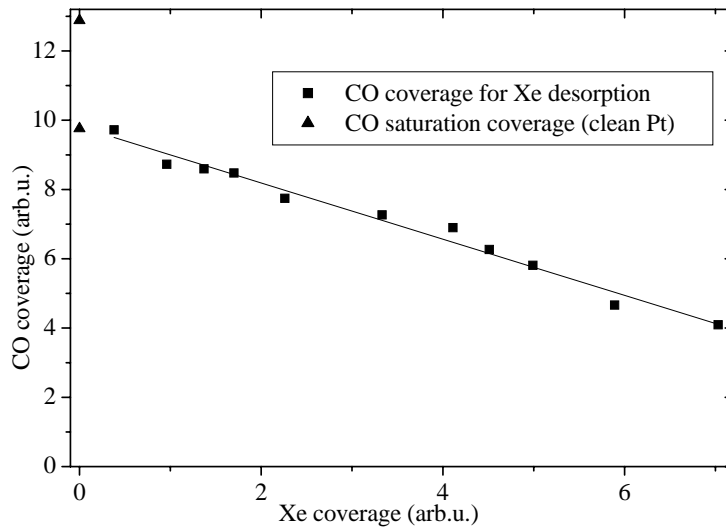
Figure 12. CO coverage when Xe desorption sets in as a function the initial Xe coverage before CO exposure starts. (Figure from ref. [63])

32

4.4 N$_2$ displacement: Results and discussion

A Ru(0001) surface was cooled via liquid nitrogen (LN$_2$) and dosed with molecular N$_2$ from the background. A physisorbed N$_2$ state exists at T_s=40 K [64]. At higher temperatures N$_2$ chemisorbs on Ru(0001). Adsorption at T_s=95 K results in a coverage of $\Theta_{N_2} = 0.35$ ML, characterized by a $\left(\sqrt{3} \text{x} \sqrt{3}\right) - R30°$ LEED pattern and a single peak in TPD at 115 K [65,66]. The desorption energy was estimated to 0.44 eV, in agreement with DFT calculations [32]. Adsorption at T_s=75 K produces an additional chemisorbed state with lower binding energy. The total coverage increases to 0.58 ML and in TPD this shows up as an additional peak at 90 K [65,66].

We did not measure the temperature directly, since the connected type C thermocouple used is rather insensitive at these low temperatures. We observed only one peak in the TPD spectrum, indicating that T_s is approximately 90 K. The presence of adsorbed nitrogen was confirmed by a clear AES signal. In the experimental setup discussed in chapter 3, a Pt(111) crystal was mounted identically on the same sample manipulator. Here a type K thermocouple was used, sensitive at LN$_2$ temperatures and it was found that the lowest T_s was 90 K. We therefore believe that the same minimum T_s is achieved for both samples.

The saturation coverage of N$_2$ achieved by us at this T_s was determined to be 0.25 ML by comparing TPD areas of N$_2$ and CO. This agreed with the coverage estimated by AES measuring peak to peak ratios of the differentiated signal of N and Ru, normalized to a known atomic N-coverage (see chapter 6). This does not fully agree with the expected coverage of ~0.35 ML at this T_s as discussed above, but may be due to the uncertainty in determining T_s. The surface temperature must therefore be slightly higher than 95 K.

The D atom beam was generated in a microwave discharge. Through double differential pumping and the use of skimmers, the beam entering the chamber was well collimated to just expose the Ru(0001) sample at an angle of incidence of 7° relative to the surface normal. The beam striking the surface was >50 % dissociated with an atom flux variable between 0.013-0.12 ML/s (1 ML/s = 1.58·10^{15} cm^{-2}s^{-1}).

The Ru(0001) surface was saturated with molecular nitrogen and a D-atom beam, with a flux of 0.013 ML/s, was pointed at the surface. Below is shown the mass 4 and mass 28 signal measured in the background with a QMS. The Deuterium beam is only partly dissociated and we therefore see a mass 4 signal. Since the reactive D atoms stick to the stainless steel walls of the UHV chamber the QMS signal from the atoms in the background is very low and the molecular signal was monitored instead. The D-atom beam strikes the surface as soon as it enters the chamber. As seen in Figure 13 N$_2$ desorbs promptly or at least within the time-constant of the vacuum system. No delay is observed as for CO/Xe/Pt(111). If the microwave discharge is turned off (no atoms in the beam) no displacement of N$_2$ is observed.
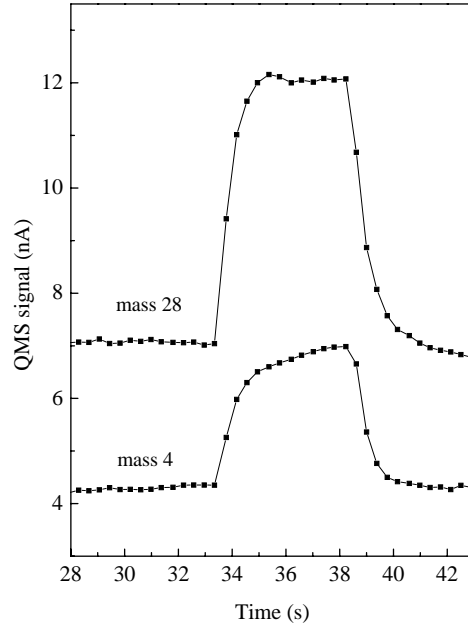
Figure 13. QMS signals as a function of time, showing that N_2 is displaced promptly by incident D atoms. D-flux: F=0.013 ML/s, $\Theta_0(N_2)\sim0.25$

The displacement rate increases with N_2 coverage. A measure of the initial displacement rate is the initial pressure-jump when the D-beam strikes the surface. In Figure 14 the initial "pressure-jump" has been plotted as a function of $\Theta_0(N_2)$, and demonstrates the linear increase with $\Theta_0(N_2)$. The D atom flux was here increased to 0.12 ML/s.
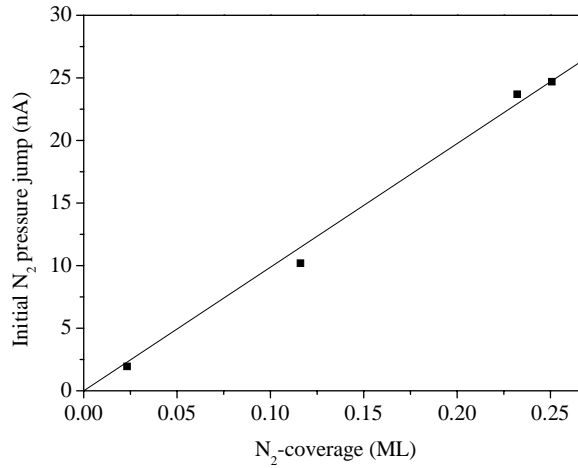
Figure 14. Initial mass 28 (N_2) "pressure-jump" as a function of initial N_2-coverage, $\Theta_0(N_2)$. D-flux: F=0.12 ML/s.

In Figure 15 is shown the mass 28 signal, i.e. the displaced N_2, over a long period for three initial coverages of N_2 and a D atom flux of 0.12 ML/s. It is seen that the partial pressure (N_2 signal) jumps to a maximum value (almost) immediately and then decays monotonically until no more N_2 is on the surface. No delay between onset of D adsorption and N_2 desorption is observed as it was for CO/Xe/Pt(111). Since N_2

34

desorption occurs immediately upon D adsorption, also at N_2 coverages far below saturation, we can here conclude that the mechanism for displacement is not thermodynamic as for Xe displaced from Pt(111) by CO. The mechanism will be discussed in more detail later.
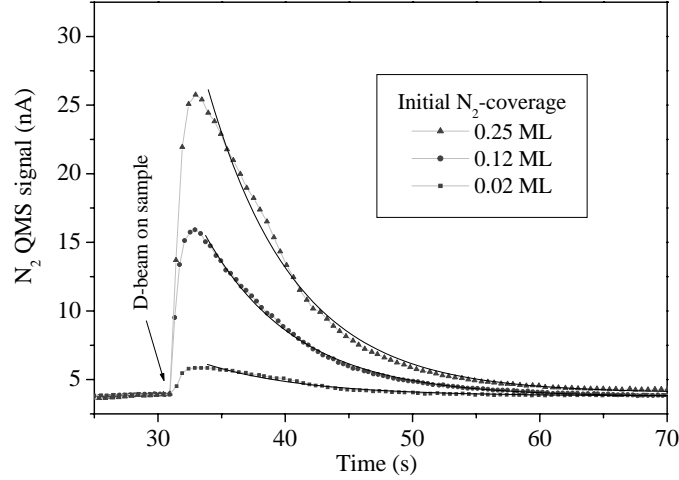
Figure 15. N_2 (mass 28) QMS signal over a long time during D-dosing. D-flux: F=0.12 ML/s. Initial N_2-coverage was $\Theta_0(N_2)$ 0.25, 0.12 and 0.02 respectively. The fit of the exponential decay is shown as solid black lines.

The decay of the N_2-desorption rate is fitted to a simple exponential function $\Theta(t) = \Theta_0 \, exp(-t/\tau)$, where Θ_0 is the initial N_2-coverage. The desorption rate is thus given by: $-\dfrac{d\Theta(t)}{dt} = \sigma F \cdot \Theta(t)$, where σ is the cross section for an incident D-atom displacing a N_2 molecule and F is the atom flux and $\dfrac{1}{\tau} = \sigma F$. The fit of the decay is shown in Figure 15.

Since the desorption rate is described by a simple exponential decay, the desorption rate is independent of D coverage on the surface which increases with time. Otherwise we would have to add a term proportional to $\Theta_D(t)$ to the rate. The same time-constant (τ=7.1 s) described the decay of all three curves. We can thus estimate the cross section from $\dfrac{1}{\tau} = \sigma F$ and find that σ=7.6·10^{-16} cm^2 for displacing a N_2 by an incident D.

An absolute value for the probability p of an incident D atom displacing a N_2 molecule has been estimated by the following equation: $p = \dfrac{N \cdot \sigma}{A}$, where N is the number of N_2 molecules adsorbed and A the area of the Ru(0001) surface. In terms of coverage Θ, this can be written as $p = \Theta \cdot n_0 \cdot \sigma$, where n_0 is the surface atom density (n_0 =1.58 10^{15} cm^{-2}). At saturation coverage Θ=0.25 ML we find p=0.3.

The probability p has also been estimated in a different way by measuring the number of N_2 molecules desorbed and the number of D atoms adsorbed in a 5 sec atom dose at

low flux (0.013 ML/s). The numbers were measured by integrated TPD signals, i.e. areas "A". For N_2, a TPD spectrum was taken after exposing the surface to D atoms and comparing to a TPD measurement of the saturated surface, $\Theta_{sat}(N_2)=0.25$ ML. The number of D atoms adsorbed was measured by the integrated TPD signal relative to the TPD area of a saturation coverage, $\Theta_{sat}(D)=1$ ML [67]. The absolute probability for desorption of one N_2 molecule for one incident D atom is thus given by:

$$p = \left. \frac{\dfrac{A(N_2, \text{sat. dose}) - A(N_2, \text{after D dose})}{A(N_2, \text{sat. dose})} \cdot \Theta_{sat}(N_2)}{} \middle/ \frac{A(D, \text{after dose})}{A(D, \text{sat. dose})} \cdot \Theta_{sat}(D) \right.$$

It was found that $p_D=0.5\pm0.1$. This is quite different from the value of 0.3 estimated from the cross section. It is unclear why, but the methods used are very different.

4.5 N_2 displacement mechanism

What is the mechanism for the observed displacement of N_2 by incident D atoms? First we consider thermodynamic displacement, which is characterized by the lateral interactions leading to desorption of the weaker bound adsorbate, when the total coverage exceeds a certain limit. D is stronger bound than N_2 and could in principle lead to thermodynamic displacement of N_2. It was already discussed that this is unlikely, since even though the initial N_2 coverage was below saturation, no delay between adsorption of D and the onset of N_2 desorption was observed.

When dosing with atoms, the displacement is instantaneous. The D-flux for the displacement results in Figure 13 is only 0.013 ML/s. N_2 reaches its maximum desorption rate within ~1 sec (the time constant of the vacuum system). In 1 sec only 0.013 ML D adsorbs. This is a very small amount and should not lead to desorption of N_2 by simple lateral repulsive interactions between two adsorbates in equilibrium with the surface.

If we instead dose with D_2 molecules, these will dissociate on the surface and could push N_2 off the surface when the D coverage is large enough. But, when only D_2 molecules are in the beam (discharge off), no displacement is observed. This was done at rather low N_2 coverage $\Theta_0(N_2)=0.12$ (half of the N_2 saturation coverage at this T_s), and there should thus be empty sites for D_2 dissociation. A TPD after this dose confirmed the presence of D on the surface ($\Theta_D=0.3$ ML). It should be noted that the D_2 dissociative sticking probability (S) is reduced strongly with adsorbate coverage. We find initially $S=0.16$ on clean Ru(0001), $S=0.05$ on Ru(0001) with 0.12 ML N_2 pre-adsorbed and further decreasing when D is accumulated on the surface. It may simply not be possible to adsorb and dissociate enough deuterium to induce desorption of N_2. But the simple exponential decay of the desorption rate shown in Figure 15, indicated that the accumulated coverage of adsorbed D atoms had no influence on the desorption rate.

For H/O$_2$/Pt(111) [59] and H/CO/Cu(111) [61] it was believed that the desorption was induced by changes in the local electronic structure of the surface associated with adsorption of the incident atom. A similar electronic mechanism could also be the case for D/N$_2$/Ru(0001). Another possibility is that the incident D atom creates a local "thermal hot spot" upon adsorption and desorption is then induced by lattice phonons.

To distinguish between an electronic and a phonon-mediated desorption mechanism we could look for an isotope effect, i.e. using H instead of D atoms. They should experience the same atom/surface potential well and therefore the same forces when approaching the surface. The energy of H and D will therefore be the same, whereas H will gain a higher velocity than D due to the lower mass.

If the displacement mechanism is phonon mediated D atoms should be more effective than H atoms due to the more effective (mechanical) energy transfer in the collision with the surface. Assuming that the target particle is at rest the fraction of kinetic energy transferred from the incident particle can be calculated from the conservation of momentum and kinetic energy in an elastic collision and is given by: $\frac{4\mu}{(1+\mu)^2}$, where μ is the mass ratio between incident and target particle. This is called the Baule formula [44]. It is only an approximate description for a complex atom-surface or atom-adsorbate collision.

On the other hand, if the displacement occurs via an electronic mechanism, it is the velocity of the atoms crossing the Fermi level that is important since a non-adiabatic mechanism must be responsible for the electronic excitation [68,69]. In this case, H atoms should be more effective since they have a higher velocity of approach to the surface than D atoms.

We did indeed observe an isotope effect. If an H-atom instead of D-atom beam was used to induce desorption, it was found that the cross section was considerably smaller. This was investigated carefully. The surface was saturated with N$_2$ for maximum signal, and to ensure reproducible coverages. When using a low flux atom beam (~0.013 ML/s), a plateau-like region, i.e. a well-defined maximum (initial pressure jump, P-jump), is formed before the decay is visible (compare eventually Figure 13 and Figure 15). This initial P-jump normalized to the atom-flux is proportional to the cross section σ for displacement, although only the relative cross section can be determined this way. It was found that $\sigma_D/\sigma_H = 1.8 \pm 0.1$. We did not measure σ_H directly but using the value for $\sigma_D = 7.6 \cdot 10^{-16}$ cm^{-2}, and the ratio above we find that $\sigma_H = 4.2 \cdot 10^{-16}$ cm^{-2}.

The absolute probability for H atoms displacing a N$_2$ molecule (at saturation coverage of 0.25 ML) has been estimated, by measuring the number of H atoms adsorbed and the number of N$_2$ molecules desorbed by TPD. It was found that $p_H = 0.2 \pm 0.1$. Using probabilities for D and H measured by this method we find relatively: $p_D/p_H = 2.5$. This is in reasonable agreement with the above finding, where the initial P-jumps were compared.

A D atom is thus twice as effective as an H atom in displacing a N_2. The observed isotope effect demonstrates that we can rule out an electronic displacement mechanism. A phonon-mediated mechanism seems to be more likely.

The observed isotope effect further speaks against thermodynamic displacement, which should be independent of isotope. Lateral interactions between adsorbed D and N_2 are expected to be the same as lateral interactions between H and N_2.

One possibility is that the N_2 is displaced by direct collision-induced desorption (CID). Romm *et al.* found that the threshold for CID of N_2 from Ru(0001) by incident Ar and Kr is E_{trans}~0.5 eV [58]. In a direct collision, Ar and Kr transfer 97 and 75 % of their kinetic energy to an adsorbed N_2 in the Baule limit [44]. D only transfers 25 % of its kinetic energy. The D atoms are incident at thermal energies, but the attractive interaction in the atom/surface potential well accelerates them. The Ru-D binding energy is 2.8 eV [67]. As an upper limit we assume that a D-atom reaches E_{trans}~2.8 eV before collision with a N_2 molecule, and estimate that 0.70 eV would be transferred to a N_2 molecule. According to Romm *et al.* this is enough to induce CID. For incident H atoms this is different, though. H only transfers 13 % of the kinetic energy; i.e. 0.36 eV is transferred to a N_2 molecule. This is not enough to induce CID, thus speaking against the possibility that only energy transfer in a direct collision between the incident atom and the N_2 molecule is the mechanism leading to desorption.

Furthermore, the cross section for CID of N_2 by Ar/Kr at E_{trans}~0.7 eV was $\sigma_{Ar}=3\cdot10^{-16}$ cm^2 [58]. This is much lower than the cross section $\sigma_D=7.6\cdot10^{-16}$ cm^2 for displacement of N_2 by D. It is also slightly lower than the cross section $\sigma_H=4.2\cdot10^{-16}$ cm^2 for displacement of N_2 by H. This suggests that pure CID is not responsible for the observations reported here. For incident H atoms, it would not even be possible to achieve CID.

4.6 Conclusion

Exposing a N_2 covered Ru(0001) surface to a D or H atom beam leads to prompt desorption of the N_2 molecules. A strong isotope effect was observed, where the cross section for displacement of N_2 by D(H) was determined to be $\sigma_D=7.6\cdot10^{-16}$ cm^2 and $\sigma_H=4.2\cdot10^{-16}$ cm^2, respectively. A D atom is thus twice as effective as an H atom in displacing a N_2. We propose that the mechanism for N_2 displacement is creation of a "thermal hot spot" by the incident atom accelerated in the atom/surface potential well. As well as phonons, there is a possibility that direct energy transfer between D(H) and N_2 leads to excitation of the N_2-Ru bond.

5 Introduction to the energetics of N_2/Ru(0001)

It is well recognized that the activated dissociation of simple gas phase molecules at metal surfaces is often the rate-limiting step in many industrially important catalytic processes. For example, the dissociative chemisorption of N_2 at the catalyst surface is rate-limiting in the Haber-Bosch synthesis of NH_3. As discussed in the introduction, this recognition has stimulated much experimental and theoretical work over the past several decades in the kinetics and dynamics of activated dissociative chemisorption. For example, Arrhenius measurements of dissociation rates at high gas pressure can in principle give the overall activation energy for dissociation, although the activation energy obtained is very sensitive to the presence of defects and steps, especially when barriers are high [26,70]. Similarly, molecular beam techniques have been instrumental in clarifying some dynamical issues in activated dissociative chemisorption, e.g. the role of precursors vs. direct dissociation mechanisms, the role of translational vs. vibrational energy in promoting dissociation over barriers, etc. When dissociation barriers are very high, however, or principally along a vibrational coordinate, molecular beam techniques may be difficult to apply due to limitations in reaching high enough translational energies to achieve significant sticking to surmount the barrier and probe the PES in adsorption.

The dynamics of dissociative chemisorption has also recently been inferred by laser state-resolved measurements of the time-reversed process of associative desorption and by then invoking detailed balance [20,31,71]. This approach appears to provide a more detailed dynamic picture than molecular beam experiments when applicable.

Most UHV surface science studies of dissociative chemisorption on metal surfaces, i.e. molecular beam studies, generally study the dissociative chemisorption on the bare metal surface in the limit of zero surface coverage. However, for industrially relevant conditions, the coverage of dissociated species is often quite high. While it is well recognized that a high coverage of the dissociated species can reduce the number of available dissociation sites, it is not always realized that the presence of dissociated species on the surface can also strongly affect the height of the dissociation barrier at available sites. We will show here that barriers between gas phase N_2 molecules and the dissociated fragments on a Ru(0001) surface can increase substantially with surface coverage due to what we believe are coverage dependent changes in the electron structure at the available sites.

We believe that the increase in overall N_2 dissociation barrier height with Θ_N observed here are very likely quite general phenomena since the origin is in general changes in electronic structure induced by surface adsorption. Consequently, we anticipate that these coverage dependent energy changes may be an important aspect of the so-called "pressure gap" in catalysis in some cases. For example, in NH_3 synthesis over reduced Fe catalysts, the coverage of adsorbed N is quite high and does play a significant role in limiting the rate of this process. On the other hand, for NH_3 synthesis over supported Ru, the high coverage of N studied here is not maintained, in fact this is one reason for its higher activity.

Before going into details about the $N_2/Ru(0001)$ system, a few general remarks will be made about how to determine the energetics of an activated system. Below is shown a simplified one-dimensional potential energy diagram to define the energetic terms for N_2/Ru.
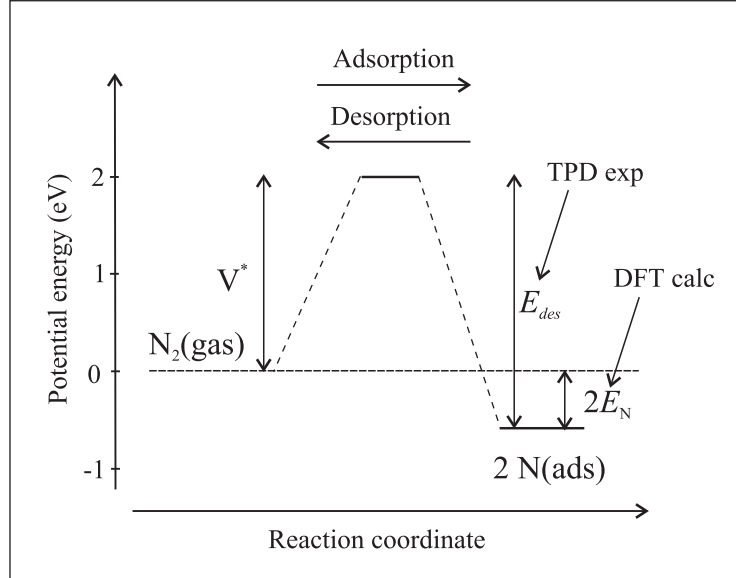
Figure 16. One-dimensional potential energy diagram visualizing the energetics of associative desorption and dissociative adsorption. V^* is the dissociation barrier, E_{des} the activation energy to desorption and E_N the adsorption energy per N-atom. All energies are relative to the N_2 + Ru(0001) asymptote.

Temperature programmed desorption (TPD) is an often used experimental method to determine the activation energy to desorption (E_{des}). One can write the desorption rate in the following Arrhenius expression:

$$R(t) = -\frac{d\Theta(t)}{dt} = \Theta(t)^n \cdot \nu \cdot exp[-E_{des}/k_B T_s(t)] \tag{5.1}$$

Where Θ is the coverage, ν the pre-exponential, T_s the surface temperature and n the order of the reaction. For N_2 associative desorption $n=2$. Now the temperature is varied linearly with time and the partial pressure rise in the UHV chamber, which will be proportional to the rate R if the pumping speed of the vacuum system is sufficiently large, is monitored with a mass spectrometer. The heating rate is normally between 2-20 K/s. The exponential term of R increases with temperature, whereas the coverage term decreases, when molecules desorb. At a certain temperature the rate reaches its maximum i.e. $dR/dT_s=0$. Solving this equation allows us to estimate the desorption energy, E_{des} when knowing the initial coverage, the pre-exponential, the heating rate and the temperature where the desorption rate peaks. This procedure is called Redhead analysis [72].

For N_2 dissociative chemisorption, adsorption energies E_N have been calculated for N adsorption on Ru(0001) for a range of coverages up to one mono-layer (ML). If we

now measure the desorption energies in a TPD experiment, we can estimate the adsorption barrier in a fairly simple manner by combining these two energies. This is easily verified by looking at Figure 16, where the relevant energies have been visualized. As already pointed out, determination of the barrier is very important when we want to understand the dissociation of molecules on metal surfaces. N_2 dissociation on Ru(0001) has attracted much attention, and as discussed in section 1.3, many studies have been performed.

The arrangement of the remaining part of this thesis will be as follows. First, a discussion of the observation of stable and metastable states of N adsorbed on Ru(0001), how we prepared the N/Ru overlayers and a characterization of these. Whereas the lower coverages have been observed earlier, the higher coverages reported here are entirely new. This will include an overall introduction to prior existing studies on the N/Ru system. A comparison of nitrogen adsorption on Ru(0001) with oxygen adsorption on Ru(0001) is also stressed. As outlined above the barrier can be determined from measured desorption energies and calculated adsorption energies. It will be shown that the barrier for N_2 dissociation on Ru(0001) increases strongly with N-coverage.

After that, an experimental study of the dynamics of the associative desorption of N_2 from Ru(0001) will be presented. First the experimental technique will be presented in general. We have used laser assisted associative desorption (LAAD) to directly measure the barrier as a function of N-coverage and also to gain further information about the dynamics. It will be shown that the associative desorbing N_2 are highly vibrationally excited and that the barrier increases strongly with N-coverage. These results triggered the interest of a theoretician, Bjørk Hammer, to actually calculate the barrier for different N-coverages. As will become clear, there is an excellent agreement between the experimental results and the theory.

Finally follows an application of LAAD to another system: Associative desorption of CO from Ru(0001).

6 Observation of metastable atomic nitrogen adsorbed on Ru(0001)

6.1 Introduction

There has been considerable interest in recent years in the interaction of both N_2 and O_2 with ruthenium surfaces. One motivation for this interest is the importance of these systems to catalysis; O_2/ Ru for oxidation and N_2/ Ru for the catalytic synthesis of ammonia. In the latter, ruthenium makes a more active (but more expensive) catalyst for NH_3 synthesis from N_2 and H_2 than the conventional reduced iron catalyst [49]. Although catalysts are in no sense well defined surfaces, there has been a long history of trying to build understanding based on chemistry at single crystal surfaces, and for Ru, the close packed Ru(0001) surface has been particularly well studied.

In some ways, the interaction of O_2 and N_2 with Ru(0001) are similar. Both break a strong diatomic bond and form strong adsorbate-Ru bonds in the process of dissociative chemisorption. Both N and O atoms adsorbed on Ru(0001) are strongly bound in hcp 3-fold sites [73-76], albeit with somewhat different long-range structures at low coverage. Density functional theory (DFT) calculations show that the binding energies for both N and O on Ru(0001) decrease rather strongly with adsorbate coverage [32,73,75,77], indicating strong indirect adsorbate- adsorbate repulsive interactions. Because both O and N adsorbates interact strongly with the localized d-bands of the Ru, this decrease in binding energy at higher coverages has been interpreted as due to the need to "share" the limited Ru d-band electrons at higher coverage [32].

There are of course significant differences between the interaction of the two species with Ru(0001) as well. Since the N-N bond is roughly 4.6 eV stronger than the O-O bond, the energetics and dynamics of dissociative chemisorption are considerably different between the two systems. Dissociation of O_2 on Ru(0001) is much more exothermic than dissociation of N_2 on the surface. Also, the initial (zero coverage) dissociative chemisorption of O_2 is unactivated and proceeds through a molecular precursor mechanism [78], while the dissociative chemisorption of N_2 is strongly activated. Most theoretical estimates and measurements suggest that this barrier is ca. 1.4 – 2 eV at low N coverages [26,27,32]. In addition, the N-N indirect repulsive interaction between adsorbed atoms [32,75] is stronger than that for O-O adsorbed atoms [73,77], presumably because N has three valence electrons/atom interacting with the limited number of Ru d-band electrons instead of two valence electrons/atom for O.

The energetics and geometrical structure for a whole series of states with different O coverage (Θ_O) adsorbed on Ru(0001), up to $\Theta_O = 1$, have recently been characterized [74,77,79,80]. All are thermodynamically stable, although there is a "kinetic barrier" for forming the higher coverage states. While several lower coverage states for N adsorbed on Ru(0001) are now known, there has been uncertainty as to the existence of higher coverage states and the maximum N coverage achievable. Because of the very high barrier to N_2 dissociation, it is impossible to build up a high coverage of

adsorbed N by direct dissociation of N_2 without major contamination. With a thermal dissociation probability as low as 10^{-12} at room temperature, unreasonably long exposures and high pressures are required for background dosing. "Filament assisted" dissociation of N_2, which enhances the dissociative sticking by a factor of 10^6, or decomposition of ammonia, followed by an anneal to a surface temperature $T_s = 615$ K has been used to prepare the p(2 x 2) -N, $\Theta_N = 0.25$ adlayer [24,81]. Similarly, extensive exposure to ammonia followed by an anneal to $T_s = 525$ K prepares the $(\sqrt{3} \, x \, \sqrt{3}\,)R - 30°$-N, $\Theta_N = 0.33$ adlayer [81]. Both have been well characterized by LEED [75]. In addition, a slightly higher N coverage of 0.36- 0.44 was also obtained by decomposition of ammonia [81] or hydrazine [82] and corresponds to a so-called heavy domain wall structure (HDW). This structure is thought to be essentially patches of the $(\sqrt{3} \, x \, \sqrt{3}\,)R - 30°$ structure with higher density at the domain walls [81,82]. An even higher N coverage has been obtained by decomposition of ammonia at surface temperatures in a sequence from 500 to 350 K, but because of the lower surface temperature much of the adsorbed N was in the form of NH_x fragments [81]. The results at lower N-coverage have recently been reviewed by Jacobi [83].

We will show that by dosing with an atomic N beam, where the strong N-N bond is broken in the gasphase before impact with the surface, a series of different adsorbate N states can be prepared on the Ru(0001) surface. For low atom beam doses, the known p(2x2) -N, $(\sqrt{3} \, x \, \sqrt{3}\,)R - 30°$-N and HDW states are produced. However, for higher atom doses we find sequential filling of several previously unknown and lower stability, high coverage states, ultimately saturating at a maximum coverage of ≈1 ML N/Ru atom. The results show a very large decrease in the thermal desorption peak temperatures with coverage so that these high coverage states would not be observable with surface temperatures used in previous experimental procedures to produce adsorbate coverages.

Recent DFT calculations for N adsorbed on Ru(0001) [32,75,84] indicate that the higher coverage states are in fact not stable relative to associative desorption. The high coverage states must therefore be metastable, with a lifetime determined by the height of the barrier between gas phase N_2 and the adsorbed N states. Combination of our experimental TPD results with the DFT calculations allows us to estimate these coverage dependent barriers. We find that barriers increase significantly with N coverage and this is in fact a necessary aspect for the metastability of the highest coverage states.

6.2 Experimental

The experiments reported here were performed in an ultra-high vacuum (UHV) system, described in chapter 2.

The ruthenium crystal, 9 mm in diameter and 1 mm thick, was aligned and polished within 0.1° of the (0001) face. A groove was spark eroded on each side of the crystal, and the crystal was clamped by Ta pieces mounted onto a Cu block, which was cooled with either flowing water or liquid nitrogen. A type C thermocouple was pressed into a small hole, spark eroded in the side of the crystal. The crystal was heated by electron

bombardment on the back of the crystal. The overall thermal time constant for cooling of the crystal (when thermal conductance dominated) was ca 1 minute.

The crystal was initially cleaned after introduction into vacuum by repeated heating cycles to 1500 K in oxygen ($2x10^{-8}$ Torr) followed by flashes to 1600 K in UHV. Heating the sample in O_2 results in the removal of C in the form of CO and annealing to 1600 K in UHV removes remaining chemisorbed oxygen. This is a standard cleaning procedure to remove C, the main chemical impurity, from the near surface region of Ru. After many such cycles, the sample was judged C free in the near surface region by the absence of a CO desorption peak following saturated adsorption of background O_2. AES is not sensitive to adsorbed C on Ru due to overlap of the C peak with a Ru peak. Ar ion sputtering was also periodically included in the cleaning procedure. No features other than those attributed to Ru were observed by Auger analysis and indicate that chemical impurities on the surface are minimal. In particular, there was no observable Fe Auger signal, implying that this common bulk impurity in Ru was below detectable Auger limits for our sample.

In addition to the undetectable level of chemical impurities on our sample, we also believe the surface defect density was quite small. LEED at 300 K showed quite sharp substrate spots with a very low diffuse background. In addition, the specular reflectivity of a 300 K He supersonic nozzle atom beam from the surface at an incident angle of 27° relative to the surface normal was ~0.9 for a Debye-Waller extrapolation to $T_s = 0$ K. Since thermal He atom scattering is very sensitive to surface defects, this high He surface reflectivity also indicates a very low surface defect density. The surface defect density was estimated as 0.25 % by CO titration. In this procedure, a 0.02 L (Langmuir, 1 L=$1x10^{-6}$ Torr*sec) CO dose resulted not only in the usual CO TPD peak at ca. 500 K, but also a small shoulder at 575 K believed to be due to CO adsorbed at surface defects. The relative intensities of the two CO TPD features allowed an estimate of surface defect density, although the nature of these defects is unknown.

The active nitrogen beam for dosing of the Ru(0001) surface was produced by a microwave discharge (2.45 GHz, 50 W) in high purity N_2 (99.999%) at ca 1 Torr pressure in a 1 cm diameter quartz tube. Following the discharge, the active nitrogen flowed through a 250 mm length of 1.8 mm id capillary tubing into the UHV system and aimed at the Ru(0001) surface. The capillary tube, which ended some 80 mm in front of the crystal surface, acted as a single long channel beam source pointing at the crystal and provided modest collimation of the beam onto the sample. The pressure build up in the chamber was $1x10^{-7}$ Torr during nitrogen dosing. The internal of the capillary tube was coated with phosphoric acid to minimize heterogeneous recombination of atoms formed in the discharge on the tube walls as they flowed into the UHV chamber. The presence of N atoms in the capillary tube was evident from the characteristic emission of the nitrogen afterglow (formed by the gas phase recombination of nitrogen atoms). Unfortunately, some impurities are required to produce a significant concentration of atoms in discharge flow systems [85]. Both the quartz discharge tube and the phosphoric acid added sufficient oxygen impurity for this purpose. As a result, the active nitrogen beam contained an unavoidable (and somewhat variable) oxygen impurity.

The active species from the microwave discharge that produces adsorbed N on the Ru(0001) surface is unknown with certainty. Discharges in N_2 can produce atoms at a few percent level, metastable molecular nitrogen and vibrationally excited ground state molecules. Generally, metastable molecules are quenched in a pure N_2 discharge [86]. The active nitrogen beam was also investigated by resonantly enhanced multi photon ionization spectroscopy (REMPI) using the 2 + 1 ionization scheme with a laser wavelength of ca. 203 nm [87]. This sensitive spectroscopy, which vibrationally resolves the N_2, showed that no vibrationally excited species produced in the discharge survived the flow down the capillary tube into the vacuum system. We therefore assume that the active species forming adsorbed N on Ru(0001) is the atoms produced in the discharge. Assuming that the sticking coefficient of the atoms on the surface is unity, we estimate an atom flux at the surface of ~0.3 ML/min ~8×10^{12} atoms/cm^2/s from the initial build up of N atoms on the surface. This is consistent with an atom concentration in the beam of a few percent and is quite typical for dissociation probabilities quoted for pure N_2 discharges.

Because the N atom beam contained an oxygen atom impurity, initial experiments showed some build up of adsorbed oxygen as well as adsorbed N on the surface with extended beam exposures. We therefore developed a "scrubbing" procedure to remove the surface O without depleting significantly the surface N coverage. This scrubbing procedure was based on exposure of the surface with adsorbates to a H atom (D atom) beam. Gas phase H atoms react with adsorbed O via an Eley-Rideal reaction to form H_2O which readily desorbs from the surface (at $T_s > 200$ K) [88]. In a similar manner, gas phase H atoms react with adsorbed N atoms, presumably to form NH_3. Subsequent anneals of the surface to $T_s \geq 485$ K ensured that no H or NH_x remained on the surface after exposure to the H atom beam. The key fact that made the scrubbing feasible was that the removal rate by gas phase H atoms of adsorbed O was ca 4 times greater than that for adsorbed N as measured by the disappearance of Auger peaks.

The H (or D) atom beam used in this scrubbing was formed by a microwave discharge in a manner similar to that for the N atom beam. The H (or D) atom beam, however, was well collimated by two stages of differential pumping to just expose the Ru(0001) surface. The dissociation efficiency for H_2 (or D_2) in microwave discharges is extremely high, and the beam striking the surface was > 50 % dissociated as determined by mass spectrometry of the direct collimated beam. The H (or D) atom flux at the surface was estimated as 0.015 ML/sec from the extent of dissociation and the overall beam flux at the surface (determined by sticking of H_2 relative to a background dose).

After dosing with the N atom beam, temperature programmed desorption (TPD) was performed using a differentially pumped quadrupole mass spectrometer (QMS) with an orifice of 5 mm in diameter placed 2 mm from the sample. In this way we ensure that only species desorbing from the front surface are detected by the QMS. Typical linear heating rates of the sample were 3 K/s. Only mass 14 and 28 were significant peaks in the TPD after atom dosing. Both mass 28 and mass 14 showed the same behavior. In order to avoid confusion with any possible CO contamination peak, mass 14 was usually chosen for detection. To minimize CO adsorption during N atom dosing the surface temperature T_s was usually kept at 400 K. This T_s is above the desorption temperature of CO when N is also adsorbed on the surface.

6.3 Results

Initial experiments involved simply looking at the N_2 TPD spectra (mass 14) following various dosing times from the atom beam. For low atom beam doses (0.5 min.), a single and broad desorption feature centered at ca 800 K is observed. This TPD feature is well known from adsorption studies using filament assisted dissociation of molecular nitrogen [24] and thermal decomposition of ammonia [81] to result from the associative desorption of atomic nitrogen on the Ru(0001) surface. At higher atom doses, we find that a series of new states are sequentially populated and desorb at lower and lower surface temperatures. As we show below, the adlayers formed by exposure to only the N atom beam are somewhat contaminated by an O impurity so we will not discuss in detail here the TPD spectra. We simply note at this stage that due to an apparent increase in N coverage (or O coverage), N_2 desorption features were observed at significantly lower T_s. We will show in later experiments that both high coverage of N and co-adsorption of large O coverage with the N each independently produce low T_s associative desorption peaks of N_2.

Auger measurements of the N (and O) coverage as a function of exposure time to the atom beam allowed us to follow the buildup of N (and O) quantitatively and is given in Figure 17.
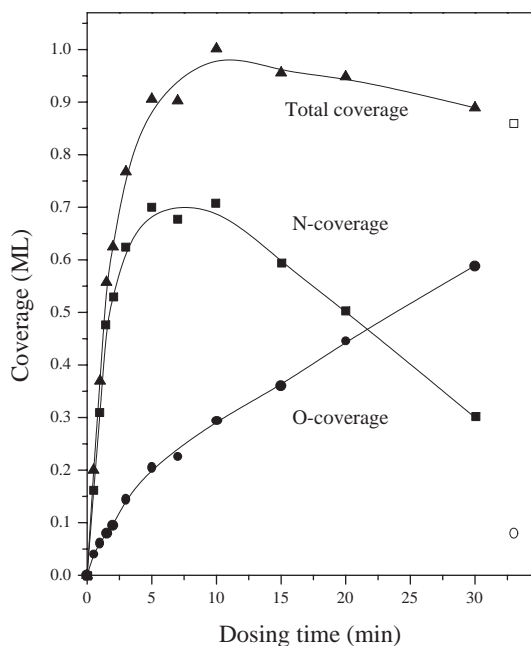
Figure 17. N coverage, O coverage and the total N + O coverage in ML/Ru atom as a function of N atom beam dose time. The open symbols refer to N and O coverages obtained after scrubbing (procedure (e) in Table I).

The relative N coverage was measured by the intensity of the 379 eV N peak in the differentiated spectrum, to that of the 231 eV Ru peak and the relative O coverage was measured by the intensity of the 503 eV peak to that of the 231 eV Ru peak. To calibrate the absolute N coverage, the Auger intensities were normalized assuming that

the saturation adlayer obtained by extended NH_3 decomposition at 610 K is the p(2x2)-N, $\Theta_N = 0.25$ adlayer [75]. This calibration agreed within 15 % to that obtained comparing the N_2 TPD intensity to the CO TPD intensity from a CO saturated surface at $T_s = 300$ K ($\Theta_{CO} = 0.56$) [89]. The O coverage was calibrated by comparing Auger intensities to that of the p(2x1) adlayer ($\Theta_O = 0.50$) formed by saturated O_2 dissociative adsorption at 300 K. The ratio of the Auger sensitivities for N and O obtained independently was in good agreement with the ratio obtained by adsorbing a small amount (0.1 L dose) of NO, which dissociates fully at low coverages [90] and results in equal amounts of N and O on the surface.

It is clear that dosing by the atom beam yields a higher N coverage than has been observed previously, but that there is a significant contamination from adsorbed O, particularly for longer exposure times. For exposures beyond a few minutes, the sum of the N + O coverage is approximately unity. Since both preferentially occupy the same hcp 3-fold sites [73-76], it is reasonable that the combined coverage saturate at Θ = 1 since repulsive interactions between the adsorbates will certainly increase drastically beyond that coverage. It should also be noted that the maximum pure oxygen surface coverage obtainable is $\Theta_O = 1$ [77]. The apparent displacement of N by O for high atom dosing is consistent with the stronger Ru-O bond compared to the Ru-N bonds (relative to associative desorption of the molecular O_2 or N_2). Our interpretation of these results is that although the atom beam has predominately N atoms, there is a small O atom impurity as well. Thus, the N + O atom coverage increases rapidly until the total coverage of N + O is 1. Then, the N is slowly displaced by the O impurity in the beam without increasing the total coverage of N + O.

For low atom beam doses, several of the well-known LEED structures for N adsorbed on Ru(0001) were observed. With increasing atom dose, the p (2 x 2) LEED pattern, the $(\sqrt{3} \, x \sqrt{3} \,)R-30°$ LEED pattern and that ascribed to the HDW structure were observed. For higher beam doses (> 2 minutes dose time), no LEED structures other than the substrate (1 x 1) structure were observed, although there was considerable increase in the diffuse background indicating disorder of the surface adlayer.

In order to clarify the nature of a "pure" N adlayer, the O scrubbing procedure described before was employed to reduce the O contamination on the surface and to build up a higher coverage of N. A variety of different N coverages were produced on the surface with low O impurity by exposure to the N atom beam, followed by scrubbing with the H atom beam and then annealing to various T_s (all greater than 485 K). Because the anneal to 485 K limits the maximum N coverage due to thermal desorption of the adsorbed N, the highest coverages were produced by following the above procedure with an additional final exposure to the N atom beam. This necessarily resulted in a small O atom impurity, but at much smaller levels than observed without scrubbing. The preparation recipe for various adlayers labeled (a) to (e), and their N atom and O atom coverages as determined by the procedures described previously, are given in Table I. For comparison with the dosing without scrubbing, the maximum N coverage obtained via this procedure and its O impurity are included in Figure 17 as the open symbols.

Table I. Summary of the experimental preparation procedures for the TPD spectra labeled a) – e) in Figure 17. Values of Θ_N for each adlayer were obtained by comparing the N_2 TPD intensity to that from a saturated CO adlayer at $T_s = 300$ K. Θ_O was obtained by the Auger intensity normalized to that for the $\Theta_O = 0.5$ adlayer prepared by saturated O_2 background adsorption.

Experiment	Preparation procedure	Θ_N	Θ_O
(a)	2 min. N atom beam exposure at $T_s = 400$ K + 1 min. H atom beam exposure at $T_s = 400$ K + $T_s = 630$ K surface anneal	0.29	0
(b)	2 min. N atom beam exposure at $T_s = 400$ K + 1 min. H atom beam exposure at $T_s = 400$ K + $T_s = 535$ K surface anneal	0.38	0
(c)	2 min. N atom beam exposure at $T_s = 400$ K + 1 min. H atom beam exposure at $T_s = 400$ K + $T_s = 500$ K surface anneal	0.54	0.02
(d)	2 min. N atom beam exposure at $T_s = 400$ K + 1 min. H atom beam exposure at $T_s = 400$ K + $T_s = 485$ K surface anneal + 2 min. N atom beam exposure at $T_s = 300$ K	0.72	0.07
(e)	5 min. N atom beam exposure at $T_s = 400$ K + 2 min. H atom beam exposure at $T_s = 400$ K + $T_s = 485$ K surface anneal + 4 min. N atom beam exposure at $T_s = 400$ K + 1.5 min. H atom beam exposure at $T_s = 400$ K + $T_s = 485$ K surface anneal + 3 min. N atom beam exposure at $T_s = 300$ K	0.86	0.08

TPD spectra for these lower impurity adlayers formed by the scrubbing are given in Figure 18. Measurements of Θ_N are appended at the side of each TPD spectrum. The conditions for the preparation, Θ_N and Θ_O of the various adlayers are those given in Table I. In the TPD, we observe a series of desorption peaks filling sequentially with increasing N atom coverage in the adlayer. While clearly a given desorption peak does shift slightly with changes in N atom coverage, there seems to be five well defined peaks in the TPD spectra; 790, 635, 565, 500 and 430 K. There also appears to be a sharpening of the peaks for lower desorption temperatures. We attribute these results to associative desorption from a series of well-defined states with different N coverage. The TPD spectra for a given adlayer showed no changes with time after the initial preparation. This indicates that the adsorbate structures probed during the TPD are at least metastable during the time scale of the experiments. Each TPD peak appears to saturate with N coverage before a new peak at lower T_s emerges. The preparation procedures (a)- (e) of Table I and Figure 18 were chosen to approximately represent saturation of each successive peak without filling in the next lower desorption peak. LEED studies indicated that preparation procedure (a) yielded a well-defined p(2 x 2) pattern, procedure (b) gave a $(\sqrt{3} \, x \sqrt{3})R - 30°$ pattern and a coverage between (b) and (c) gave the HDW LEED pattern. Only very diffuse LEED

patterns (other than the 1 x 1) were observed under preparation conditions (c)- (e) and no attempt was made to analyze them further. The TPD spectra from adlayers formed without the scrubbing were generally similar, except that intensities in the higher temperature N_2 TPD peaks decreased with exposure beyond ca. 2 min.
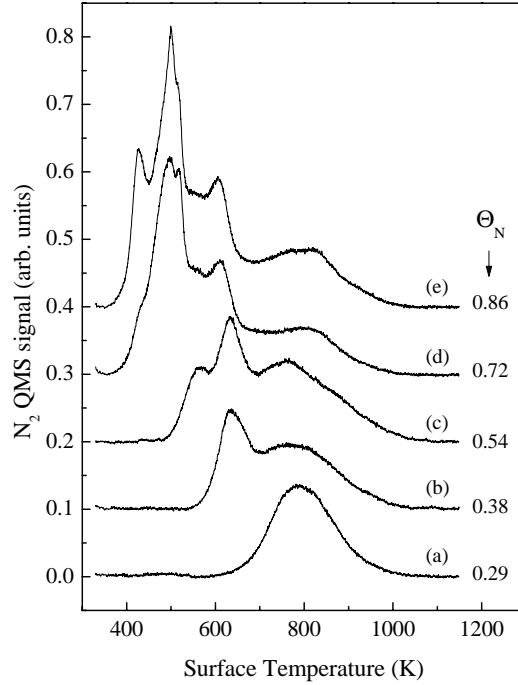
Figure 18. N_2 TPD spectra for various coverages of nitrogen Θ_N adsorbed on Ru(0001). The preparation procedures for the curves labeled (a)- (e) are given in Table I.

Assuming all desorption peaks are due to second order associative desorption from the majority terrace sites, conventional Redhead analysis [72] allows us to estimate desorption energies (E_{des}) for each "state" from the desorption temperature peaks. These are given in Table II. These estimates used a pre-exponential for desorption for all states consistent with that obtained by Tsai and Weinberg [91] of 1.3×10^{-3} $cm^2 \cdot s^{-1}$. The value of $E_{des} = 2.0$ eV obtained here for the lowest coverage state ($\Theta_N = 0.29$) is in good agreement with earlier experimental work; 1.91 eV [91] and 1.97 eV [24]. As the coverage is increased we find a large decrease in E_{des}. Since it is entirely possible that the desorption is more like first order (at the lower coverages) than second order, we have also estimated desorption energies using first order desorption and the pre-exponential of Tsai and Weinberg (2×10^{12} s^{-1}). These give E_{des} of 1.1, 1.3, 1.5, 1.7 and 2.1 eV for the various TPD peaks. All values are within 0.1 eV of those assuming 2nd order desorption. Thus the assumed order of desorption does not affect the overall conclusion that as the coverage is increased we find a large decrease in E_{des}.

Table II. Analysis of N_2 TPD spectrum in Figure 18. Θ_N is the N atom coverage for the preparation procedures a) – e) outlined in the text and Table I, and obtained by a comparison to CO TPD intensities. These preparation procedures correspond approximately to the coverage where a given TPD feature fully saturates. E_{des} is the desorption energy calculated by a simple Redhead analysis for the given peak assuming second order desorption kinetics.

TPD peak (K)	Θ_N	E_{des} (eV/ molecule)
790	0.29	2.0
635	0.37	1.6
565	0.54	1.4
500	0.72	1.3
430	≥ 0.86	1.1

Because of the high O impurity in the initial experiments at high coverage (before scrubbing was introduced), it was also interesting to measure the effects of co-adsorbed O on the N associative desorption. Adsorption of N from the beam to $\Theta_N \approx 0.25$ followed by saturated background exposure to O_2 also produced a significant lowering of the N_2 associative desorption peak temperature as demonstrated in Figure 19. Note, however, that there is only a single low T_s peak at ≈ 500 K and no remaining desorption of N_2 at $T_s \approx 800$ K after dosing with O_2. Under these exposure conditions, the total coverage was $\Theta_N + \Theta_O \approx 0.5$. The low N_2 associative desorption temperature of ca. 500 K when O is present on the surface has been observed several times previously, e. g. by thermal desorption following dissociative adsorption of NO on Ru(0001) [92], but has not been given any discussion or interpretation. No NO TPD was observed under these conditions.
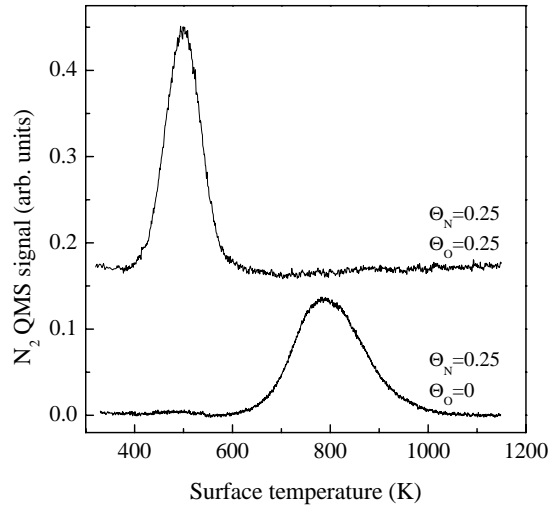
Figure 19. N_2 TPD spectra for an initial nitrogen coverage $\Theta_N \approx 0.25$ without and with co-adsorbed oxygen ($\Theta_O \approx 0.25$)

6.4 Discussion

Several low coverage states of N adsorbed on Ru(0001) have been previously well characterized experimentally. These include the p(2 x 2)-N, $\Theta_N = 0.25$ adlayer, the $(\sqrt{3} \, x \sqrt{3}\,)R - 30°$ -N, $\Theta_N = 0.33$ adlayer and a higher coverage heavy domain wall structure (HDW) consisting of $(\sqrt{3} \, x \sqrt{3}\,)R - 30°$ -N patches with domain walls of local (1 x 1)- N structure, $\Theta_N = 0.36$- 0.44 adlayer [81,82]. The p(2 x 2)-N is the only stable structure at $T_s = 615$ K, the $(\sqrt{3} \, x \sqrt{3}\,)R - 30°$ -N structure is produced at $T_s = 525$ K and the HDW structure at $T_s = 420$ K. LEED [75] and STM [90] studies demonstrate that N adsorbs in the HCP 3-fold hollow site on the Ru(0001) surface for all known structures. The LEED experiments [75] yield a N adsorption distance above the surface plane of ca. 1 Å and demonstrate that no substrate reconstruction and only modest relaxation occurs upon adsorption. STM experiments involving variable temperature anneals determined the indirect interactions between adsorbed N atoms [76]. They obtained a repulsive N-N nearest and second nearest neighbor interaction and an attractive third nearest neighbor interactions. With these indirect N-N interactions, they were able to rationalize all of the observed low coverage structures. Of particular importance for this work is that the authors conclude that the nearest neighbor interaction must be quite repulsive, > 0.2 eV. This means that any higher coverage states must be considerably less stable than those measured previously.

One curious aspect is that electron energy loss spectroscopy (EELS) studies indicate that the Ru-N vibrational frequency increases with coverage despite the fact that the energy/atom must decrease with coverage [24,81]. A similar increase in the vibrational frequency with coverage has been observed for O/Ru(0001) vibrations and attributed to a steeper binding well due to repulsive O-O interactions, despite a lowering of the binding energy due to the same repulsive interaction [93]. Presumably, the same explanation is valid for N/Ru(0001) adlayers.

Our interpretation of the series of TPD spectra is that the broad highest temperature feature is desorption from low coverage up to and filling the well known p(2x2) adlayer of N adsorbed on Ru(0001) with $\Theta_N = 0.25$. This assignment is in complete accord with all of the previous studies and was confirmed by the LEED measurements of preparation (a). The lower temperature peaks are interpreted as desorption from a series of higher coverage and less stable adlayers of adsorbed N. The TPD peak at 635 K is assigned as desorption from the $(\sqrt{3} \, x \sqrt{3}\,)R - 30°$ adlayer structure with $\Theta_N \approx$ 0.33. This assignment agrees approximately with the measured Θ_N, with the anneal temperature necessary to produce this structure [81], and with the LEED measurements of preparation (b). Previous procedures ("filament assisted" adsorption or NH_3 dissociation) have not been able to resolve a well-defined TPD peak for this state. In approximate agreement with measured Θ_N values, we tentatively assign the peak at 565 K to an adlayer with $\Theta_N \approx 0.5$, the peak at 500 K to an adlayer with $\Theta_N \approx$ 0.75 and the peak at 430 K to the adlayer with $\Theta_N \approx 1$. None of these states have been observed previously and their structure is presently unknown. LEED studies at the higher coverages were inconclusive since at best very weak and diffuse additional LEED spots were observed. However, the sharp and well-resolved TPD peaks do suggest the formation of moderately well defined adlayers at a given coverage. The assignment chosen facilitates comparison of the experimental results with theoretical

calculations of coverage dependent adlayer stability. It is unlikely that any N adsorbs into subsurface sites since the observed N coverage (both by TPD and Auger) saturates when $\Theta_N + \Theta_O = 1$. In addition, the scrubbing procedure that lowered the N coverage slightly, only diminished the lowest temperature TPD peak. Since scrubbing is a surface process (Eley- Rideal reaction with H), we infer that the lowest temperature TPD peak is due to repulsive interactions of species on the surface and not due to a subsurface feature.

Using density functional theory, the adsorption energies E_N for a series of known and (previously) unknown higher coverage N adsorbate states on the Ru(0001) have recently been calculated [26,32,75]. Initial calculations were based on using the so-called PW91 exchange- correlation functional [32,75]. It has recently been suggested that a slightly different functional, the so- called RPBE functional, gives improved adsorption energetics [94]. A summary of the DFT calculations is given in Table III. Calculations with both functionals predict the same important trend, i.e. that the binding energy decreases drastically with N coverage. Following ref. [94], we assume that the RPBE calculations are more accurate and use these for comparison with our experiment. These show that the stability of the adsorbate states decreases drastically with N coverage, from -0.29 eV/N atom for $\Theta_N = 0.25$ to +0.86 eV/N atom for $\Theta_N = 1$, relative to the gas phase molecule. Thus states with $\Theta_N \geq 0.5$ are in fact not predicted to be thermodynamically stable on the surface. These calculations justify fully the qualitative concept of a strong indirect repulsive interaction due to the sharing of available Ru d-band electrons mentioned in the introduction. These DFT calculations are also in complete accord with the strong nearest neighbor N-N repulsive interaction measured in the STM experiments [76]. Since the high coverage states are not thermodynamically stable, it is not surprising that they had not been observed previously.

Table III. Density functional theory calculations for average N atom adsorption energies E_N for an assumed adlayer structure of coverage Θ_N. Results are given as eV/atom relative to an origin given by the ½ N_2 + Ru(0001) asymptote. Results are quoted for calculations based on two different exchange-correlation functionals (PW91 and RPBE) and based on the following: a) A. Logadottir and J.K. Nørskov, private communication. b) Ref. [32], c) Ref. [75], d) based on estimating the RPBE adsorption energy from PW91 via E_N (RPBE) $\approx E_N$ (PW91) + 0.36 eV and e) Ref. [26]. The RPBE results are anticipated to be more accurate.

Θ_N	E_N (eV/atom) PW91	E_N (eV/atom) RPBE
0.17	-0.62[a]	-0.28[a]
0.25	-0.65[a], -0.77[b], -0.7[c],	-0.29[a]
0.33	-0.47[c]	-0.11[d]
0.5	-0.24[a], -0.19[b], -0.2[c],	+0.12[a,e]
0.75	+0.2[c]	+0.56[d]
1.0	+0.5[a], +0.6[c],	+0.86[a]

As mentioned in the introduction, the other dominant feature of N_2/Ru(0001) interactions is the high barrier to dissociation. This barrier results in a very low dissociative sticking probability for background N_2 [25,26]. The exact height of the barrier and the resulting thermal dissociation rate for N_2 on Ru surfaces has been somewhat controversial. Initial molecular beam experiments of N_2 dissociative

sticking on Ru(0001) suggested a high dissociation barrier of ~2 eV [27], but the experimental data in this work are not consistent with several newer, but as yet unpublished, molecular beam experiments [28,30,95]. Thus, we are uncertain as to how to evaluate their experiment and conclusions. The thermal dependence of the rate of the N_2 dissociation on Ru(0001) at high pressures gives an activation barrier of only 0.4 eV on a reasonably good single crystal [26]. However, if the (low density) natural steps on the surface are poisoned by co-adsorption of Au, a much higher barrier of 1.3 eV is obtained [26]. The authors suggest that the rate of dissociation in many experiments is dominated by the defects and that this may account for much of the discrepancy in comparing various measurements of dissociation rates. Another recent technique that has evolved to determine barrier heights (and other dynamic aspects) is to measure the translational energy (and internal state distribution) of molecules formed by associative desorption from the surface [20,22]. Recent measurements of N_2 formed by associative desorption from Ru(0001) [31] present a puzzling picture for the barrier since the energy dependence of the desorption flux peaks at low translational energies (consistent with a low barrier) but tails to high translational energies (consistent with a high barrier). The results are basically interpreted in terms of a very broad barrier distribution (energy dependent sticking function).

Some of the DFT calculations mentioned earlier have also probed the full minimum energy path to dissociation from gas phase N_2 to adsorbed N atoms at a total N/Ru coverage of 0.5 [32]. These calculations find a path which passes through the known molecularly adsorbed state ($E_M = -0.44$ eV/N_2), through a metastable molecular state bonded parallel to the surface ($E_{MS} = 0.4$ eV/N_2), through a barrier with a stretched N-N bond ($V^* = 1.36$ eV/N_2) and into the N adsorbate state ($E_N = -0.77$ eV/ N atom). All energies are relative to an origin defined by the infinitely separated N_2 + Ru(0001). These initial calculations were based on using the PW91 exchange- correlation functional. Use of the improved RPBE functional gave a theoretical barrier height $V^* = 1.9$ eV [26].

Thus, despite the contradictory experimental evidence, we agree with ref. [26] that the barrier at low coverage is high ≥ 1.4 eV on terrace sites but that defects (steps, etc.) may significantly lower the barrier. We will show evidence below that the barrier actually increases significantly above this value of 1.4 eV at higher N coverage.

$E_{des}(\Theta_N)$ estimated from the thermal desorption experiments represents the energy difference between the adsorbate state and the barrier,

$$E_{des}(\Theta_N) = V^*(\Theta_N) - 2 E_N(\Theta_N) \tag{6.1}$$

Combining $E_{des}(\Theta_N)$ obtained here from the TPD measurements with $E_N(\Theta_N)$ from the DFT calculations allows predictions of $V^*(\Theta_N)$. This is shown in Figure 20 and numerical values given in Table IV. It is immediately apparent in Figure 20 (and Table IV) that V^* increases with Θ_N. The increase in $V^*(\Theta_N)$ is, however, less than the decrease in $E_N(\Theta_N)$. Of course, a shifting down of the desorption peak temperatures with Θ_N is the experimental consequence of this fact. Both the existence of this increase in V^* with Θ_N and the magnitude of its change relative to that of E_N are consistent with the explanation of the DFT calculations in terms of the necessity to

share Ru d-band electrons at high N coverage[§]. Direct measurements of $V^*(\Theta_N)$ using the technique of laser assisted associative desorption will be present later (chapter 8), which confirm that the barriers increase substantially with Θ_N.
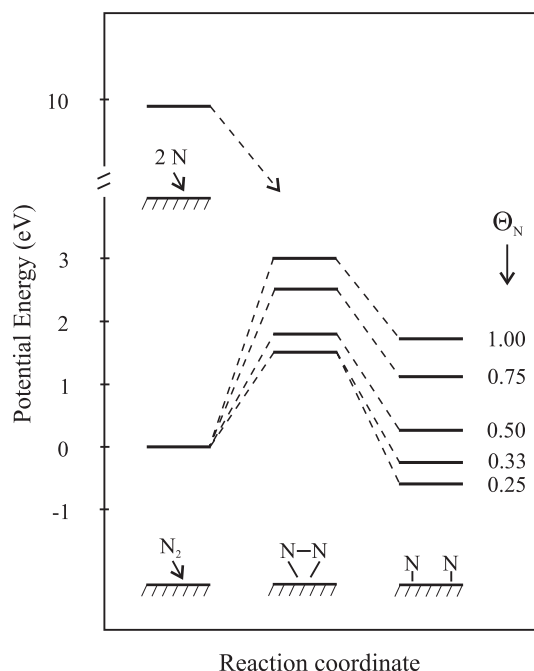
Figure 20. Schematic energy diagram for the interaction of N_2 and 2N with the Ru(0001) surface. The origin of energy is taken as the N_2 + Ru(0001) asymptote. The left side is the entrance channel for dissociative chemisorption. The right hand side is the atomic adsorbed state and is based on the DFT RPBE adsorption energies (see Table III). The center is the estimate of $V^*(\Theta_N)$ by combining the theoretical adsorption energies with the desorption energies obtained from the TPD (see Table II).

Figure 20 illustrates the difficulty in preparing the high coverage states. The prediction that states with $\Theta_N \geq 0.5$ are not thermodynamically stable relative to N_2 + Ru(0001) means that it is difficult to prepare such states via N_2 dosing, even "filament assisted" adsorption since this process is endothermic. More importantly, the barrier to dissociative chemisorption increases substantially at higher coverage so that the energy cost for dissociating N_2 also increases. However, as Figure 20 graphically illustrates, dissociating the N_2 in the gas phase provides more than enough energy to readily overcome all barriers and form all adsorbate states. The fact that the metastable high

---

[§] New DFT calculations by B. Hammer have shown that the "differential adsorption energies" are different from the "average adsorption energies" used here. These calculations were not yet available when the results presented in this chapter were published and will be discussed later in more detail, but briefly here. The "average adsorption energy" is the total adsorption energy per atom at a given coverage. This corresponds to the energy difference between the adsorbate state and when *all* atoms are desorbed from the surface. However, when a TPD experiment is performed at higher coverage, not all of the adsorbates are removed from the surface in a given TPD peak. Thus, differential adsorption energies are more relevant for calculating V^* from E_{des}. The average adsorption energies from Table III have been used here and since this was how the results were published in ref. [2], no attempt has been made to use the differential adsorption energies at this point. When the N_2 LAAD results and B. Hammers new DFT calculations have been presented later, differential adsorption energies will be used instead. These new calculations showed that at higher coverages, the average adsorption energies are lower than the differential and the barriers presented here are then in principle to low at higher coverages.

coverage states are observed via N atom impingement at all and appear metastable for $\geq$ 30 min. implies that they must have a significant surface lifetime.

Table IV. Best estimates of coverage dependent N_2 dissociation barrier heights $V^*(\Theta_N)$ on Ru(0001) by combining TPD experiments and DFT calculations. $E_{des}(\Theta_N)$ from Table II assuming the TPD peaks correspond to desorption from $\Theta_N = 0.25, 0.33, 0.5, 0.75$ and 1 respectively. $E_N(\Theta_N)$ from Table III is based on the RPBE values. Barrier heights in eV are relative to the N_2 + Ru(0001) asymptote.

Θ_N	$V^*(\Theta_N) = E_{des}(\Theta_N) + 2E_N(\Theta_N)$ (eV)
0.25	1.4
0.33	1.4
0.5	1.7
0.75	2.4
1.0	2.9

It has recently been shown that the thermal activation energy for dissociative chemisorption of N_2 on Ru(0001) is lowered at step sites relative to terrace [26]. By detailed balance, this may imply that the thermal desorption energies $E_{des}(\Theta_N)$ measured in the TPD experiments are those characteristic of desorption from the step sites. However, the relative importance of the steps vs. terrace sites in the TPD experiments will depend in a complex way on the step density, coverage, diffusion rate to step sites, heating rate, etc.. A model incorporating all these features is currently being developed. Even if the step sites do dominate thermal desorption, this merely implies that the desorption energies determined from the TPD experiments must be interpreted as lower limits to desorption energies from the terrace sites. If this is the case, then the barriers at the terraces may be somewhat higher than those of Figure 20 and Table IV.

As mentioned in the introduction, the energetic and geometrical structure for a whole series of states of O adsorbed on Ru(0001) have also recently been studied [73,77]. While the lower coverage (2 x 2)- O, $\Theta_O = 0.25$ and (2 x 1)- O, $\Theta_O = 0.5$ have long been known, newer work has demonstrated that (2 x 2)- 3O, $\Theta_O = 0.75$ and (1 x 1)- O, $\Theta_O = 1$ are also stable on the surface [77,80]. There is, however, a "kinetic barrier" to the formation of the $\Theta_O = 0.75$ and $\Theta_O = 1$ states so that either high pressures of O_2 or indirect methods (NO_2 dissociation) are necessary to prepare these states. The nature of this "kinetic barrier" is ill defined. It may just be a true energy barrier that occurs at high O coverage, in a similar manner as the energy barrier for N_2 dissociation increases with N coverage. However, since the dissociation is so exothermic, the high coverage states are thermodynamically stable, in agreement with the DFT calculations. Figure 21 summarizes the energetics obtained for the O_2/Ru(0001) system. It has also been observed that at sufficiently high exposures O atoms can be forced into subsurface sites [96].
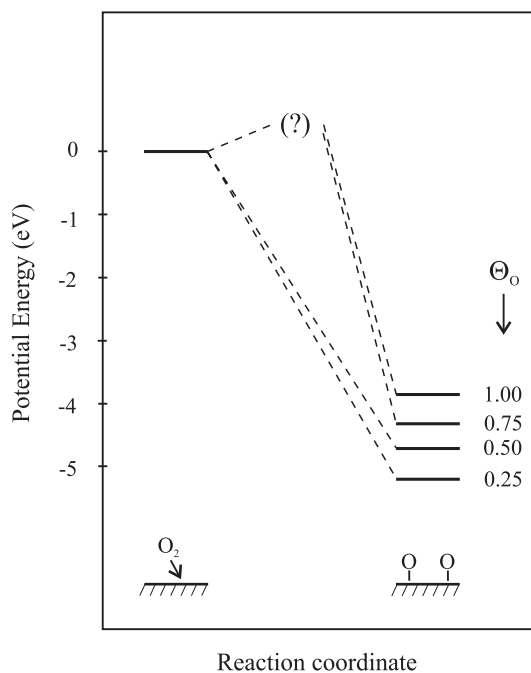
Figure 21. Schematic energy diagram for the interaction of O_2 with Ru(0001). The adsorbed atomic state on the right side is based on DFT calculations of adsorption energies. For $\Theta_O = 0.75$ and 1.0, the "kinetic barrier" is indicated as a (?).

Comparison of Figure 21 with Figure 20 highlights the similarities and differences between O_2/Ru(0001) and N_2/Ru(0001) interactions. As stated earlier, both dissociation processes are exothermic at low coverage to produce adsorbed atomic states on the surface. Because the O_2 bond is 4.6 eV weaker than the N_2 bond, the dissociation of O_2 on Ru(0001) is much more exothermic than that of N_2, even though the Ru-N bond is 1.5 eV stronger than the Ru-O bond. Both systems support many different adsorbate states of different coverage up to a maximum coverage of $\Theta = 1$. For the (1 x 1)- O structure, O occupies all available 3- fold HCP sites [77]. Since N binds to Ru also in the 3- fold HCP sites at lower coverage [90], we assume that the (1 x 1)-N structure also occupies all available 3- fold HCP sites as well. The binding energy decreases with Θ for each and this is described as an indirect repulsive interaction between the adsorbates due to the competition for available Ru d-band electron [32,97]. We also see that since the binding energy decreases more rapidly for N than for O with coverage, the N-N indirect repulsive interaction between adsorbed species is stronger than that for O-O. This is interpreted as due to the fact that N has three valence electrons/atom interacting with the Ru d-bands instead of two for O. Hence, the competition for Ru-d electrons with coverage is enhanced. Because of the large exothermicity and modest indirect repulsive interaction, all adsorbate states of oxygen on Ru(0001) are thermodynamically stable. On the other hand, both because of the smaller exothermicity and larger adsorbate repulsive interactions, only low coverage states for nitrogen on Ru(0001) are thermodynamically stable. The relative strengths of the O_2 vs. N_2 bonds is also fully in accord with the absence of a barrier to dissociation for O_2 at low coverage and the presence of a large barrier for N_2 dissociation. Both systems show, however, evidence that barriers increase with adsorbate coverage, although the nature of the barrier at high O coverage is not well characterized.

Given the discussion above about the similarities and differences between the N_2 + Ru(0001) and O_2 + Ru(0001) interactions, we can now rationalize the behavior of Figure 19 where co-adsorption of O shifts the TPD peak of the $\Theta_N = 0.25$ state from T_s = 790 K to T_s = 500 K. Both O and N bind at the same HCP site. Therefore, the adlayer can exist in either phase-separated domains or as mixed phases, depending upon details of all the lateral interactions. We have no way of knowing which situation exists at this total coverage ($\Theta_N + \Theta_O \approx 0.5$), although a low total coverage forms a mixed phase [98]. If the adlayer is phase separated, then the O co-adsorbate merely compresses the N layer to patches of a local high coverage and this accounts for the lower peak desorption temperature. However, if a mixed phase exists, then the shifts of the desorption temperature must be due to a repulsive interaction by a co-adsorbed O. Since both N-N and O-O exhibit indirect repulsive interactions that derive from the same physical origin (competition for Ru d-electrons), we suggest that either neighbor can cause a local repulsive interaction to both the adsorption energy of adsorbed N and to V^*. Since we anticipate that shifts in E_N are greater than shifts in V^*, it is also anticipated that the desorption temperature for a given Θ_N would decrease with co-adsorbed oxygen.

6.5 Conclusion

There has been considerable confusion as to the maximum coverage obtainable for N adsorbed on Ru(0001) and whether high coverage adsorbate states exist on this surface. Since the electronic interaction of N with Ru(0001) is similar to that of O with Ru(0001), and the latter supports a coverage $\Theta_O = 1$, it is tempting to speculate that a state with $\Theta_N = 1$ may also exist. In large part this has been unresolved due to experimental difficulties. There is a very high barrier for direct dissociation so that enormous exposures are required for N_2 and even "filament assisted" N_2 dosing. Indirect methods of preparation of a N adlayer (NH_3 or N_2H_4 dissociation, Eley-Rideal dissociation of NH_3 adsorbate by H [99], ion beam or electron beam dissociation of NH_3 adsorbate [100] all require anneals to higher T_s to dissociate NH_x fragments. We report here a way to produce high coverage states of nitrogen atoms on Ru(0001) using an N atom beam formed by microwave discharge. Since the atom beam contains a considerable O atom impurity, it was necessary to "scrub" the O from the surface via an Eley-Rideal reaction with a gas phase atomic H beam. The results show that in fact a coverage of $\Theta_N \approx 1$ can be formed by atom dosing. A whole series of states of different coverage are observed on the surface as separate TPD peaks by varying the atom dose. The lowest coverage states agree with previous observations, but the higher ones are entirely new.

Density functional calculations (DFT) for N adsorbed on Ru(0001) [26,32,75] indicate that the higher coverage states are in fact not stable relative to associative desorption. They must therefore be metastable, with a lifetime determined by the height of the barrier between gas phase N_2 and the adsorbed N states. Combination of our experimental TPD results with the DFT calculations allows us to estimate these coverage dependent barriers. We find that the barrier heights increase significantly with N coverage and this is in fact a necessary aspect of the metastability of the highest coverage states.

7 Laser Assisted Associative Desorption – calculations of heating and desorption

Exposing a surface to a short and intense laser pulse results in a temperature jump (T-jump), with approximately same duration as the laser pulse length. Adsorbates on the surface will thermally desorb if the temperature is sufficiently high. The general term for desorption induced by laser heating is Laser-Induced Thermal Desorption (LITD). Since desorption only occurs over a very short time range, time-of-flight (TOF) techniques can be used to determine the translational energy distribution of the desorbing molecules. Laser heating of metal surfaces will be examined in the following and a number of calculations will be presented, that help us to understand the parameters influencing the laser heating as well as the thermal desorption.

We will apply the technique of pulsed rapid laser heating to study the *dynamics* of associative desorption of diatomic molecules. This new application is termed Laser Assisted Associative Desorption (LAAD).

Laser heating is known to cause crystal damage under some circumstances. In order to avoid that, it is necessary to minimize peak temperatures, temperature gradients and the fluence the surface is exposed to. These issues will be discussed later in this chapter.

Finally, an experimental method to measure the T-jump due to laser heating will be presented. It will be shown that time-of-flight distributions of LITD of CO follow a Maxwell-Boltzmann distribution described by the surface temperature. The measured temperatures are shown to be in good agreement with the calculated.

7.1 Laser heating of metal surfaces

A metal surface is irradiated with a laser pulse. The light is absorbed in the uppermost layer, the skin depth (~100 Å), where the photon energy is transferred to metal electrons, which rapidly lose their energy through electron-electron and electron-phonon collisions, transferring the energy to the lattice. The time for the decay into heat is for most metals on the order of a few picoseconds at room temperature [101]. The system reaches local thermal equilibrium and can be described by a temperature when the laser pulse duration is considerably longer than the relaxation time, i.e. when the temporal pulselength is longer than about 100 ps. The Alexandrite laser in our laboratory has a pulselength of ca 100 ns and a wavelength in the near IR region (750 nm). In order to avoid photochemical processes, the photon energies has to be kept low. Lasers for photochemical studies on surfaces are mainly in the UV range.

The heating rate for a 100 ns pulse with energy of a few tens of mJ is about 10^9 - 10^{10} K/s, much higher than what is obtainable with conventional heating methods like electron bombardment and resistive heating. This opens up for a lot of new experiments. For example, adsorbates can either dissociate or desorb upon heating. Depending on the kinetics of a given adsorbate/surface system the rapid surface heating favors desorption over decomposition, even if slow heating would lead to

complete dissociation on the surface. This change of reaction pathway with heating rate will be discussed in more detail in section 7.3.

Using rapid laser heating it is thus possible to study the kinetics of surface reactions. Detecting the reactants, intermediates and the products of a reaction at the surface is difficult. Instead it is possible to place a small amount of the adsorbates in the gas phase where sensitive detection is possible with e.g. a mass spectrometer. Each T-jump desorbs a small fraction of the adsorbates and allows us to follow a reaction in time by performing subsequent T-jumps [102].

A well-focused laser pulse can also be used to set up coverage gradients on the surface, which can be used to study surface diffusion. ([103] and references in [102]).

7.2 Calculation of the surface temperature

Temperature profiles induced by laser heating can be calculated from the classical heat conduction equation:

$$\nabla \cdot J(\vec{r},t) + \rho c \frac{\partial T(\vec{r},t)}{\partial t} = W(\vec{r},t) \qquad (7.1)$$

$J(\vec{r},t)$ is the thermal energy crossing unit area per time, $T(\vec{r},t)$ is the temperature, ρ the density, c the specific heat capacity of the metal, $\vec{r} = (x,y,z)$ the spatial position and t the time. $W(\vec{r},t)$ is the energy source, in this case the power density deposited by the laser. Fourier's law is used to relate the heat flux and the temperature gradient:

$$J(\vec{r},t) = -\kappa \nabla T(\vec{r},t) \qquad (7.2)$$

Where κ is the thermal conductivity. Eq. (7.2) is inserted in eq. (7.1) and we get a relation between the temperature and the deposited energy [104].

$$\rho c \frac{\partial T(\vec{r},t)}{\partial t} = \kappa \nabla^2 T(\vec{r},t) + W(\vec{r},t) \qquad (7.3)$$

The energy source can be expressed in terms of the laser intensity I, the optical reflectivity R, and the absorption coefficient α:

$$W(\vec{r},t) = (1-R)\alpha e^{-\alpha x} I(x,y,t) \qquad (7.4)$$

Radiative heat loss can be neglected. According to the Stefan-Boltzmann formula, the radiated power, "Black body radiation", from a surface, with emissivity ε, is given as $\varepsilon \sigma T^4$, where the Stefan-Boltzmann is given by $\sigma = 5.67 \times 10^{-12}$ Wcm^{-2}K^{-4}. Setting $\varepsilon = 1$ (max), the thermal radiation from a surface with temperature 700 K is about 1 W/cm^2, and therefore negligible compared to the absorbed photon flux density from the incoming laser radiation with intensities normally on the order of 10^6 W/cm^2. Furthermore, it will be shown that the heat conduction into the bulk is so fast (Figure 23), that heat lost to thermal radiation also after laser irradiation is negligible. It is

assumed that the metal does not undergo any phase changes (melting, evaporation etc.) or chemical transformations (e.g. oxidation) during laser irradiation. Furthermore the material is assumed to be isotropic, i.e. κ is a scalar instead of a tensor. In order to use these classical expressions thermal equilibrium is required in order to describe the system by a temperature. This is, as discussed before, a reasonable assumption.

7.2.1 One-dimensional solution

For a well-focused laser beam we may consider the metal as semi-infinite, i.e. from the surface, the bulk extends infinitely into all three dimensions as shown in Figure 22. The thermal energy is deposited into the top 0.1 µm on an area corresponding to the laser beam. The depth of heat penetration during the laser pulse is also small compared to the diameter of the beam. The thermal diffusion length l_{th}, during the laser pulse, can be expressed by the thermal diffusivity D_{th}, ($D_{th}=\kappa/\rho c$), and the temporal pulselength t_p as: $l_{th}=(D_{th}t_p)^{1/2}$. For $t_p=100$ ns, l_{th} is a few µm for most metals (e.g. 1.6 µm for Pt and 2.0 µm for Ru)
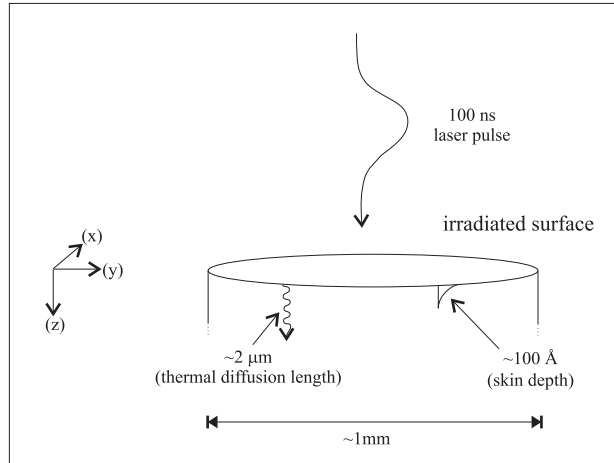
Figure 22. The geometry shows the heated part of the surface. From this, one clearly can accept the one-dimensional approximation.

The largest temperature gradients will therefore be in the z-direction, i.e. into the bulk, and heat diffusion in the surface-plane (x,y) can be ignored. This simplifies solving eq. (7.3) to a one-dimensional problem. Detailed calculations can be found in [104,105]. Ready [105] gives the solution for a spatially uniform pulse in this form:

$$T(z,t) = \frac{1-R}{(\kappa \rho c \pi)^{1/2}} \int_0^t \frac{I(t-t')exp(-z^2/4\kappa t')}{(t')^{1/2}}dt' \; + \; T_0 \tag{7.5}$$

The surface temperature, at $z=0$, is then given by:

$$T(t) = \frac{1-R}{(\kappa \rho c \pi)^{1/2}} \int_0^t \frac{I(t-t')}{(t')^{1/2}}dt' \; + \; T_0 \tag{7.6}$$

61

T_0 is the initial bias temperature. Spatial variations are calculated by multiplying with the "spatial amplitude", the (x,y)-part of the intensity. At long times, the diffusion in the (x,y)-plane becomes significant and the temperature calculated from eq. (7.6) is higher than in reality. For laser beams with very strong spatial variations the temperature gradients in the surface plane may cause heat diffusion from the beam center and outwards. In the following calculations the one-dimensional solution will be used. The validity of this model has been proved experimentally, by measuring the time evolution of the surface temperature in several ways (see e.g. [101,106])

The temperature profile, from a given intensity, has been calculated by numerical integration of eq. (7.6). An analytical solution for $T(t)$ is possible only for simple time dependencies of the intensity. Examples can be found in e.g. [105,107].

The temperature dependence of the physical parameters[*] in eq. (7.6) is neglected. The error is small as long as the temperature jump is not too large. E.g. κ for Pt increases 5 % between 300 and 800 K. For most metals over the temperature range from room temperature to their melting point, ρ remains constant and the relative variation of κ, D_{th} and c does not exceed 10 % [107]. The reflectivity will change as the temperature increases, but this is also neglected. The following calculations have been done for Ru, but can simply be transferred to other metals by using the appropriate physical parameters in eq. (7.6), which only enter as a pre-factor.

7.2.2 Spatially homogeneous beam

First, the spatial variation is not included. A Gaussian temporal distribution is a good approximation for most pulsed lasers including the one in our laboratory.

$$I(t) = I_0 \cdot exp\left[-4 \cdot ln\, 2 \cdot \left(\frac{t - t_0}{t_p}\right)^2\right] \tag{7.7}$$

t_p is the fwhm temporal pulselength and t_0 defines the center in time of the pulse. The temperature profile following irradiation with a Gaussian laser pulse has been calculated. Figure 23 shows $T(t)$ for t_p=100 ns and an intensity of I_0=6.5 MW/cm^2. All intensities stated will be peak intensities. The laser profile is also plotted on the same figure. It is seen that the temperature profile has about the same width (fwhm) in time as the laser pulse. The very fast increase in temperature is caused by the high intensity of laser irradiation followed by a fast decrease due to the heat conduction into the bulk as soon as no more energy is deposited at the surface. The "delay" of $T(t)$ compared to $I(t)$ is due to the large temperature gradients in the beginning. A little later, the layer below the surface is warm and thus reduces the heat flow into the bulk. Finally, it takes some time for the surface to cool again. After 50-100 times t_p the temperature has reached its initial value T_0, but at this time the validity of model is not very good since

---

[*] Numerical values for the parameters at room temperature and a wavelength of 750 nm (normal incidence):

  Ru: κ=1.17 W/cmK, ρ=12.2 g/cm^3, c=0.238 J/gK, R=0.62,

  Pt: κ=0.72 W/cmK, ρ=21.47 g/cm^3, c=0.133 J/gK, R=0.706

lateral diffusion becomes significant. In reality the complete cooling of the surface may go faster.
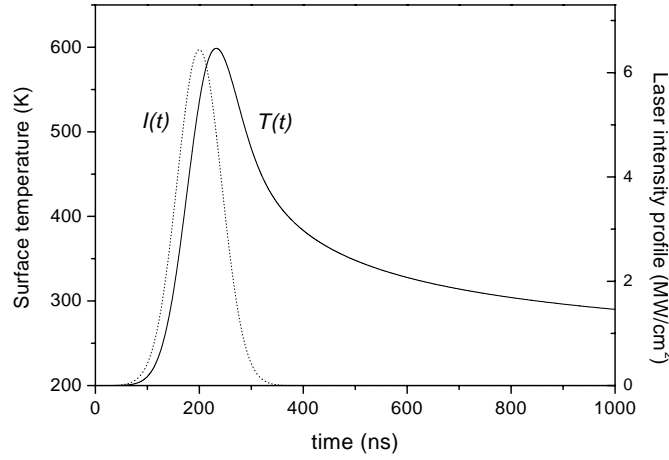
Figure 23. Calculated surface temperature $T(t)$ (solid line) and laser temporal profile $I(t)$ (dotted line) as a function of time.

The peak temperature induced by a Gaussian pulse can be estimated from the maximum of the calculated $T(t)$. That results in the following formula [102]:

$$T_{peak} = \frac{1.67 \cdot (1-R)}{(K \rho c \pi)^{\frac{1}{2}}} I_0 \sqrt{t_p} + T_0 \qquad (7.8)$$

where I_0 is inserted in W/cm^2 and t_p in sec. Using the parameters for Ru, we can write the temperature jump as:

$$T_{peak} - T_0 = 0.194 \cdot I_0 \sqrt{t_p} \qquad (7.9)$$

Again with I_0 inserted in W/cm^2 and t_p in sec. The constant has units of cm^{2}K/Ws$^{\frac{1}{2}}$.

The rate, $R(t)$, of recombinative desorbing molecules is assumed to follow a second order Arrhenius expression:

$$R(t) = -\frac{d\Theta}{dt} = \Theta^2 \nu \, exp[-E_{des} / k_B T(t)] \qquad (7.10)$$

Where Θ is the adsorbate coverage, relative to the number of surface atoms, ν is the "pre-exponential", E_{des} is the desorption energy and k_B is Boltzmann's constant.
We assume to start with a surface that is saturated with adsorbates ($\Theta_0 = 1$). Diatomic molecules leave the surface by associative desorption upon heating during the T-jump. The total coverage change is assumed to be small, and thereby Θ^2 can be assumed to stay constant when $R(t)$ is calculated.

As a "test system" was used the following kinetic parameters: E_{des}=1 eV and ν=10^{13} s^{-1} in the calculations. This corresponds to a desorption temperature which peaks at about 400 K in a normal TPD experiment (Temperature Programmed Desorption). Below is shown the calculated temperature and desorption rate following a 100 ns Gaussian laser pulse with I_0=6.5MW/cm^2. The laser-induced temperature jump starts at 200 K and reaches 600 K. The important thing to note is that since the rate depends exponentially on temperature desorption is only occurring in a rather small range of temperatures close to T_{peak}. This will be further discussed later.
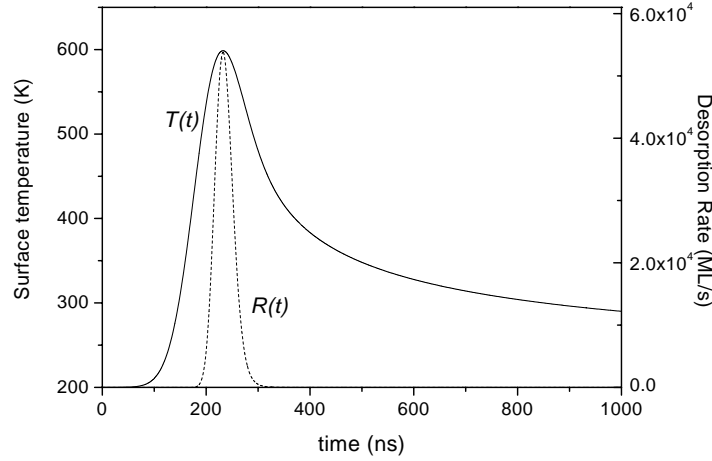
Figure 24. Calculated surface temperature $T(t)$ (solid line) and desorption rate $R(t)$ (dashed line) as a function of time.

7.2.3 Including spatial beam variation

The change in coverage will now be calculated. To find how much desorbs during each laser pulse it is important to take the spatial variation of the laser beam into account. As mentioned in section 2.3 the spatial profile of the laser beam incident on the surface was approximately Gaussian. The intensity as a function of radius (r) and time (t) is then given by:

$$I(r,t) = I_0 \cdot exp\left[-4 \cdot ln\,2 \cdot \left(r/r_p\right)^2\right] \cdot exp\left[-4 \cdot ln\,2 \cdot \left(\frac{t-t_0}{t_p}\right)^2\right] \qquad (7.11)$$

I_0 is the peak intensity, r_p is the fwhm spatial pulsewidth, t_p is the fwhm temporal pulselength and t_0 defines the center in time of the pulse. Only the time dependence enters in the integration. The radial variation can simply be found by multiplying with the spatial profile factor: $exp\left[-4 \cdot ln2 \cdot \left(r_i/r_p\right)^2\right]$.

The pulse energy for a spatially and temporally Gaussian shaped pulse can be calculated by integrating over space and time [102]:

$$E = \pi^{3/2} \left[8(\ln 2)^{3/2} \right]^{-1} I_0 t_p r_p^2 \approx 1.2 \cdot I_0 t_p r_p^2 \tag{7.12}$$

Figure 25 shows the temperature $T(r,t)$ as a function of radius and time, and the corresponding rate, $R(r,t)$. A laser beam diameter (fwhm) of r_p=2 mm is used. It is seen that desorption occurs only from those parts of the surface, that reach a sufficiently high temperature, again in a narrow time and temperature window.
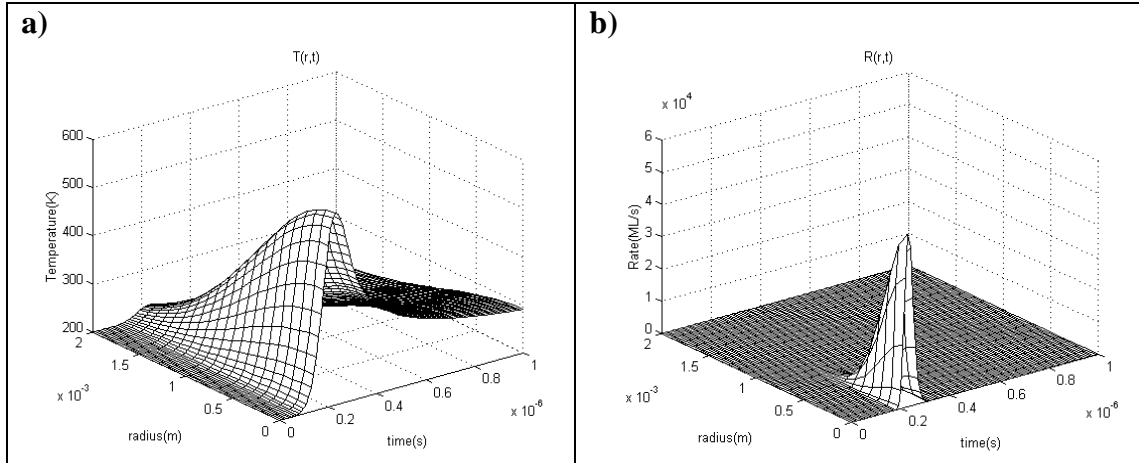
Figure 25. a) Calculated surface temperature and **b)** Desorption rate as a function of time and radius of the irradiated spot. t_p=100 ns, r_p=2 mm.

Calculation of the total coverage change is done in the following way:
The desorption rate, and thus the contributions to the total coverage change from the different areas of the irradiated spot, will be different because of the decreasing intensity with radius in the Gaussian beam. On a small ring with radius r_i, width dr, and area $A_i = \pi \cdot ((r_i + dr)^2 - r_i^2)$, the temperature $T(r_i, t)$ is varying only in time. Let $\Delta \Theta_i$ be the coverage change from the area A_i at radius r_i. This is calculated by inserting $T(r_i, t)$ in $R_i(t)$ (eq. (7.10)) and integrating the rate.

$$\Delta \Theta_i = \int R_i(t) dt \tag{7.13}$$

To get the total coverage change, the contribution from each ring has to be weighted with the area A_i and normalized to the "beam area" $\pi \cdot (r_p/2)^2$.

$$\Delta \Theta_{tot} = \sum_i \frac{A_i \cdot \Delta \Theta_i}{\pi (r_p/2)^2} \tag{7.14}$$

The amount desorbed has been calculated for a 100 ns Gaussian pulse. In Figure 26 is plotted the coverage change $\Delta \Theta_{tot}$ as a function of peak temperature reached in the T-jump. The temperature dependence is clearly exponential as expected from the rate.
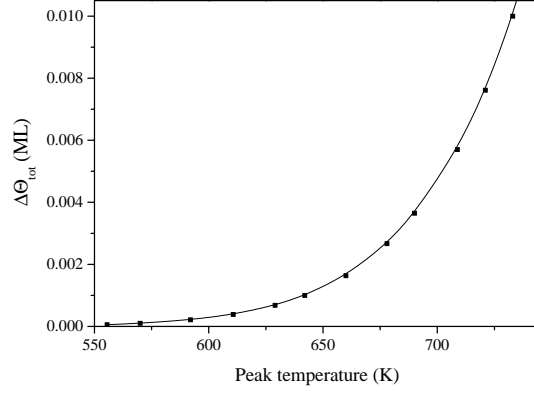
Figure 26. The amount desorbed in one laser pulse, given by the coverage change as a function of peak temperature. $T_0=200$ K.

We want to remove $\sim 10^{-3}$ ML of the adsorbates. This is enough to be detected but probably below the limit where collisions in the gas phase change the internal state distribution. Since the temperature varies in time during the T-jump, desorption will take place over a range of temperatures. Ideally, we would like the desorption to be isothermal when we later analyze the data. We can calculate what part of the coverage change that occurs in a temperature interval around T_{peak}, and show that a large fraction of the molecules desorb close to T_{peak}. This is done by integrating the rate only for temperatures above T', using a modified eq. (7.14), and comparing that to the total integrated rate of all temperatures, i.e. $\Delta\Theta_{tot}$. This is done for different values of T' and the fraction desorbed, $\Delta\Theta_{fraction}/\Delta\Theta_{tot}$, in a given temperature range from the peak temperature is plotted as a function of this interval, T_{peak}-T', in Figure 27. This is called "the distribution in temperature", and is shown for a 100 ns laser pulse desorbing $1\cdot10^{-3}$ and $1\cdot10^{-2}$ ML respectively.
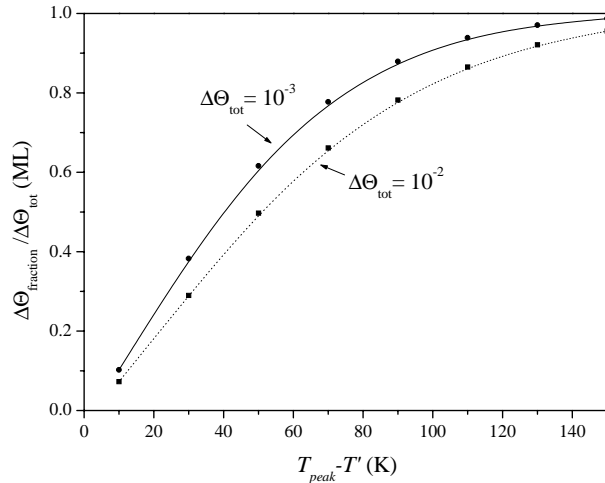
Figure 27. "The distribution in temperature", i.e. the fraction desorbed as a function of temperature interval from the peak temperature. The peak temperatures and intensities were 643 and 733 K, and 7.2 and 8.7 MW/cm^2 for $\Delta\Theta_{tot}=1\cdot10^{-3}$ and $1\cdot10^{-2}$, respectively.

Let us first look at the upper curve in Figure 27. It can be seen that 90 % of the molecules desorb within 100 K from the peak temperature for a 100 ns pulse where $1 \cdot 10^{-3}$ of a monolayer desorbs. In the same figure is also plotted the distribution in temperature for $\Delta\Theta_{tot}=1\cdot10^{-2}$. Here $\Delta\Theta_{tot}$ is ten times larger and a higher intensity and therefore a higher T_{peak} is needed to desorb a larger amount in the same time. This results in a somewhat broader distribution since the rate has a significant value over a larger temperature range. The bias temperature was 200 K and peak temperatures and intensities were 643 and 733 K, and 7.2 and 8.7 MW/cm^2 for $\Delta\Theta_{tot}=1\cdot10^{-3}$ and $1\cdot10^{-2}$, respectively. If a near-isothermal distribution is desired it is better to desorb a small amount in each pulse. Also the peak temperature is smaller this way, reducing the risk of introducing damage to the crystal, as discussed in section 7.4.

7.3 Heating rate dependent reaction pathways

As mentioned in the introduction of this chapter, rapid laser heating can favor one reaction pathway over another, depending on the heating rate. Let us assume a surface is covered with adsorbates, which can undergo two reactions, e.g. desorb or dissociate upon heating. For simplicity we just look at the rate-constants given by the expressions, $\nu \cdot exp(-E/k_BT)$. If the pre-exponentials and activation energies for the two reaction pathways are related by $\nu_{des} > \nu_{dis}$ and $E_{des} > E_{dis}$ the rate of desorption will dominate over dissociation above a certain temperature. An example taking $\nu_{des}/\nu_{dis}=400$ and $E_{des}=1.5$ eV and $E_{dis}=1.07$ eV is illustrated in Figure 28 , where the rate-constants for the two reaction pathways are plotted as a function of temperature.
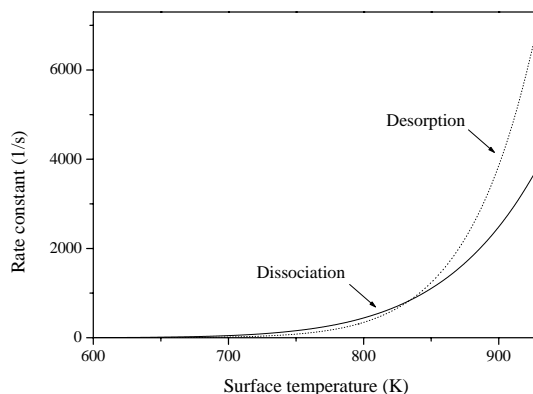
Figure 28. Rate constants for two reaction pathways as a function of temperature.

Dissociation dominates at low temperatures, but if the surface is heated very rapidly, only a small fraction is lost to dissociation before a sufficient temperature is reached for desorption to dominate. On the other hand, since the minimum energy pathway dominates at low temperatures, slow heating will result in all adsorbates being dissociated before sufficiently high temperatures for desorption is reached. This discussion can of course be generalized for branching between any two, or more, reaction pathways. For a proper quantitative treatment it is also important to take the coverage term of the rate into account. This can be included and it can be shown how the branching ratio for the two pathways depends on heating rate [102].

An example is associative desorption of methane, CH_4, from Ru(0001). If a surface with adsorbed methyl CH_3 (and hydrogen) is heated slowly, all methyl dissociates. If on the other hand rapid laser heating is used, associative desorption of methane is achieved and allows us to investigate this high-energy pathway, the time-reversed of dissociative adsorption. We have studied this in detail and the results will be reported elsewhere [108]. Another example, which will be discussed in detail later, is associative desorption of N_2 from Ru(0001). Here the two reaction pathways are associative desorption from different surface sites. Low barrier defects lead to preferential desorption from these sites in a slow heating, TPD experiment, whereas rapid laser heating lead to desorption from the terrace sites, where the activation energy but also the pre-exponential is higher.

The difference between pre-factors used in the calculation above is rather high for desorption vs. dissociation. Although, when looking at desorption from majority terrace vs. minority defect sites a simple approximation is that $\nu_{defects} = \rho_{defects} \cdot \nu_{terrace}$. With defect densities ($\rho_{defects}$) less than a percent the big difference in pre-factors used is thus very reasonable.

7.4 Laser-induced surface damage

When using powerful lasers to heat the surface, we have to make sure that damage of the crystal is avoided. Certainly the surface temperature during the laser heating has to be below the melting point of the crystal. Furthermore, when a material is exposed to a T-jump of several 100 K within 100 ns in the uppermost layer, enormous temperature gradients on the order of 10^9 K/m are built up and invoke a lot of stress on the crystal. This can create damage of the crystal structure in the near-surface region if the strain exceeds the elastic regime of the material. This conventional picture of laser damage of materials is well known because of its importance to high power laser mirrors and materials. Other, non-stress related mechanisms can also induce damage. Some examples of damage and our findings will be discussed here. Special precautions were taken to make sure no laser-induced damage of the Ru(0001) surface occurred during the experiments. The bottom line is that we did not see any evidence for damage.

Frohn *et al.* investigated the effect of irradiating a Pt(111) surface with a Nd:YAG laser (10 ns, 1064 nm) [109]. The surface was investigated on the microscopic level with a Scanning Tunneling Microscope (STM) *in situ* before and after irradiation with a single laser pulse. They found that the threshold for damage observable with STM was at a T-jump of ~500 K. The damage was assigned to creation of screw dislocations and dislocation lines caused by slip along the {111} planes of the bulk. It was found that one T-jump of 700 K introduced a defect density of approximately 1 %. In another study Hoogers *et al.* used an excimer laser (120 ns, 308 nm) to irradiate a Rh(111) surface [110]. They exposed the surface to laser pulses on an area large enough for probing with LEED (low energy electron diffraction). They observed a decrease in the LEED intensity with the number of laser scans due to disordering of the surface. They discussed the damage in terms of a stress-strain model and concluded that the onset temperature for disordering is a T-jump of 650 K.

Also a non-stress related mechanism for introducing surface damage has been observed. Ernst *et al.* observed a restructuring of a Cu single crystal surface after irradiation with a 10 ns Nd:YAG laser [111]. The damage was wavelength dependent - observed for 532 nm but not for 1064 nm at the same absorbed intensity. The restructuring was thus not related to the T-jump itself but to a process directly involving the incoming photon. By STM it was found that adatom-vacancy pairs had been created. Also He-scattering was employed in the study. The mechanism of this photo-physical damage involved long-lived primary excitations of localized d-electrons through interband transitions together with phonon excitation.

In all the above studies it was found that low levels of damage could be removed by annealing, and eventually sputtering the surface. Temperature gradients depend on the heating rate and thereby on the pulse length. The dependence on wavelength makes it difficult to transfer results from one system to another. Furthermore, different materials may respond differently.

Initial laser heating experiments in our laboratory were done with a Pt(111) crystal. We stayed well below the T-jump limits were damage should occur. Still damage of the Pt(111) crystal was visible to the eye, after it had been exposed to about 15000 laser shots on the same spot in total with only a few anneal/sputter cycles in between. This damage was not measurable with He-scattering or CO TPD and is therefore not on the microscopic level. The length scale of damage is important. Small scale (microscopic) damage is readily removed by annealing. The long scale damage seen on Pt(111) does not anneal out, but also it introduces little microscopic defects. Therefore the surface science is probably not too affected by this.

A possible explanation for the long scale damage is "macroscopic surface rippling", known from laser mirror damage. The process is initiated by some kind of irregularity, or creation of adatom-vacancy pairs [111], at the surface that permits coupling of light into surface plasmon waves from an incident laser beam [107,112]. Further incident light beam interferes with the surface plasmon wave to form a local interference pattern, or grating, in e.g. electron density or temperature, into which further light could couple, eventually cause melting or actual dislocation of the surface atoms in the "grating". The grating formation enhances coupling into the surface, and damage builds up in a positive feedback mechanism. This interference is present due to the spatial and temporal coherence and the polarization of the incoming light. We thus reduced the degree of coherence and polarization of the laser light. Coherence was reduced by sending the beam through a long optical fiber and removing the tuner from the laser cavity, which broadened the spectral range to a few nanometer and destroyed the phase coherence. Transmission through the fiber also scrambled the polarization, checked by measuring the intensity after passing a rotatable linear polarizer.

Some experiments with laser heating of polycrystalline Ta and Ni were done to investigate the surface damage. Damage was monitored with a light microscope. It was shown that the threshold for damage was not related to the peak intensity (the T-jump) but to the fluence, i.e. the number of photons absorbed. This is consistent with the photo physical mechanism suggested by Ernst *et al.* [111]. Sending the laser light through a fiber reduced the damage of the surface significantly. The metals used were not clean on a microscopic scale, and the experiments were done under low vacuum or

in air. It is unclear how this affected the results. The important finding is the reduced damage when minimizing the coherence and polarization of the light. The fluence-threshold for damage increased by approximately a factor 10. Also, it was found that different facets of the polycrystalline Ta and Ni surfaces showed different degrees of damage for the same exposure, some with no visible damage at all. It is therefore necessary to use a facet like the one of the single crystal of interest to draw definitive conclusions.

Experiments on Ru(0001) were progressed very carefully. We made sure that the same spot on the surface was only exposed to a low number of shots, 60 at max, before the crystal was annealed to high temperatures. If a high number of shots were necessary to achieve high S/N (signal to noise) in desorption, the crystal was moved a bit, thus exposing a new non-irradiated spot to the laser. It was possible to cover up to 60 spots on the surface, and thus gaining high S/N. The surface quality before and after laser irradiation was investigated with specular He-scattering [113] and CO TPD, both techniques being very sensitive to defects. No problems were ever observed. Also no macroscopic damage, visible to the eye, was ever seen. It seems that the experimental procedure made sure that no surface damage was induced by the laser heating of Ru(0001). Furthermore, it may certainly be possible that Ru is more immune against creation of laser damage, e.g. Ru is a much harder material compared to Pt and that Ru is more immune against the photo physical damage. We were satisfied with damage never showing up, though, and did not study this in detail.

7.5 Surface temperature measurement

As already discussed, the surface temperature plays a major role in describing the laser induced desorption. As shown previously in this chapter, the temperature can be calculated if we know the exact intensity deposited at the surface by the laser pulse. Gaussian temporal and spatial profiles were used in the calculation. This represents quite well the temporal pulse shape of the Alexandrite laser. The spatial profile, after propagating through the fiber, is also nearly Gaussian. But when the beam is imaged onto the surface, we do not know the exact spot size on surface. Also the temperature dependence of the material parameters κ, ρ, c and R was neglected. Instead of only calculating the temperature, an indirect measurement was also made.

It is not easy to measure the surface temperature T_s during the T-jump, since only the surface is heated, and the time scale of temperature variation is very short. A non-surface contact method is needed. One way is to desorb an adsorbate with the laser-induced T-jump and measure the distribution of translational energies, assuming the molecules are in thermal equilibrium with the surface. For CO/Ru(0001) the activation barrier to desorption is given by the binding energy, i.e. there is no additional barrier between the molecule in the gas phase and the adsorbed state [114,115]. When the surface is heated with the laser, molecules are thermally activated and are anticipated to leave the surface with translational energies determined solely by the surface temperature. We can write a theoretical expression for the expected TOF distribution depending on the surface temperature. Measuring the TOF and fitting the data to this expression gives us thereby T_s.

Let us first look at the theoretical distribution. Molecules desorbing from a surface can be compared with molecules leaving an oven through a small hole (an effusive source). Consider first an oven at a temperature T. A gas at thermal equilibrium inside the oven can be described by a Maxwell-Boltzmann distribution of velocities:

$$g(v)dv = \frac{4b^{3/2}}{\sqrt{\pi}} v^2 \, exp\left(-bv^2\right)dv \qquad (7.15)$$

Where v is the scalar velocity (i.e. the speed), $g(v)dv$ is the number-density of molecules with a velocity in the range $(v,v+dv)$ and b is a constant describing the width of the distribution $\left(b = m/2k_BT\right)$, where m is the mass, T the temperature and k_B the Boltzmann constant. Now, let there be a small hole in the oven. The probability that a molecule leaves the oven is proportional to its velocity; faster molecules hit the wall more often. Therefore the flux of molecules out of the oven, in the normal direction, is given by:

$$j(v)dv = v \cdot g(v)dv \qquad (7.16)$$

Eq. (7.15) describes a gas (in equilibrium) momentarily present in a given volume, whereas eq. (7.16) describes a gas flux impinging on a surface, passing a "surface" or desorbing from a surface. We measure the flight times from surface to a detector, and therefore need to convert the distribution from velocity to time domain. Conservation of the number of particles, $j(v)dv = n_{flux}(t)dt$, allows us to write the flux as a function of time in the following way:

$$n_{flux}(t) = j(v)\frac{dv}{dt} \qquad (7.17)$$

Since $v=x/t$, where x is the flight distance from source to detector, the Jacobian (dv/dt) results in a factor t^{-2}. The time-of-flight distribution in flux domain is thus given by:

$$n_{flux}(t)dt = 2b^2 x^4 t^{-5} \, exp\left(-b(x/t)^2\right)dt \qquad (7.18)$$

The detector, in our case a mass spectrometer, is sensitive to the density of molecules in the detection volume. Fast molecules spend less time in the ionizer region. The flux and density distributions are therefore related by $n_{flux}(t) \propto v \cdot n_{density}(t)$ and we can write the expression for the desorbing molecules in a form, which can be used to fit the TOF data:

$$n_{density}(t)dt = at^{-4} \, exp\left(-b(x/t)^2\right)dt \qquad (7.19)$$

Here a is a normalization constant, $b = m/2k_BT$ and x is the flight distance. We can calculate the flux weighted mean translational energy (of molecules desorbing from a surface) by averaging over the Maxwell-Boltzmann distribution and find $\langle E_{trans} \rangle = 2k_BT$.

7.5.1 Results

To measure the temperature rise due to the laser irradiation, we dose the Ru(0001) surface with 10 L CO at 425 K, resulting in a coverage of approximately 0.25 ML, i.e. a partly saturated, well ordered $\sqrt{3}x\sqrt{3}$ overlayer [116]. We then cool the sample to room temperature and perform the laser-induced thermal desorption (LITD) of CO, measuring the TOF distribution. The measured TOF is a sum of TOF's from spots all over the surface, with 10-20 shots on each spot. The TOF was fitted with eq. (7.19) varying the two parameters: the temperature T and the "amplitude" a. Figure 29 shows a typical measured CO TOF and the fit. As shown earlier, the molecules desorb over a range of temperatures. This would result in a broader distribution, than just described by eq. (7.19). But it is clear from Figure 29 that there is a good agreement between data and the fit of one desorption temperature, in this case T_{des}=812 K. This, and the fact that the calculation in section 7.2.3 showed that the main fraction of the molecules desorb in a narrow temperature range close to the peak temperature, tells us that the assignment of "one temperature" is plausible.
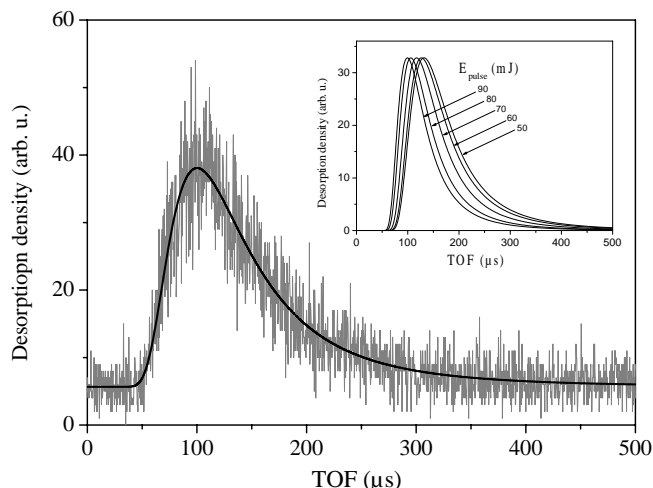
Figure 29. Time of flight distribution for CO LITD from Ru(0001) after a temperature jump induced by a 130 ns laser pulse of 60 mJ with the sample initially at room temperature. The solid curve represents the fit using a flux-weighted Maxwell-Boltzmann distribution (eq. (7.19)). The insert shows fits to CO TOF's for laser pulse energies ranging from 50 to 90 mJ (The corresponding fitted temperatures are shown in Figure 30).

As an insert in Figure 29 are shown only the fits to CO TOF's under different laser intensities. The TOF clearly shifts to shorter flight times at higher laser intensities, and the resulting higher surface temperatures. Figure 30 shows the surface temperature jump, as a function of laser pulse energy, obtained by fitting the CO desorption TOF. The desorption yield decreases strongly with the temperature during the T-jump, and the lowest used pulse energies represent approximately the detection limit, where a reasonable S/N could be achieved. Measurements for two different temporal pulse lengths are shown. At some point the Alexandrite laser rod was replaced and one of the consequences was a change in pulse length from 130 to 100 ns. Most of the nitrogen LAAD experiments have been done at 130 ns. It is evident that the shorter pulse results

in a higher temperature at same pulse energy. This is the natural consequence of depositing the same amount of energy in shorter time.

The peak temperatures in the T-jumps have been calculated using eq. (7.9), where eq. (7.12) was used to determine the peak intensity I_0 from the measured pulse energy and beam diameter. The laser beam is transmitted through a fiber with inner diameter 0.4 mm and focused onto the sample with a lens. The magnification is 3X and the beam diameter at the sample is thus 1.2 mm, by assuming perfect geometrical optics imaging from the fiber tip onto the surface. A measurement outside vacuum confirmed this within a few tenth of a mm. The angle of incidence was 57° (to the surface normal) and the spot on the surface is elliptic. Therefore eq. (7.9) was modified by multiplying the right hand side with the area ratio of an ellipse and a circle. This results in the following formula for the T-jump, only valid under the conditions just outlined.

$$T_{peak} - T_0 = 5.7 \cdot \frac{E}{\sqrt{t_p}} \qquad (7.20)$$

The pulse energy is inserted in J, the pulse length in sec and the constant has units of K/J·s$^{1/2}$. T_0 is the bias temperature. The pulse energy used in the formula is the value measured outside the UHV chamber. A correction for the transmission through the chamber window is included in the constant.

Using the above formula, the T-jumps are calculated and compared with the values determined by CO LITD. The calculated values depend strongly on the peak intensity and thereby on the estimated area of the laser beam spot on the sample. Determination of the exact beam spot size on the surface is very difficult, and the diameter of the laser beam is therefore allowed to vary until the best agreement with the temperatures from CO LITD is obtained. The results are shown in Figure 30. For the 130 ns pulse best agreement was found for a laser beam spot diameter of r_p=1.45 mm, and for 100 ns we found r_p=1.37 mm. The deviation from the measured/assumed diameter of 1.2 mm is thus very small.

We would expect that the measured T-jump depends linearly on the pulse energy, and that this straight line would intersect (E_{pulse}=0, T-jump=0). From Figure 30 it can be seen that this is clearly the case for the 100 ns pulse, whereas some deviation is observed for the 130 ns pulse. It is important to remember that we are comparing a calculated value for just the peak temperature with a value determined fitting a TOF of desorbing molecules. As the calculations in section 7.2.3 showed the molecules desorb over a range of temperatures, close to the peak temperature though[*]. The overall agreement between the model calculations and the measurements do confirm the assignment of one temperature.

---

[*] Shot to shot fluctuations of the laser pulse energy are only on the order of 5 %, and will not lead to significant changes in TOF's from shot to shot
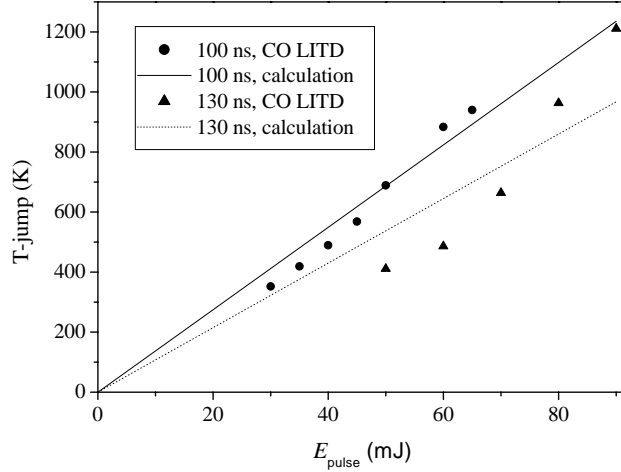
Figure 30. The surface temperature jump (bias temperature subtracted from fitted temperature) as a function of laser pulse energy during laser heating estimated from fitting CO LITD time of flights. Results for two temporal pulse lengths (t_p) are shown: 100 ns (circles) and 130 ns (triangles). The calculated T-jumps are shown as straight lines: 100 ns (solid line) and 130 ns (dotted line).

Allers *et al.* showed in an experiment measuring TOF of CO during a TPD experiment, that CO desorbing from Pt(111) and Ni(100) follows a Maxwell-Boltzmann distribution with average energy ~$1.9k_BT_s$, i.e. nearly $2k_BT_s$ and a desorption temperature, i.e. the temperature from the fit, very close to the surface temperature, T_{des}~$0.95T_s$ [117]. Thus, thermal desorption of CO should measure the surface temperature. There is no dynamic reason, i.e. a barrier, to preclude this. LITD measurements by Wedler and Ruhmann showed that CO desorbed from Fe(110) [118] using a 30 ns laser for the T-jump could also be well described by a Maxwell-Boltzmann distribution with a desorption temperature T_{des} equal to a calculated peak temperature T_{peak}, using the same model described earlier in this chapter. However, this was only possible for rather low laser intensities (T_{peak}<600 K). At higher laser intensities it was found that T_{des}<T_{peak}. It was suggested that this was due to the fact that, complete LITD occurred at high intensities before the T-jump reached its maximum values [119]. We find no evidence for a similar behavior here as evident from Figure 30. This would otherwise show up as a deviation from the linear dependence of the T-jump as a function of pulse energy, where the measured T-jump would level off and saturate in the limit of high pulse energies. LITD by Burgess *et al.* with 10 ns laser pulses of CO from Cu(100) showed Maxwell-Boltzmann behavior at all intensities/ temperatures, but T_{des} from the fit was lower than the T_{peak} predicted from TPD [120]. It is unclear, though, how this temperature T_{peak} was determined.

We did observe that the presence of impurities and/or defects could influence the measured T_{des}. This showed up as changes in T_{des}, up to ± 50 K, for repeated CO LITD experiments under same conditions of laser intensity etc. Careful cleaning of the sample removed these problems and resulted in reproducible results. We kept the number of laser shots on the same spot low and obtained S/N by collecting TOF's from a large number of different spatial spots on the surface. This minimizes the risk of inducing surface damage. Investigations of the surface after irradiation with

74

specular He-scattering and CO TPD indicated that the laser irradiation under our conditions did not create any defects.

We took great care to measure the temperature via laser desorbed CO using the same conditions as the "real LAAD experiment" where T_s is to be known; Making sure that e.g. the laser beam focus and pulse energy were the same.

7.6 Conclusion

The calculations of laser heating of a metal surface demonstrated that irradiating a metal surface with a short laser pulse results in a T-jump with approximately same duration as the laser pulse. Desorption is occurring over an even shorter time range, and TOF techniques can thus be used to measure translational energy distributions of the desorbing molecules. Although desorption is occurring over a finite temperature range, it was shown that the main fraction desorbs close to the peak temperature, resulting in nearly isothermal desorption.

LITD experiments of CO desorbing from Ru(0001) showed that the TOF's were described by Maxwell-Boltzmann distributions and the temperature (T_{des}) from the fit described the surface temperature (T_s). The surface temperatures measured this way were in good agreement with the calculated values and confirm the assignment of one temperature to the T-jump.

It is known that the rapid laser heating can induce damage to the crystal in the near surface region under some circumstances. Some of these findings in the literature were discussed, and it was demonstrated that damage to the Ru(0001) crystal was not observed under the conditions employed by us.

8 Laser Assisted Associative Desorption of N_2 from Ru(0001)

8.1 Introduction

After having introduced laser assisted associative desorption (LAAD) in the previous chapter, the technique will now be applied. It will be demonstrated here that LAAD provides great insights into the dynamics of associative desorption and its time reversed process, dissociative chemisorption. This technique does *not* require laser state-resolved detection and is generally applicable, regardless of the height of the barrier or whether it is along a translational or vibrational coordinate. Furthermore, it is quite insensitive to the presence of defects and steps on the surface and can be used over a wide range of adsorbate coverages. In this chapter a dynamical study of the interaction of N_2 with a Ru(0001) surface will be presented. We will show that these experimental results are in excellent agreement in detail with density functional theory (DFT).

First a very brief summary of the interaction of N_2 and N with Ru(0001) which has attracted much attention recently due to the possible role of supported Ru as an end catalyst for NH_3 synthesis. The rate-limiting step is the dissociative chemisorption of N_2. On Ru(0001), dissociation is strongly activated. Low coverage states of N adsorbed on Ru(0001) ($\Theta_N = 0.25$ and $0.33\,\text{ML}$) are well known and have been characterized experimentally [83,121] and theoretically [32,75]. We have shown that a series of higher coverage states are also formed in addition by exposure to a N atom beam, ultimately saturating at a coverage $\Theta_N \approx 1\,\text{ML}$ (see chapter 6). By comparing with DFT calculations of the binding energies of N on Ru(0001) as a function of N coverage it was suggested that all states for $\Theta_N \geq 0.5\,\text{eV}$ were only *metastable*, with lifetimes determined by the barrier between gas phase N_2 and the adsorbed N.

The essence of the LAAD application described here is to measure the translational energy distribution of N_2 formed by associative desorption from a Ru(0001) surface following a laser induced temperature jump. Neglecting tunneling and coupling to the lattice, we anticipate that the total energy of the desorbing N_2 is given approximately by the barrier height relative to the $N_2 + \text{Ru}(0001)$ asymptote. Because both internal and translational excitations are anticipated in this associative desorption [20,31], the overall measured translational energy distribution represents a sum of the translational distributions for each internal state weighted by the population of that state. If the vibrational state $\nu=0$ is sufficiently populated to be detected, then the translational energy observed for this state corresponds approximately to the barrier height, since rotational excitation is small for this system [31].

8.2 Results

After exposure of a Ru(0001) crystal to a N atom beam to produce a N atom coverage Θ_N LAAD experiments were performed by irradiating the surface with a pulsed

Alexandrite laser with a wavelength of 750 nm and duration 130 ns. Since the wavelength is in the near IR, laser induced photochemistry is highly unlikely. Thus, the resulting excitation of the surface is well described as a thermally induced temperature jump (T- jump). The surface temperature T_s is shown to basically follow the laser temporal profile as described in section 7.2 (Figure 23).

Since the T-jump and resulting N_2 desorption occur only for ca 100 ns, time of flight (TOF) techniques can be used to measure the translational energy distribution. The desorbing N_2 was detected normal to the surface with a differentially pumped quadropole mass spectrometer. The ionizer is placed 97 mm from the surface and views a solid angle of 8×10^{-4} sr. To determine absolute TOF from the surface to the detector, extensive calibrations of the TOF delays through the mass spectrometer were necessary and a convolution over finite ionizer length (5 mm) was performed in the analysis (see section 2.4). Most LAAD experiments were performed with N^{15}, due to a lower background at mass 30. No isotope effect was observed.

Because laser irradiation is known to cause surface damage under some circumstances [107,122,123] (see section 7.4), we took special care to only irradiate with a few laser shots (typically 5-40) at a given spot on the surface while collecting TOF data. Then, the laser was moved to a new non-irradiated spot and the LAAD experiment was continued, etc. Since the sample movement can be controlled very precisely, the laser beam position is kept fixed and the sample is then moved around in small steps. In this way we preserve the same angle of incidence. Typically 40-60 separate spots were studied on the surface for a given prepared Θ_N. There was no observable difference from spot to spot or with different number of laser shots at each spot, except for increased S/N with increasing number of shots, of course. Nor were there any differences from day to day as the experiments were repeated under identical conditions. All indicate that laser damage is not a problem under our experimental conditions. In addition, further investigations of the surface quality after LAAD showed no increase in surface defects as observed by CO TPD and specular He atom scattering.

The T-jump achieved for a given laser power was calibrated by measuring the TOF of CO laser desorbed from the Ru(0001) surface. As described in section 7.5, TOF distributions were well described by Boltzmann distributions desorbing at $2k_BT_s$.

An example of the TOF distribution for N_2^{15} obtained by LAAD for an initial coverage $\Theta_N = 0.6$ is given in Figure 31, representing an average of 1800 laser shots spread over 60 spatial spots on the surface. The yield of N_2 desorbing per laser shot is very small («10^{-3} ML), therefore the TOF produced by many laser shots could be averaged without changing Θ_N significantly. Since the time window in the TOF data taking was small (320 ns), raw TOF data were smoothed using a 5 point Savitzky-Golay algorithm. The corresponding translational energy is given at the top of Figure 31. It is evident that the overall TOF distribution consists of a series of partially overlapping narrower peaks. The spacing in energy between the peaks is approximately equal to the vibrational quanta of N_2, which is 0.28 eV for N_2^{15}. We assign these individual peaks to desorption of N_2^{15} in different vibrational states ν, with the higher vibrational states occurring at longer TOF, i.e. lower translational energy. Assuming $\nu = 0$ is sufficiently populated to be observed in the TOF, then the high energy threshold corresponds approximately to the barrier height V^*.
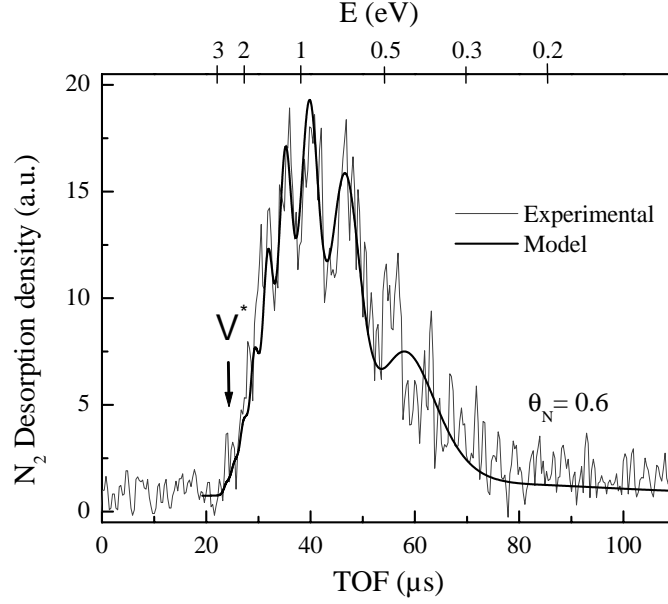
Figure 31. TOF distribution for laser assisted associative desorption of N_2[15] following a T-jump to 875 K. The translational energy (*E*) is indicated on the top axis. The energy of the barrier V^* (relative to gas phase N_2) is marked with an arrow.

8.2.1 Model

In order to test this interpretation more quantitatively, a model for associative desorption of N_2 is described in the following.

8.2.1.1 Desorption model based on detailed balance

The traditional way to analyze desorption data is based on the principle of detailed balance. Let $D_\Theta(E,T_s)$ be the desorption density for Θ_N and T_s at translational energy E. Neglecting rotation of the N_2, which is known to be small anyway [31], we can write this desorption density [18] as

$$D_\Theta(E,T_s) \propto \sqrt{E}\, exp(-E/k_B T_s)\sum_v exp(-\varepsilon_v/k_B T_s)S_\Theta(E,v) \qquad (8.1)$$

where ε_v is the zero point corrected vibrational energy of the desorbing N_2 in vibrational state v and $S_\Theta(E,v)$ is a dissociative sticking coefficient for $N_2(v)$ at incident translational energy E on a surface with coverage Θ_N. Only the normal direction is considered. Considerable experience with fitting molecular beam experiments of dissociative sticking suggests that $S_\Theta(E,v)$ is empirically well represented by the following flexible form [18,22,124]

$$S_\Theta(E,v) = P(v)\frac{1}{2}\left[1 + erf\left(\frac{E - E_0(v)}{W}\right)\right] \qquad (8.2)$$

where $P(\nu)$ is a relative intensity factor for sticking of vibrational state ν, E is the translational energy and $E_0(\nu)$ is the center point of the "S" shaped *error* sticking function for the vibrational state ν and W is the width of the *error* function. $E_0(\nu)$ is given by $E_0(\nu) = U^* - \eta_\nu \varepsilon_\nu$, where U^* is a barrier defined by $U^* = E_0(0)$ and $\eta_\nu \varepsilon_\nu$ is the lowering of the effective barrier for the state ν (η_ν is the vibrational efficacy). The figure below shows (some of) the sticking functions for each vibrational state.
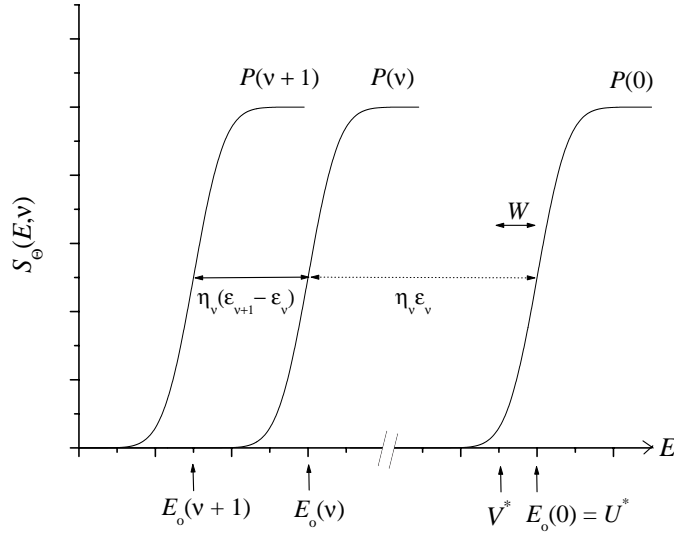
Figure 32. Sticking functions for each vibrational state ν, plotted as a function of translational energy E. The centers $E_0(\nu)$ and the width W are indicated. Also the barrier $U^*=E_0(0)$ as well as the minimum energy barrier V^* are indicated.

In the classical 1-dimensional picture, the sticking probability would be 0 for translational energies below the barrier ($E<U^*$) and 1 for $E>U^*$ and $S(E)$ would thus be a step-function. The finite width W has been explained by quantum effects [125], i.e. tunneling through the barrier and reflection from the potential wall at energies above the barrier height, and due to a distribution of barrier heights, where the center point E_0 is the "central barrier" (U^*). W could depend on T_s, as observed in some experiments [126,127]. This has been interpreted in terms of a broadening of the distribution of barriers by thermally induced corrugation [22,128,129], and to a T_s dependence due to energy exchange between the incident molecule and lattice phonons [130]. This will be neglected here. W could change with ν. This is neglected, though, and a fixed value of W will be used later.

As evident from Figure 32, it is not possible to define a single unique barrier due to the gradual increase of *S(E)*. One can either choose the "central barrier" in terms of $U^*=E_0(0)$, or let the barrier be equal to the "minimum energy barrier" defined by the threshold of $S_\Theta(E,\nu=0)$. The threshold for sticking is not exactly defined, but a good estimate is to subtract the width from the center, thus defining the minimum energy barrier by: $V^* = U^*-W = E_0(0)-W$.

8.2.1.2 Direct desorption model

Instead of using the approach of detailed balance, A.C. Luntz derived a direct model to describe associative desorption of an activated system without assuming detailed balance [131]. This model is used to analyze the N_2 LAAD data and will be described below.

Conservation of the total energy from the transition state into the desorbed product implies approximately that,

$$E_{tot} \approx U^* + k_B T_s = E + \varepsilon_v + \delta \qquad (8.3)$$

where U^* is the barrier and $k_B T_s$ the thermal energy in the transition state, $\frac{1}{2}k_B T_s$ from the reaction coordinate and $\frac{1}{2}k_B T_s$ for a vibrational mode perpendicular to the reaction coordinate. Only molecules desorbing in the normal direction are detected and it is assumed that the process is adiabatic with respect to hindered rotation, and translation parallel to surface, i.e. they do not end up in translation normal to the surface or vibration of N_2. E is the translational energy and ε_v is the zero point corrected vibrational energy. δ reflects two terms; First, the energy loss or gain from translation and vibration to modes of the lattice or other N_2 modes (rotation) during the desorption event. Secondly, a distribution of barriers. It is assumed that δ is given by a Gaussian distribution of width W and with $\langle\delta\rangle \approx 0$. The total desorption probability is a sum of probabilities from individual vibrational states centered at translational energies

$$E_0(v) = E_{tot} - \eta_v \varepsilon_v \qquad (8.4)$$

where $\eta_v \varepsilon_v$ is the lowering of the effective barrier in producing state v (η_v is the vibrational efficacy). Thermally averaging this leads to the desorption density

$$D_\Theta(E,T_s) \propto \sqrt{E}\, exp(-E/k_B T_s) \sum_v exp(-\varepsilon_v/k_B T_s) \left\{ P(v) \left[1 + erf\left(\frac{E - E_0(v)}{W} \right) \right] \right\} \qquad (8.5)$$

$P(v)$ is the relative probability of desorption into state v. Identifying the terms inside the {} as the sticking function, $S_\Theta(E,v)$, for dissociative chemisorption of the vibrational state v, leads to a form for $D_\Theta(E,T_s)$ known from the detailed balance arguments (see eq. (8.1) and eq. (8.2)) [18]. Details about this direct desorption model can be found in ref. [131].

The observed TOF desorption density, $D_\Theta(t)$, is a function of time. This can be related to the desorption density as a function of energy by, $D_\Theta(t)dt = D_\Theta(E,T_s)dE$ i.e. $D_\Theta(t) \propto \frac{1}{t^2} D_\Theta(E,T_s)$. This relation was employed and eq. (8.5) was used to fit the data. The TOF distribution is thus "described" by: $E_0(v)$, W, $P(v)$ and T_s, where the barrier enters via $E_0(v)$, or rather $E_0(0)$, as discussed below.

How do we extract a barrier? The Gaussian barrier distribution does not allow a unique definition of a minimum. A good approximation, though, is to subtract the width W

from the "center barrier" U^*, which, from eq. (8.3) and eq. (8.4), is given by $U^*=E_0(0)$ - $k_B T_s$. We thus find for the minimum energy barrier:

$$V^*=U^*-W \qquad (8.6)$$

This value for the minimum energy barrier is the one most appropriate to compare with the DFT calculations presented later. Detailed balance will be applied later, and the parameters $E_0(v)$, W and $P(v)$ determined by LAAD will be used to calculate sticking probabilities to compare with molecular beam experiments. Thermal experiments measure the activation energy to dissociation, i.e. the adiabatic minimum energy barrier which will be directly compared with V^* found by LAAD.

We now make several assumptions about the parameters. To describe vibrational inversion in desorption, which is known to be the case for N_2 desorbing from Ru(0001) [31], "limitations" on the parameters in eq. (8.5) are introduced. The approach we used, is to describe the vibrational population by keeping the vibrational efficacy fixed and letting $P(v)$ vary with v. $P(v)$ then represents the intensity distribution of the various TOF peaks. Another approach is to choose $P(v)\sim 1$, approximately constant for all v, and let the vibrational efficacy, η_v, vary to describe the observed vibrational population in desorption, e.g. $\eta_v>1$ describes an inverted vibrational distribution. Murphy *et al.* assumed that $P(v)=1$ for all v, i.e. $v=0$ and 1 which where the only states they detected, and found for the vibrational efficacy that $\eta_v=1.3$ [31]. That vibrational inversion in principle can be described by both approaches can be verified by calculating the desorption yield of each state by integration of the state dependent desorption flux, which is found by removing the summation over v from eq. (8.5) and multiplying the state dependent density with the velocity ($\propto \sqrt{E}$).

Looking at Figure 31 it is evident, that the v states are separated in translational energy by ε_v, consistent with an assumption of $\eta_v=1$, constant for all v. This assumption of a high vibrational efficacy is consistent with a barrier strongly in the vibrational coordinate.

In order to avoid arbitrarily assigning a value for $P(v)$ to each peak, we have used the approach of information theory [132,133] to reduce the assignment of values to $P(v)$ to one parameter: The so called vibrational "surprisal" λ, describing the dynamical constraints. This approach has been very successful in describing detailed state resolved atom-molecule collision experiments in the gas phase [132,133]. We want to determine the distribution of vibrational states v in an exothermic reaction, where the total energy E_{tot} is released into vibration and translation. If we have no prior information about the outcome of the reaction, the simplest approach would be to assume that the E_{tot} is distributed statistically into v according to the final density of states. This prior-expectation probability distribution, $P^0(v)$, is called the statistical distribution. However, associative desorption is reflecting a complex potential energy surface and the dynamics of the process may very well result in a distribution, $P(v)$, different from $P^0(v)^\#$. For example, barriers along the vibrational coordinate should

---

The term "surprisal" is related to: If you don't get what you expected beforehand i.e. if $P(v)\neq P^0(v)$, then you are "surprised".

produce strong vibrational excitation, while barriers along the translational coordinate results in molecules preferentially desorbing with translational energy and only little energy in vibration. The simplest way to describe the dynamical effects that produce $P(\nu)$ is via information theory to characterize the minimum necessary dynamic constraints. This approach has been very successful in describing state-resolved atom-molecule reactions in the gas phase in terms of a few so-called "surprisal" parameters λ_i. For example, vibrational state distributions in exothermic chemical reactions like $AB+C \rightarrow A+BC(\nu)$, are described by a single vibrational surprisal parameter λ. Actually, the same λ also describes the selective vibrational energy consumption in the reverse endothermic reaction.

Assuming the molecule is described as a rigid-rotor harmonic oscillator, application of information theory to associative desorption of N_2 gives

$$P(\nu)= P^0(\nu)exp(-\lambda f_\nu)/Q \tag{8.7}$$

where $f_\nu \approx \varepsilon_\nu / E_{tot}$ is the fraction of the total energy available for desorption that is present as vibrational energy in a given state ν and Q is a normalization constant such that $\sum_\nu P(\nu)=1$. The statistical distribution to produce the vibrational state ν, given the total energy E_{tot} available for desorption, is given by $P^0(\nu)= 2.5(1- f_\nu)^{3/2} E_{tot}^{-1}$. A wide range of associative desorption processes can be described this way: When $\lambda=0$ a statistical distribution is described. When $\lambda<0$, we have greater importance of vibrational excitation relative to translation (excess vibrational energy release), even vibrational inversion for $\lambda<<0$. When $\lambda>0$, translational excitation dominates. $P(\nu)$ is determined by one parameter λ for all ν. This means we can describe the vibrational state distribution by fitting λ to the observed distribution. As will be clear, it turned out that the same value for λ described all N_2 LAAD experiments, under all conditions, reported here.

Given the above model [131], $D_\Theta(E,T_s)$ and hence the TOF distribution is determined by only three parameters: V^*, λ and W, as well as T_s. For the LAAD shown in Figure 31 $T_s= 875$ K. The three parameters in the model are well constrained by the observed TOF distribution. A value of $W \approx 0.1$ eV is necessary from the partial resolution of the individual ν states in the TOF. In principle, W could vary with ν and T_s, but this is neglected and we assume a constant value for W. λ must be a large negative number to make $P(\nu)$ peak at higher ν, i.e. to describe a strong vibrational inversion. V^* is chosen so that the high kinetic energy threshold in the model agrees with the experimental TOF. The theoretical model curve in Figure 31 is produced with the "best fit" parameters $W = 0.09$ eV, $\lambda = -12$ and $V^* = 2.5$ eV. The actual labeling of the ν for each peak is not possible. This produces some uncertainty in the determination of V^*. In this fit, we have assumed that desorption of $\nu = 0$ defines the threshold. If $\lambda << -12$ so that $\nu = 0$ is not sufficiently populated to be observed in desorption, equally good fits to the data are obtained with V^* correspondingly higher. However, when $\lambda >> -12$, agreement with the experiment is decidedly worse. The barrier V^* is therefore a lower limit and we thus interpret the experiment to say $V^* \geq 2.5$ eV. Clearly S/N also limits the ability to establish this lower bound, perhaps by an additional uncertainty of ± 0.2 eV.

The overall agreement between the model and experiment in Figure 31 is excellent and clearly demonstrates that the spacing between the partially resolved peaks is due to vibrational excitation. We believe the disagreement in the peak observed at 55 µs in the TOF (predicted at 58 µs) is due to a breakdown of the assumption $\eta_v = 1$ near the top of the barrier. Our measurements are fully consistent with simple adiabatic dynamics anticipated from the ab-initio potential energy surface from DFT calculations [31,32], where a high barrier was found to lie almost exclusively along the vibrational coordinate.

State resolved experiments of associative desorption of N_2 from Ru(0001) [31] showed a population inversion between $v = 1$ and $v = 0$, consistent with $P(v)$ peaking for $v \geq 7$ as observed by us. Murphy, et al. observed desorption from an individual vibrational-rotational state peaking at low (ca. thermal) translational energies, but also a tailing to much higher translational energies [31], in qualitative disagreement with us. It has been suggested that these results are strongly influenced by desorption from steps/defects [26].

8.2.2 Insensitivity to defects

Since our results are fully consistent with the anticipated dynamics on the majority terrace sites, this implies that the LAAD measurements are quite immune to the presence of minority low barrier steps and defects. There are two reasons for this. First, during a T-jump of only 100 ns, adsorbed N does not have sufficient time to diffuse to the steps/defects which otherwise might dominate associative desorption, due to the lower barrier [26]. The diffusion of N atoms on Ru(0001) has been studied with STM (scanning tunneling microscopy) by Zambelli *et al.* [134] by dissociating NO at steps on the surface and following the N atoms in time and space. They found that the N atoms are not trapped at steps or preferentially populate step sites but readily diffused away from the step site where they were "created". The spatial distribution away from the step, after some time, was described by a Gaussian, and the diffusion coefficient followed an Arrhenius expression: $D = D_0\, exp\left(- E_{diff} / k_B T_s\right)$. They determined the activation energy for diffusion to be $E_{diff} = 0.94$ eV and the prefactor $D_0 = 2 \cdot 10^{-2}$ cm^{2}s^{-1}. We can now estimate the "diffusion distance" during the T-jump from: $<x> = \sqrt{2Dt_p}$, where t_p is the laser pulse length. Using $T_s = 875$ K and $t_p = 100$ ns, we find $<x> \approx 12$ Å. The lattice constant of Ru(0001) is ~ 2.7 Å. With only approximately 0.25 % steps/defects on the surface, the probability of two N-atoms diffusing to the same defect-site is much lower than recombination on the majority terrace sites. We therefore believe, that on the time-scale of the T-jump, only the terrace sites contribute significantly to the desorption.

Furthermore, although the activation energy for desorption from defect sites is lower, the pre-exponential in the rate-constant, $k_i = v_i\, exp\left(- E_{des}^i / k_B T_s\right)$, for desorption from the majority terrace sites is much higher. A good approximation is $v_{defect} = \rho_{defect} \cdot v_{terrace}$, where ρ_{defect} is the concentration of defect sites, $\rho_{defect} = 0.0025$ is a reasonable value for our crystal. As discussed in section 7.4, if $E_{des}^{terrace} > E_{des}^{defect}$ and $v_{terrace} > v_{defect}$, $k_{terrace}$ will dominate above a certain temperature (see Figure 28). Dominant desorption from

terrace sites is only achieved due to the use of laser heating, though. At lower temperatures, k_{defect} will dominate, but the rapid laser heating raises T_s so fast that no significant desorption takes place at lower T_s.[*]

8.2.3 Temperature dependence

We also investigated the dependence on the surface temperature where desorption occurs. Two LAAD experiments were made, at the same coverage, using two different laser intensities. The desorption temperatures were 875 and 1600 K. Figure 33 below shows the two TOF distributions. Approximately the same number of laser shoots where employed for the two experiments. The lower T_s curve is enlarged by a factor 1.8. First we note that the S/N is improved at the high T_s. It also is clear, that the "vibrational resolution" is nearly washed out at the high T_s. Although the total energy available for desorption increases by 0.06 eV due to the increased $k_B T_s$ term of eq. (8.3), the observed overall shape and position in time is nearly unchanged.
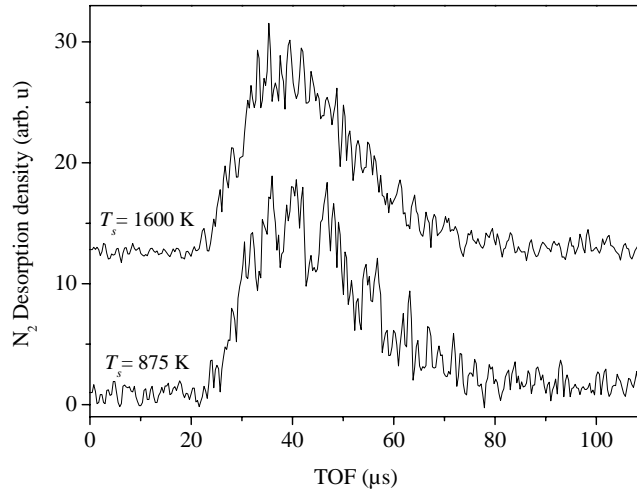
Figure 33. Measured LAAD TOF distributions for the same N-coverage, $\Theta_N= 0.6$ ML, under laser intensities where desorption occurred at 875 and 1600 K, respectively. The TOF at 875 K is the same as shown in Figure 31.

In Figure 34 the theoretical TOF distributions are calculated using the model outlined earlier. The parameters used were: $V^*= 2.5$ eV, $W=0.09$ eV and $\lambda=-12$. Averaging over the ionizer region was included. It is clear that the vibrational resolution is decreased when T_s is increased. The individual peaks from each vibrational state seem to broaden with T_s.

---

[*] At low coverage it is known that $E_{des}^{terrace} > E_{des}^{defect}$ [26]. At higher coverages $E_{des}^{terrace}$ is reduced strongly (see chapter 6 and section 8.2.5). Probably E_{des}^{defect} also reduces with coverage such that $E_{des}^{terrace} > E_{des}^{defect}$ at all coverages. Rapid laser heating is thus necessary to favor desorption from terraces at all coverages.
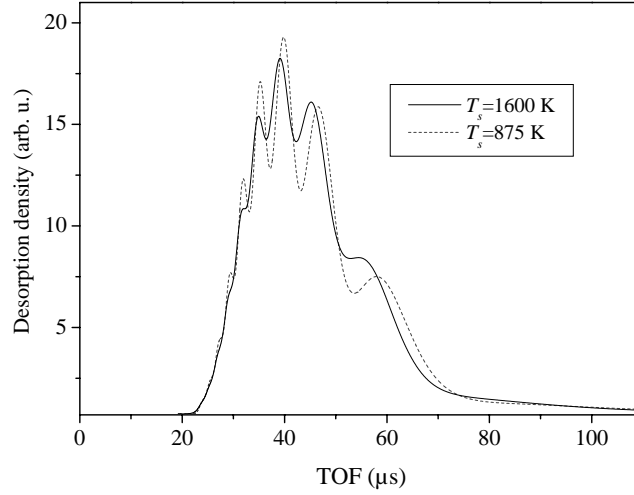
Figure 34. Calculated TOF distributions for two surface temperatures. T_s=1600 K (Solid line), T_s=875 K (Dashed line). V^*=2.5 eV, W=0.09eV and λ=-12.

Looking closer at the desorption function eq. (8.5) can give the explanation. The intensity and width of each state in the desorption is given by the overlap between $\sqrt{E}\,exp\!\left(-E/k_BT_s\right)$ and the *error* function $S_\Theta(\nu,E)$ (eq. (8.2)). In Figure 35a, $\sqrt{E}\,exp\!\left(-E/k_BT_s\right)$ is plotted for the two temperatures together with $S_\Theta(\nu,E)$ for only one state, for clarity. The center point was chosen at E_0=1.0 eV, and a width W=0.09 eV was used. All functions are scaled to same height. For increasing T_s, $\sqrt{E}\,exp\!\left(-E/k_BT_s\right)$ broadens, while $S_\Theta(\nu,E)$ remains unchanged (we assumed, that the width is independent of temperature). The overlap between the two functions is increased, resulting in desorption over a wider energy range, i.e. a broadening of each state ν. This effect is even clearer at a larger width W, shown in Figure 35b.
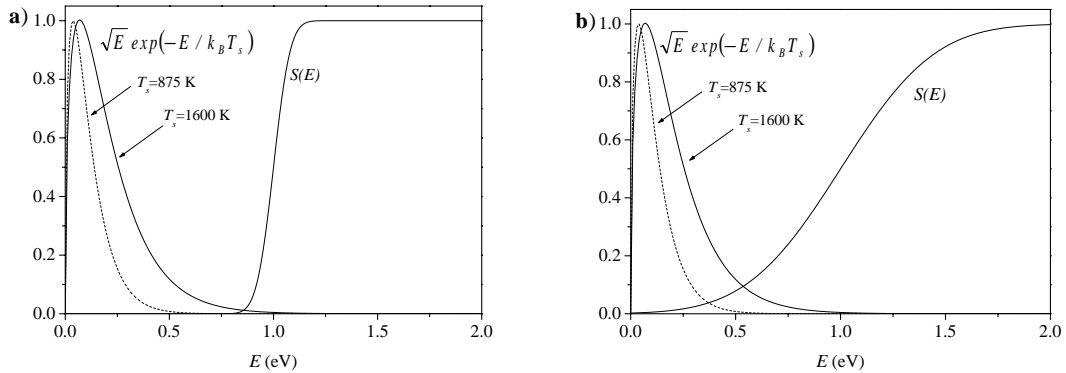
Figure 35. $\sqrt{E}\,exp\!\left(-E/k_BT_s\right)$ for two surface temperatures, T_s=875 and 1600 K, and $S_\Theta(\nu,E)$, for a state ν, where E_0=1.0 eV. All plotted as a function of translational energy E. The figure illustrates how the overlap between the two functions changes with T_s. The width of the *error* function is **a)** W=0.09 eV, **b)** W=0.5 eV.

As seen in Figure 33 (and Figure 34 as well) the shift of the TOF distribution is very small, if observable at all, as the temperature is increased. This actually confirms that

the choice of a small width W to describe N_2 associative desorption from Ru(0001) is correct. In Figure 35b $\sqrt{E}\,exp(-E/k_B T_s)$ is plotted again for T_s=875 and 1600 K, together with $S_\Theta(v,E)$ where the width now is increased to W=0.5 eV. It is clear, that the broader *error* function results in a larger overlap, and thereby a much broader desorption for each state v. Furthermore, the overlap also shifts to higher energy with increasing T_s, whereas the overlap for the narrow width is at approximately the same position in energy. To show the effect on the desorption, the TOF distributions for one state, using the functions in Figure 35a and b, have been calculated and are shown in Figure 36a and b. The peak positions of the TOF's are shifted by 0.8 µs (~0.05 eV) for W=0.09 eV and 27.5 µs (~0.34 eV) for W=0.5 eV.
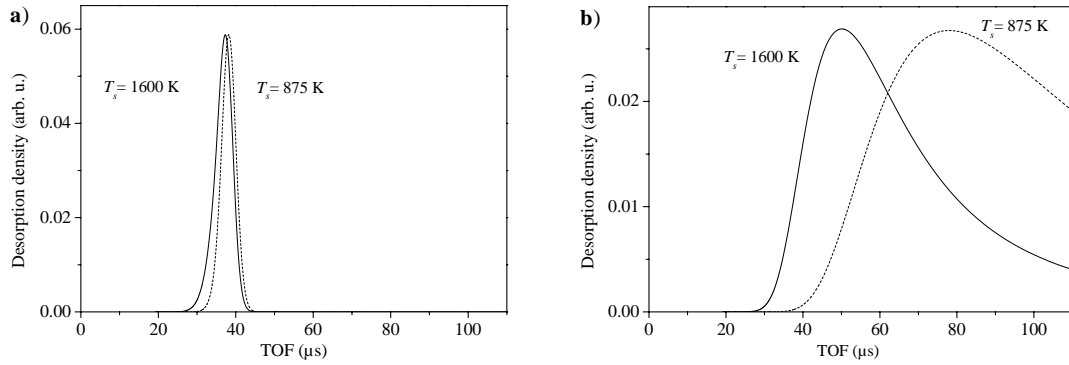
Figure 36. Surface temperature dependence of the calculated TOF distributions for one state, assuming E_0=1.0 eV. T_s=1600 K (Solid line), T_s=875 K (Dashed line). **a)** W=0.09eV, **b)** W=0.5eV.

If one would try to fit the N_2 TOF distributions, without any prior knowledge of the system, assuming that only one vibrational state was produced in desorption, it would be necessary to choose a very large width W in order to reproduce the overall rather broad observed TOF. Clearly, we would then expect to see, besides a smooth distribution without vibrational resolution, a very strong TOF dependence on T_s, similar to the one seen on Figure 36b. This is clearly not observed in the experiment (see Figure 33). The only effect of the increased surface temperature is the slight broadening of the desorption distribution for each state, illustrated in Figure 36a for one state and in Figure 34 for the total distribution. In conclusion, the observed TOF distribution is a sum of narrow TOF's originating from N_2 desorbing in different vibrational states. As mentioned earlier a narrow width of W~0.1 eV is necessary to retain the vibrational resolution. The insensitivity of the observed TOF to surface temperature further confirms that the widths have to be narrow.

8.2.4 Coverage dependence

LAAD measurements have been made as a function of Θ_N and are given in Figure 37. There is a decided shift in the TOF distribution to higher translational energies with increasing Θ_N and this is taken as evidence for an increase of the barrier with Θ_N. Although vibrational resolution is apparent at higher Θ_N, it is not observed for the lower Θ_N. Since the lower coverage states are stronger bound (larger activation energy

to desorption) it was necessary to use a higher laser intensity to achieve desorption. As explained above, a higher desorption temperature results in a thermal broadening of each vibrational state. Furthermore, because of the lower desorption yield at lower Θ_N, even at the increased temperature, it was necessary to average TOF experiments for several independent N exposures in addition to averaging each exposure over the different spatial spots to achieve high S/N. Because each N exposure produced a slightly different Θ_N, the vibrational resolution was further washed out due to the shift of V^* with Θ_N. Assuming that $\lambda = -12$ for all Θ_N, application of the model outlined previously gives the lower bounds to barriers $V^*(\Theta_N)$ marked on Figure 37 as arrows. The justification for assuming a constant λ with Θ_N is that the N-N bond length at the transition state was nearly independent of Θ_N in the DFT calculations discussed later.
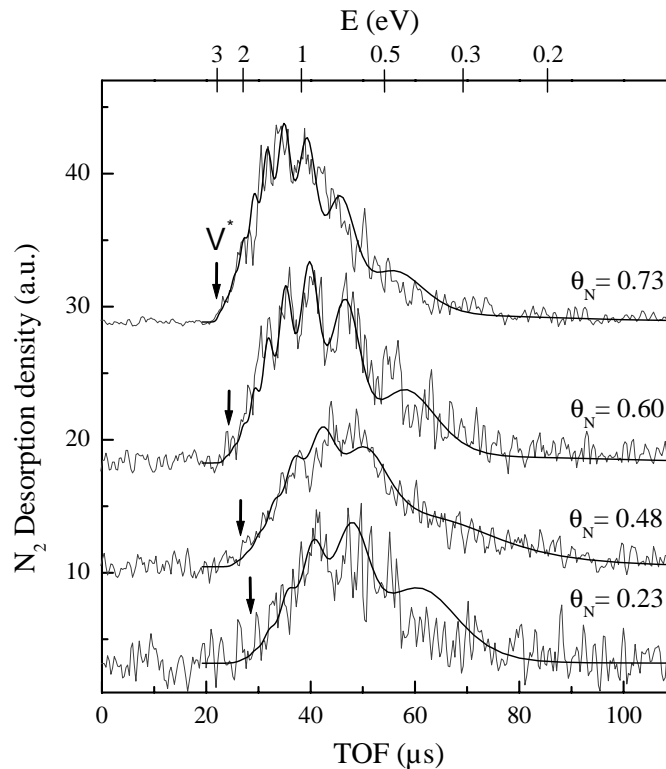
Figure 37. TOF distributions for LAAD of $N_2{}^{15}$ as a function of N-coverage. The translational energy (E) is indicated on the top axis. The energies of the barriers V^* (relative to gas phase N_2) are marked with arrows. LAAD occurred at 800, 875, 1000 and 1700 K for $\Theta_N = 0.73$, 0.60, 0.48 and 0.23 ML respectively.

The barriers are given in Table V and are seen to increase from approximately 2 eV at low Θ_N to 3 eV at the highest Θ_N. A similar increase in barrier with Θ_N was indirectly inferred from thermal desorption measurements as a function of coverage and will be discussed later.

Table V. Measured (V_{LAAD}^*) and calculated (V_{DFT}^*) values for the coverage dependence of the minimum energy barrier.

Θ_N (ML)	0.23	0.32	0.48	0.60	0.73	-
V_{LAAD}^* (eV)	1.8	2.0	2.1	2.5	2.8	-
Θ_N (ML)	0.25	-	0.50	-	0.75	1.00
V_{DFT}^* (eV)	2.1	-	2.2	-	3.5	4.8

8.2.5 DFT calculations

In order to understand the origin of the barrier increase with Θ_N, Bjørk Hammer performed DFT calculations of the transition from adsorbed N to gas phase N_2 as a function of Θ_N. The calculations will be described in the following. Figure 38 shows the results of these calculations with respect to N_2 (g) and clean Ru(0001). Four consecutive N_2 desorption events (A, B, C, and D) are described in a c(4 x 4) surface super cell which initially accommodates eight N atoms in its eight hcp sites. The RPBE exchange-correlation functional is used [94]. See also ref. [70] for further calculational details. The surface super cell is repeated periodically whereby effectively N_2 desorption in the range $0.25 \le \Theta_N \le 1$ is investigated.
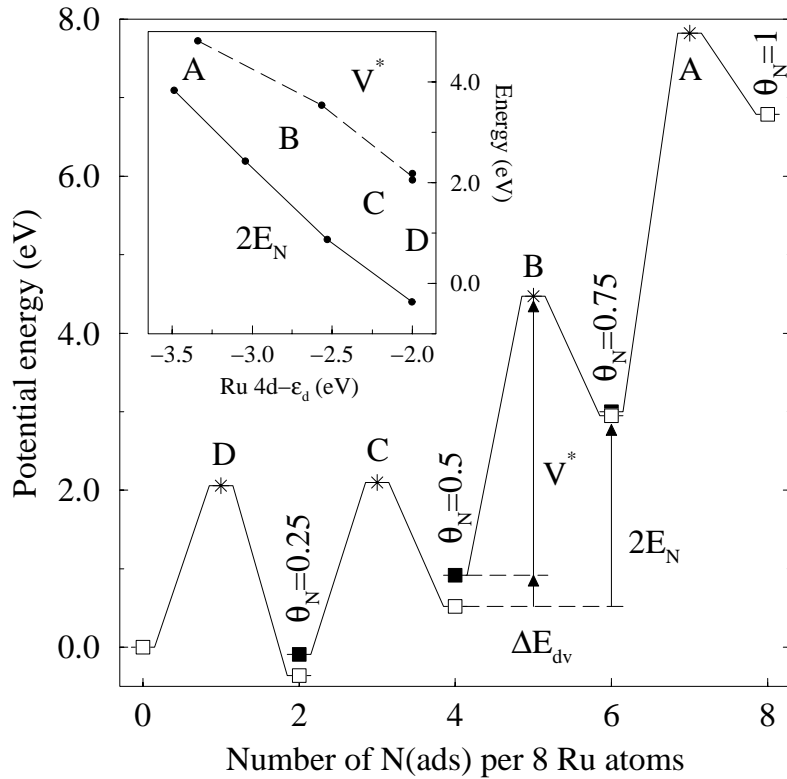
Figure 38. Calculated potential energy diagram for desorption of N_2 from Ru(0001)-c(4 x 4) initially at Θ_N =1. The inset shows (twice) the differential adsorption energy of N, E_N, and the energy barrier for dissociation at a di-vacancy as a function of the Ru 4d-band center, ε_d.

89

In Figure 38, the potential energy levels of the various stages of the adiabatic N_2 desorption events are indicated by open squares (most stable configuration of the surface at a given coverage), asterisks (transition state for the association of two N atoms from neighboring hcp sites), and solid squares (meta-stable surface configuration including a N di-vacancy where the desorption took place). Since the time scale of the LAAD experiment is very short compared to annihilation of the di-vacancy, the barrier, V^*, is evaluated from the level including such a di-vacancy to the level of the transition state in the case of the desorption events A, B, and C (see indications on Figure 38).

After the N_2 molecule is desorbed, the di-vacancy can annihilate as explained in Figure 39 below. When two nitrogen atoms recombine and desorb from the surface, immediately after the desorption event the configuration left behind is in an "excited state" (solid squares in Figure 38). The remaining N atoms can rearrange to an energetically more favorable configuration (open squares in Figure 38) for the new lower coverage, lowering the energy by ΔE_{dv}. This energy is not carried away by the desorbing N_2 and therefore not measured by LAAD. The barriers from the DFT calculation are therefore given in Table V without the di-vacancy energy term. Consequences of this di-vacancy will be discussed when comparing with adsorption later (in section 8.2.8), but as seen in Figure 38 above the true dissociation barrier is given by $V^* + \Delta E_{dv}$. In adsorption ΔE_{dv} is thus the energy needed to form a di-vacancy where dissociation can take place. Note that at the lowest coverage, $\Delta E_{dv}=0$, and there is thus no difference between V^* and the barrier to adsorption.

(d)   (c)   (b)   (a)
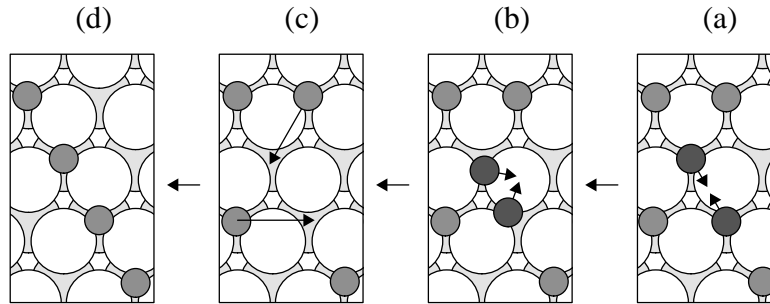
Figure 39. Reading from right to left is pictured an associative desorption event with $\Theta_N=0.75$ initially (a). Two N atoms recombine on the surface and desorb (b). The remaining N atoms now rearrange (c) to minimize the energy for a N adlayer at $\Theta_N=0.5$ (d). Reversing the arrows and reading from left to right pictures the corresponding dissociative adsorption event. (Figure by B. Hammer [135])

Assigning Θ_N for each calculated V^* corresponding to the N-coverage in the super cell before the desorption, the obtained values are given in Table V. Judging from the table, there is excellent agreement between these DFT calculations and the values obtained by the LAAD experiment, both in the magnitude of the barrier and in its coverage dependence. Correction for the zero point energy has not been included in the calculations. This will only lower the barrier by approximately a tenth of an eV, though [26].

It has previously been demonstrated that there is a strong correlation of both surface adsorption energies and barriers to dissociation on transition metals with the center of

the metal d-bands [136]. In the inset of Figure 38 it is shown that such a correlation also exists for the coverage dependence of differential chemisorption energies and energy barriers. The Ru 4d-band centers ε_d as a function of Θ_N are constructed as geometrical means of the first moments of the 4d-projected DOS at Ru sites neighboring the reaction site. The ε_d at these sites decrease with Θ_N, because the Ru atoms have their electronic 4d states shifted down compared to the clean surface value as a consequence of the bonding to the pre-adsorbed N. Both the atomic chemisorption energies and the energy barriers increase with the decrease in ε_d because the lower in energy the Ru 4d electrons are, the less they are capable of interacting chemically with the electronic levels on the adsorbed N as well as on the transition state [136].

8.2.6 Comparison with TPD

We now compare the barriers measured by LAAD, and calculated by DFT, with the barriers derived from the measured desorption energies in the TPD experiment combined with calculated adsorption energies, as described earlier in chapter 6. We here use the newest DFT calculations just presented in section 8.2.5. As the inset in Figure 38 shows, the differential adsorption energy increases linearly with coverage. Combining these with the E_{des} at the coverages where E_{des} were measured (see Table II), barriers have been calculated and are plotted in Figure 40 together with the barriers from LAAD and DFT. The agreement between the three methods is very good. The LAAD values seem to be the lowest, but we have to remember that the barriers determined by LAAD are only lower limits, since the labeling of the vibrational states is unknown.
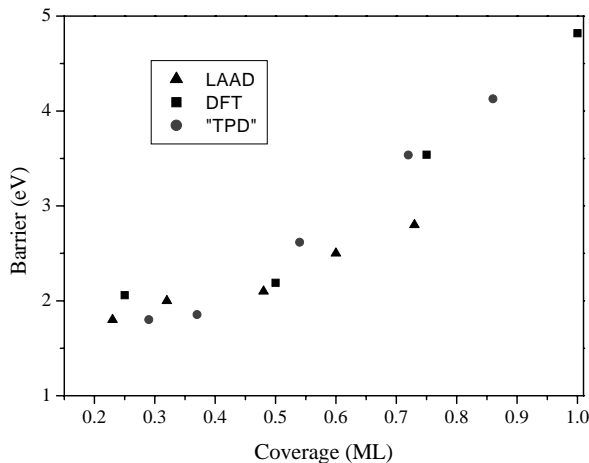
Figure 40. Barriers determined by the three methods: LAAD, DFT and "TPD", i.e. a combination of E_{des} from TPD and E_N from DFT.

The "TPD-barriers" shown here differ somewhat from the values shown earlier in chapter 6 (Table IV and Figure 20), which at higher Θ_N appear to be lower. The discrepancy can be explained as follows. The adsorption energies used in the latest DFT calculations (presented in section 8.2.5) were "differential adsorption energies", i.e. the adsorption energy describing a change in coverage. The adsorption energies used earlier were "average adsorption energies", which is the total adsorption energy

per atom to prepare a specific coverage initially starting at $\Theta_N=0$, i.e. the energy difference between the adsorbed state and when *all* atoms are desorbed from the surface. However, when a TPD experiment is performed at higher coverage, not all of the atoms are removed in a given TPD peak. Each peak in the TPD spectrum represents desorption from one state where only a fraction of the adsorbed N atoms desorbs. The desorption energy (E_{des}) measured by TPD should correctly be combined with the *differential* adsorption energy in order to determine the barrier for a fair comparison with barriers from LAAD and DFT.

8.2.7 Influence of coadsorbed oxygen

To investigate the effect of co-adsorbed oxygen, we deliberately dosed with oxygen after N-dosing resulting in $\Theta_N=0.21$ ML and $\Theta_O=0.30$ ML. A N_2 LAAD experiment was performed, and the barrier determined from this was $V^*=2.1$ eV. The adsorption energy, for nitrogen coadsorbed with oxygen, is given by $2E_N= V^*-E_{des}$, where E_{des} is the activation energy for N_2 associative desorption for nitrogen coadsorbed with oxygen. This can be estimated from the TPD spectrum in Figure 19 to be $E_{des}=1.3$ eV. Inserting the values for V^* and E_{des} from above we find $E_N= 0.4$ eV (per atom relative to the ½$N_{2(gas)}$+Ru(0001) asymptote). This is very close to the adsorption energy for pure nitrogen at the same total coverage ($\Theta_N=0.5$ and $\Theta_O=0$). From the DFT calculations shown in Figure 38 we find $E_N=0.44$eV for $\Theta_N=0.5$.

In both cases E_N is positive and nitrogen is therefore only metastable at the total coverage of 0.5 ML, with respect to associative desorption. That the presence of large amounts of oxygen destabilizes adsorbed nitrogen was already discussed in chapter 6. We have shown here, that the oxygen-nitrogen repulsive interaction quantitatively plays the same role in destabilizing the N binding energy as just pure N-N repulsive interactions. Calculations of the Ru-4d band centers ε_d for N and O coadsorbed have not been done. But from the above findings we can predict that ε_d would be shifted down by the same amount whether pure N, or N and O is adsorbed, as long as the total coverage is the same. In other words, the present coadsorbed oxygen results in a downshift of ε_d that results in a weaker interaction between the Ru-4d electrons and the N leading to weaker bound nitrogen.

As well as a decrease in the N-stability when O is coadsorbed, also the barrier is affected. For pure nitrogen ($\Theta_N=0.23$, $\Theta_O=0$) we found $V^*=1.8$ eV, increasing to $V^*=2.1$ eV for the same N-coverage now with O coadsorbed ($\Theta_N=0.21$, $\Theta_O=0.30$). Again the presence of O has the same quantitative effect on the barrier as it had on the adsorption energy, since the barrier for pure nitrogen ($\Theta_N=0.48$, $\Theta_O=0$) at the same total coverage was also 2.1 eV.

Care was taken to keep the oxygen contamination at a minimum, when preparing the surface with N for all nitrogen LAAD experiments presented here. For $\Theta_N<0.5$ ML, no oxygen was present. For higher Θ_N, we always had $\Theta_O<0.07$ ML. We believe that this small amount of oxygen has no significant effects on the N_2 LAAD experiment and the interpretation.

8.2.8 Comparison with adsorption

The experimental results presented here showed that one can measure the barrier via measurements of N_2 energies following associative desorption. One could also measure the barrier to dissociative chemisorption directly, e.g. via N_2 energy dependent molecular beam studies [27]. Since they are essentially time reversed experimental scenarios, the results of both seemingly different measurements should be related by detailed balance. While detailed balance may in fact be a good approximation for low Θ_N, we wish to argue here that at high Θ_N we anticipate that detailed balance will *not* be a good approximation.

DFT calculations [32] indicate that the minimum energy path for dissociation connects the transition state to N atoms at two adjacent 3 fold hcp sites. At high Θ_N, it is unlikely that there is an ensemble of two adjacent empty hcp sites. Thus, it is unlikely that the phase space available for the dissociated state allows a gas phase N_2 molecule to follow the minimum energy path. In essence, there is a steric constraint to the dissociative chemisorption and dissociation can then only occur through some higher energy path. The steric constraint is thus formation of the di-vacancy discussed in section 8.2.5.

On the other hand, there is no such steric constraint for associative desorption at high Θ_N since adjacent hcp sites are likely occupied and must merely deform somewhat to encounter the transition state or minimum barrier configuration (see Figure 39b). At low Θ_N, steric constraints in dissociative chemisorption are probably minimal and thus should see the same barrier as associative desorption.

If we want to predict the activation energy E_a for dissociation at low coverage as measured in a high-pressure thermal kinetic experiment, we want to know the adiabatic minimum energy barrier. The barrier V^* measured in LAAD as given in Table V, was the "central barrier" minus the width W. If we now apply detailed balance and compare with adsorption, the adiabatic minimum energy barrier is probably most correctly given by the threshold of the *error* function. The threshold for sticking is not exactly defined, due to the "S" shaped sticking function, but subtracting the width W from the centerpoint will be a good estimate and V^* will therefore be a reasonable value for the threshold energy and thereby the minimum energy barrier, i.e. $E_a \sim V^*$ (see eventually Figure 32). From LAAD we found $V^*=1.8$ eV at low coverage and would thus predict $E_a=1.8$ eV.

The LAAD experiment measures the barrier at the terrace sites, but for N_2/Ru(0001) it is known that the barrier at steps/defects is substantially lower [26]. A thermal high-pressure experiment would thus measure the activation energy for N_2 dissociation at the steps/defects. Dahl *et al.* found an activation energy $E_a=0.4$ eV on a clean Ru(0001) surface. However, if the (low density) natural steps on the surface were poisoned by coadsorption of gold, $E_a=1.3$ eV was obtained [26]. This is still much lower than the value predicted by LAAD and we believe that even if the steps are decorated with gold, the E_a obtained this way still not measures the barrier on the terrace sites. It was already mentioned by Dahl *et al.* that $E_a=1.3$ eV could be the

activation energy to free up a step site, i.e. gold diffusing away and allowing N_2 to dissociate at the step. The LAAD experiments agree with that.

High-energy molecular beam experiments should mainly probe the majority terrace sites. For N_2/Ru(0001) it was shown for a crystal with ~1 % steps/defects, that poisoning of the lower barrier with Au sites only reduced the sticking probability measured with the beam by a factor of two [26]. It is therefore reasonable to compare the LAAD experiments with molecular beam experiments.

As discussed previously, the barrier determined from LAAD is not exactly the same as the adsorption barrier at higher coverages and detailed balance is not a good approximation. This was due to the "di-vacancy term". By adding the energy ΔE_{dv} needed to form a di-vacany, i.e. two empty adjacent hcp sites where the minimum energy barrier dissociation can take place, we could still predict the dissociation behavior at higher coverages. Only low coverages will be considered in the following, though.

Using the results from LAAD at low coverage we will now predict the initial ($\Theta_N \approx 0$) dissociation probability that would be measured in a molecular beam experiment. The lowest coverage investigated with LAAD was Θ_N=0.23, where a barrier of 1.8 eV was measured. It can be seen in Figure 40, that the barrier seems to level off at low coverage and a barrier measured at Θ_N=0.23 is therefore also a good value for the barrier at $\Theta_N \approx 0$. Using LAAD parameters for $V^* = 1.8$ eV, we have calculated the dissociative sticking by invoking detailed balance and compared that with existing molecular beam experiments. We thus assume that the parameters V^*, W and $P(\nu)$ describing the desorption are also valid for adsorption.

The dissociative sticking probability can be calculated by the following summation over sticking functions for each vibrational state, weighted by a Boltzmann factor representing the population of the corresponding vibrational state.

$$S_\Theta (E,T_{vib}) = \sum_\nu F_B (\nu,T_{vib}) S_\Theta (E,\nu) \tag{8.8}$$

Where $F_B (\nu,T_{vib}) = e^{-\varepsilon_\nu / k_B T_{vib}} / \sum_\nu e^{-\varepsilon_\nu / k_B T_{vib}}$. The vibrational temperature, T_{vib}, of the gas in the supersonic nozzle beam is approximately equivalent to the nozzle temperature. $S_\Theta (E,\nu)$ is given by eq. (8.2) with the centerpoint given by $E_0 (\nu) = V^* + W - \eta_\nu \varepsilon_\nu$, where V^* is the "minimum energy barrier" measured in LAAD and again η_ν=1 for all ν as in desorption. The amplitudes $P(\nu)$ have to be treated carefully, though. In analyzing the desorption experiments, the observed vibrational inversion was described by $P(\nu)$ varying with ν. The values of $P(\nu)$ describing desorption were relative values, i.e. probabilities, where the normalization $\sum_\nu P(\nu)=1$, was due to conservation of probability. In other words, no absolute values can be assigned to $P(\nu)$. When applying detailed balance, $P(\nu)$ will determine where the sticking function $S_\Theta (E,\nu)$ for state ν saturates at high translational energies, since $S_\Theta (E,\nu)$ is proportional to $P(\nu)$. Determination of absolute sticking probabilities is

therefore not possible. An upper limit can be set, since the largest $P(\nu)$ can not exceed 1, due to the obvious limitation $S_\Theta(E,\nu) \le 1$, for any ν. For a barrier of $V^* = 1.8$ eV the values for $P(\nu)$ determined from LAAD were $P(\nu=0,1,2,3,4,5,6) = (0.0005, 0.0024, 0.011, 0.044, 0.15, 0.40, 0.39)$. These values for $P(\nu)$ were used directly in the following comparisons with beam experiments without any scaling.

In the direct comparison, we find that the experimental data of a previous molecular beam study of N_2 dissociation on Ru(0001) [27] are inconsistent with the LAAD results. On the other hand, more recent molecular beam experiments [29] are in almost quantitative agreement with the LAAD predictions. In Figure 41a are shown the dissociative sticking probabilities for the molecular beam experiments of Egeberg *et al* [29] and the calculated values inferred from LAAD using the exact same conditions of translational energy and nozzle temperature (T_n) as in ref.[29]. The agreement is very good. In Figure 41b the sticking data from Romm *et al.* are shown together with calculated values from LAAD. Exact nozzle temperatures and translational energies were obtained from M. Asscher [137]. Clearly these data are in disagreement with the prediction from LAAD, especially at low energy. Finally, we made a dissociative sticking experiment at one translational energy $E=1.5$ eV ($T_n=1150$ K) and found $S_0=1.8 \times 10^{-5}$. The calculated value from LAAD is $S_0=1.6 \times 10^{-5}$, i.e. nearly identical, although a comparison based on only one data point is not telling much.
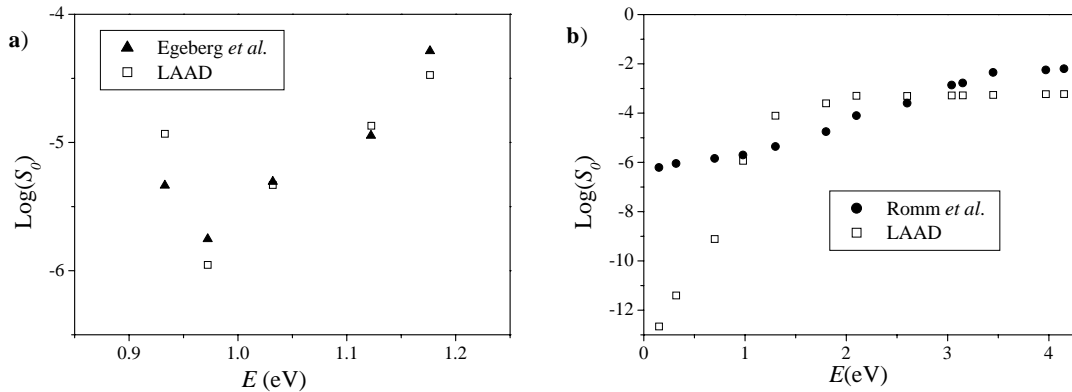
Figure 41. Dissociative sticking probabilities as a function of translational energy. Results from two molecular beam experiments (solid symbols) and LAAD inverted to sticking (open symbols) are shown.

We have also calculated the expected sticking probability in the limit of large translational energies, and found that S_0 saturates at $\sim 4 \cdot 10^{-3}$ (for $T_{vib} \sim 2000$ K). At experimentally achievable nozzle temperatures only the lowest vibrational states are populated in the beam (eq. (8.8)). These will have a very low sticking probability, even for translational energies well above the barrier, due to the predicted low $P(\nu)$, when ν is small. This must mean that translational energy only couples very weakly to the reaction coordinate, in full accord with a barrier mainly in the vibrational coordinate. The majority of the impinging molecules are therefore expected to scatter off the surface. Papageorgopoulos *et al.* studied the scattering of N_2 from Ru(0001) [138]. They used a supersonic beam of N_2 at translational energies up to 1.8 eV and observed that for an incident angle of 40° the scattered molecules had lost up to 45 % of their incoming translational energy. Only the translational energy of the scattered molecules

was detected, and the energy loss can therefore be explained by excitation of internal degrees of freedom, rotation and vibration, of the N_2 as well as loss to phonons of the Ru-solid. Vibrational excitation of molecules scattering from a surface has been observed for e.g. H_2/D_2 ($v=0 \rightarrow v=1$) scattering from Cu(111) [139].

That S_0 is predicted by LAAD to saturate at a value $S_0 \ll 1$ is in agreement with the findings of Romm *et al.* who found that S_0 saturated at $\sim 10^{-2}$ [27]. This limit was reached at translational energies of ~ 4 eV (see Figure 41b), much higher than expected for a barrier of 1.8 eV. A reasonable explanation for this discrepancy could be that Romm *et al.* have an error in the absolute beam translational energy scale. Jane H. Larsen already pointed out, that it is theoretically impossible to achieve such high translational energies under the beam conditions (nozzle temperatures and seeding ratios) employed [95]. This could also explain the disagreement in the slope of $S_0(E)$, which would increase by compressing the translational energy scale given by Romm *et al.*, although this would not change the disagreement in the absolute value of S_0 at low energy.

In conclusion, if the energy scale is changed there seems to be a qualitative agreement between the data of Romm *et al.* and the S_0 predicted by LAAD at translational energies above 1 eV, including the leveling off of S_0 at high energy. At lower energy the molecular beam is probably more sensitive to defects and the high S_0 at low energy observed by Romm *et al.* could be due to defects on their crystal.

In a more recent study, Romm *et al* present measurements of S_0 for two different isotopes of nitrogen, N_2^{14} and N_2^{15} [140]. They find an isotope effect where the ratio $R=S_0(N_2^{15})/S_0(N_2^{14})$ is >1 at low and high translational energies, passing through a minimum ($R=0.25$) at $E=1.6$ eV. At max, the isotope effect is thus a factor of 4, in favor of N_2^{14} dissociation. It should be noted though, that they are comparing two very small numbers since S_0 is on the order of 10^{-5} in the energy range where the isotope effect is observed. Such small dissociation probabilities are difficult to measure accurately and uncertainties of a factor of two, in opposite directions for N^{14} and N^{15}, would completely cancel out the apparent isotope effect.

To explain the isotope effect they suggest a non-adiabatic tunneling mechanism. The model calculations are only fitting the experimental data poorly, though.

In strong contrast, LAAD measurements, at two coverages $\Theta_N=0.5$ and 0.7 ML, using the two isotopes N^{14} and N^{15}, did not show any differences at all in the TOF distributions. It was proposed by Kosloff [141], that the desorption yield would be much higher for N^{14}. Also this was not observed. Romm *et al.* used the leveling off at low S_0 at high E as evidence for the non-adiabatic model [27], but as discussed earlier, we suggest an alternative explanation, the low P(v)'s at low v. Furthermore, the barriers from the LAAD experiment were in very good agreement with the adiabatic DFT calculations by B. Hammer and we see no reason to conclude non-adiabatic effects.

8.3 Conclusion

In summary, we have described the application of LAAD to determine both the dynamics and energetics of N_2 associative desorption from Ru(0001). This technique seems rather immune to complications caused by low barrier minority sites. We find that N_2 is preferentially produced in high vibrational states and that the barrier between gas phase N_2 and the adsorbed N atoms increases substantially with Θ_N. Both the energetics and dynamics are in excellent agreement with DFT calculations for the process. The DFT calculations show that the origin of this increase in barrier with coverage can be understood in terms of coverage dependent shifts of the Ru 4d band centers. It was shown that the application of detailed balance leads to prediction of dissociation probabilities in agreement with recent molecular beam experiments.

9 Laser Assisted Associative Desorption of CO from Ru(0001)

9.1 Introduction

Motivated by the success of the N_2 LAAD experiments, we studied another very interesting system: CO on Ru(0001) which also experiences a high dissociation barrier, mainly along the vibrational coordinate.

CO is considered to be a "model-system" for the interaction of a diatomic heteronuclear molecule with a metal surface. Furthermore, the adsorption and dissociation of CO on transition metal surfaces have been intensively studied due to its importance in many catalytic reactions such as oxidation of CO, methanation (CO + $3H_2 \rightarrow CH_4 + H_2O$) and Fisher-Tropsch synthesis [142,143]. Mainly nickel catalysts are used but ruthenium has also shown to contain good catalytic properties for the above mentioned reactions.

Recent density functional calculations have shown that the barrier to CO dissociation on Ru(0001) is 1.0 eV, mainly along the vibrational coordinate [129]. On other metals the barrier is 1.4 eV on Ni(111) and 2.9 eV on Pt(111) [144][*]. No dissociation has been observed in molecular beam experiments on either surface [114,115,145,146]. On Ni(111) CO dissociation does occur under high pressures [142], but not under UHV conditions (see references in [145]). On Pt(111), CO dissociation has not been observed, presumably due to the endothermicity of that reaction [147]. CO has been observed to dissociate on Ru(0001) at high pressures, with the step sites being most effective [143,148-150]. No dissociation of CO has been seen under UHV conditions[#], only electron induced dissociation [152]. Furthermore, a recent molecular beam experiment showed no dissociation for kinetic energies up to 2 eV [114,115].

To study a high barrier system like this, even if the barrier is mainly along the vibrational coordinate, we can try to use the experimental technique of laser assisted associative desorption (LAAD). We need to deposit C and O atoms on the surface, create a temperature jump with a short laser pulse and measure the kinetic energy of the desorbing molecules using time-of-flight (TOF) techniques. By application of the principle of detailed balance, we can then relate the desorption process to adsorption.

Deposition of O is easy, since O_2 dissociates readily on the Ru(0001) surface [153]. Deposition of C on the surface is a little complicated. Carbon can exist in different phases on the surface, from isolated atoms to islands of graphite. If we want to study

---

[*] These calculations used the PW91 exchange-correlation functional. For N_2 dissociation, the barrier increased substantially when the RPBE functional was used instead. A similar increase can be expected for CO dissociation [135].

[#] Lauderback and Delgass did observe dissociation of CO under UHV conditions, at background doses of a few hundred Langmuir [151]. This is in disagreement with everybody else and could be due to a crystal having a lot of defects.

the associative desorption of C with O, control of the C state is necessary. The easiest way to prepare C/Ru(0001) is to dissociate C-containing molecules like methane (CH_4) or acetylene (C_2H_2) on the surface and heat the sample to a temperature where hydrogen desorbs and only C is left on the surface.

9.2 C/Ru(0001) Adlayer preparation

It is known that adsorbed carbon can be in a number of different states on Ru(0001), ranging from so-called carbidic C where the adsorbed C atoms are isolated to the more stronger bound graphite. This depends strongly on temperature. In the study of associative desorption of C+O, we need to prepare the surface with isolated C and O atoms. The associative desorption reaction involves then only the breaking of a C-Ru and a O-Ru bond and formation of a C-O bond. This is the process, which is relevant to relate to dissociative adsorption.

The procedure to we have employed to prepare C/Ru(0001) will be outlined here. First, a methane beam was used. 3 % CH_4 was seeded in He and the nozzle temperature was set at 1057 K. The kinetic energy of the CH_4 was measured by TOF to be 0.85 eV. We could not analyze C/Ru with AES due to overlap in energy of the C Auger peak with a Ru peak. A titration method where the C is reacted off the surface by depositing oxygen and heating the surface was used instead. The procedure is the following. After the surface has been exposed to a methane beam, and the sample has been annealed to a temperature (600 K) where all H is desorbed, the surface is saturated with oxygen at room temperature (RT) and a TPD experiment is performed. The sample is heated with 10 K/s and the produced CO is monitored with a mass spectrometer. This is often called temperature programmed oxidation (TPO).

The following figure shows the TPO after a 2 min methane dose at different surface temperatures followed by an anneal to 600 K and a saturation dose (10 L) of O_2. The first desorption peak at ~420 K is molecularly CO adsorbed from the background, shifted down in temperature due to the presence of oxygen [154]. Peaks above that temperature are from the associative desorption of C + O. It is clearly seen that the amount of C increases strongly with the surface temperature where the dosing takes place, from RT to 500 K and thereafter levels off. The initial sticking probability S_0 was measured by the King & Wells technique [43], showing that S_0 increased linearly from 6 % at RT to 8 % at 600 K at the CH_4 kinetic energy used here. Even though the initial sticking coefficient does not show a big T_s effect, the large difference in C-coverage for the 2 min dose is probably due to blocking of surface sites by adsorbed H at higher coverage. Hydrogen desorption is completed at ~450 K [155]. Figure 42 clearly shows that dosing at 600 K is most efficient. It should be mentioned that a single TPO was sufficient to remove all carbon.
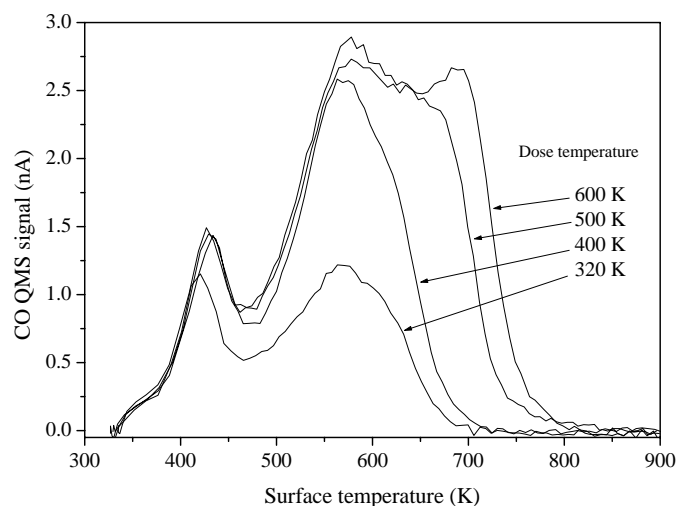
Figure 42. TPO following a 2 min CH_4 beam dose (0.85 eV) at various surface temperatures. Before the TPO an anneal to 600 K removes any remaining H.

The anneal temperature, after the CH_4 dose, also plays an important role. Below is shown the TPO (from RT to 900 K) after depositing the same amount of carbon by dosing with methane for 2 min at T_s=400 K followed by an anneal to different temperatures. The anneal was done by heating with 10 K/s and cooling immediately after the anneal temperature was reached.
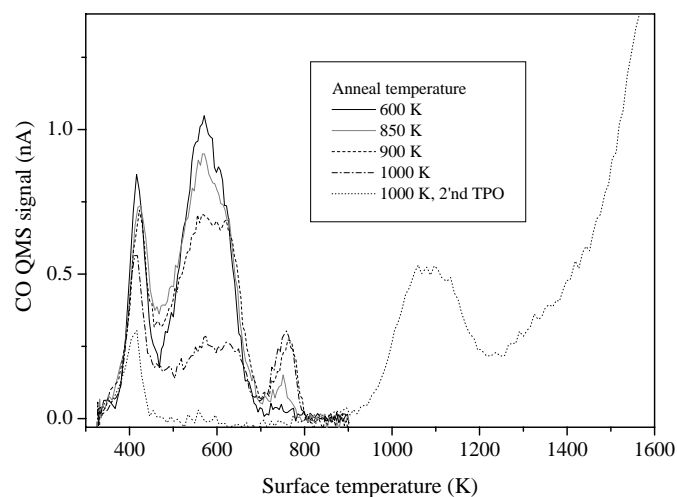
Figure 43. TPO following a 2 min CH_4 beam dose (0.85 eV) at T_s=400 K and an anneal to the various temperatures indicated on the figure.

First, an anneal to 600 K shows the same behavior as in Figure 42, one single TPO peak at ~570 K. Anneals to 500, 700 and 800 K gave the same result as 600 K and are therefore not shown here. After an anneal to 850 K a small TPO peak at 750 K starts to appear and is growing as the anneal temperature is increased. This must be a new "C-state". After every experiment, oxygen was redosed and a second TPO was performed, now to 1600 K. No C was seen, except after the anneal to 1000 K, where a peak at much higher temperature, 1100 K, was observed in the second TPO. This is believed

to be graphite, where C-C bonds stabilize the C on the surface and makes it more difficult to react off with O.

It is known that, if Ru(0001) is exposed to extensive amounts of CH_4 at high pressures and elevated temperatures graphite is formed on the surface [156]. Hrbek reports that decomposition of ethylene (C_2H_4) on Ru(001) followed by an anneal to 700 K results in the formation of "highly reactive carbidic carbon", whereas if the anneal temperature is 1300 K "graphitic carbon" is formed [157]. Hoffmann quotes TPO desorption temperatures for these types of carbon to be 500-700 K and 900-1100 K respectively. Also, Lauderback an Delgass find similar TPO's after deposition of C by dissociating CO on Ru(0001) [151]. They also find that, an anneal above 663 K results in a shift in the TPO desorption temperature from 540 to 740 K, shifting to even higher temperatures at increasing anneal temperature. This is in good agreement with our findings.

Repeating the above experiments using C_2H_2 as the C-source resulted in the same TPO's.

In conclusion, C can be in a number of different "states" on Ru(0001), depending strongly on temperature. Presumably what happens in transition from one state to another is that new bonds (C-C) are formed through an activated process, taking the C from being isolated atoms (carbidic C) to graphite, which is stronger bound. At least the activation energy for the reaction C+O is increased as evident from the higher desorption temperature. We believe that the peak at 570 K is due to isolated C-atoms on the surface, or at least C atoms only bound the surface with no chemical bonds to each other.

9.3 LAAD experiments

LAAD was performed after preparing a Ru(0001) surface with C-atoms (the state observed desorbing at 570 K in TPO,) at a coverage Θ_C~0.05 ML and then saturating the surface with O-atoms by a background dose of 10 L O_2 at RT, Θ_O~0.5 ML. The surface was irradiated with a 100 ns laser pulse, creating a temperature jump, and TOF distributions of CO formed in associative desorption were measured with a mass spectrometer. The reaction is written below.

$C_{ads} + O_{ads} \rightarrow CO_{gas}$
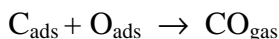
The sample temperature was biased at T_s=430 K, close to but below the associative desorption temperature. The laser pulse energy used was 50 mJ, shooting 30 times at the same spot (10 shots/sec) before moving to a new non-irradiated area. In total 900 laser shots were used to collect the TOF shown in Figure 44a. After the LAAD experiment, a TPO was performed showing that only a small fraction of the C was removed in the laser desorption. Only the peak at 570 K was seen. Another TPO did not show any C.

To analyze the data, we first note that the desorbing CO molecules are rather slow despite the >1 eV barrier. The TOF could be fitted using a flux-weighted Maxwell-

Boltzmann distribution (eq. (7.19)). The fit is shown in Figure 44a as the solid line. The desorption temperature "extracted" from the fit was T_{des}=842 K. This should be compared to the temperature reached in the laser induced T-jump measured by LITD of molecular CO, where it was shown in section 7.5 that $T_{des} \sim T_s$. 10 L CO was dosed at 425 K, and the sample was cooled to RT, where the CO was laser desorbed, using exactly the same laser intensity, i.e. the same laser induced T-jump (see also section 7.5). The TOF distribution for CO LITD is shown in Figure 44b. Fitting the data with eq. (7.19) results in a surface temperature of T_s= 866 K. We have to take into account that the sample is biased at different temperatures, T_0= 315 K for the CO LITD and T_0= 430 K for the CO LAAD. The temperature reached during the CO LAAD experiment is thus T_s= 981 K. This is slightly higher than the T_{des}= 842 K determined from fitting the CO LAAD TOF distribution and the associative desorbing CO is thus slightly sub-thermal. The main point is, though, that in contrast to N_2, which also was formed over a large barrier, the associative desorbing CO does not come off the surface at high energies.
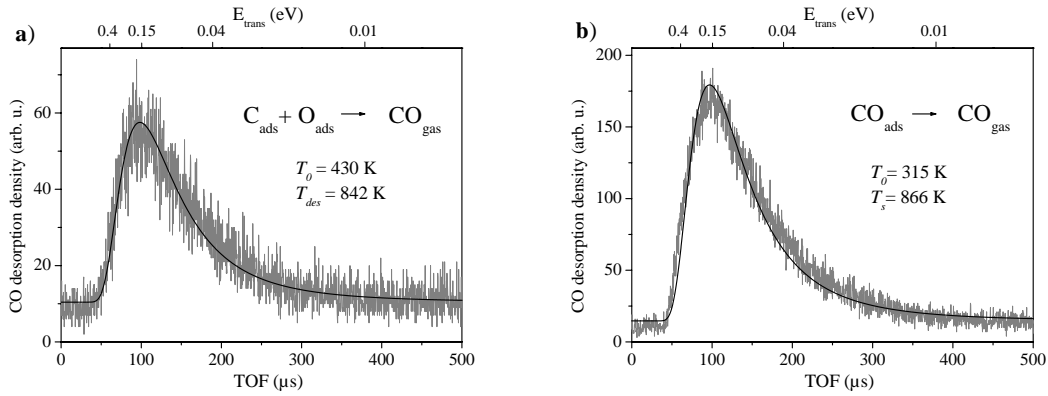
Figure 44. TOF distributions and fits (solid line) for **a)** LAAD of CO from Ru(0001). **b)** LITD of CO from Ru(0001). The translational energy is indicated on the top axis. The same laser intensity is used in both experiments.

We made sure that we are looking at the C+O reaction and that no adsorbed molecular CO interferes. As seen from e.g. Figure 42 molecular CO desorbs already at ~420 K from a C+O covered surface [154]. At the bias T_s = 430 K, molecular CO is therefore unstable and there is no contribution from background adsorbed CO. This was verified by preparing the surface as for a LAAD experiment, i.e. dosing with methane at 600 K cooling to RT, dosing with oxygen and raising T_s to 430 K. Instead of LAAD, a TPD experiment was now done. The only CO desorbing was at 570 K which is the peak due to C+O. This also made sure that no CO is formed on the surface from the adsorbed C and O before the laser heating. Furthermore, two LAAD experiments were performed by only preparing C/Ru(0001) and thereafter only O/Ru(0001), no mass 28 (CO) was observed in the TOF. This proves that we are indeed looking at associative desorption, $C_{ads}+O_{ads} \rightarrow CO_{gas}$.

In contrast to LAAD of N_2, where a lot of energy was released into translation and vibration, we do not see the same for LAAD of CO, despite the high barrier in both cases. We thus have to explain how the energy available at the barrier is lost before desorption of CO takes place. For CO on Ru(0001) there exists a strong molecular well with a binding energy of 1.66 eV [89,158]. This deep well strongly influences the

adsorption dynamics as explained below. We believe that the presence of a deep molecular well is responsible for substantial energy "scrambling" and dissipation of the energy available from the barrier resulting in the low translational energy of the observed CO in LAAD.

First the sticking will be discussed. A recent molecular beam experiment by Kneitz *et al*. determined the initial sticking probability (S_0) of CO on Ru(0001) [114,115]. They found S_0=0.92 at a translational energy E_{trans}=0.09 eV, only decreasing to S_0=0.58 at E_{trans}=2.0 eV.

The gradual decrease in S_0 is inconsistent with the simple one-dimensional soft-cube models, described shortly in the following. An incoming molecule with a translational energy E_{trans} loses the energy Δ to the lattice in the collision with the surface atoms. The model assumes a flat surface where only the normal component of the energy, $E_n = E_{trans} \cos^2\varphi$, where φ is the incident angle, is able to transfer energy to the lattice. If $\Delta > E_n$, the molecule will be trapped in the molecule-surface potential well and stick to the surface. If $\Delta < E_n$, the molecule will be reflected from the surface, having lost the energy Δ, i.e. scatter inelastically. The model predicts a step decrease in S_0, rounded off due to the finite surface temperature, at a certain threshold energy E_c, determined by the masses of the molecule and surface atoms, the molecule-surface well depth and the lattice vibrational frequency. S_0=1 if $E_n < E_c$ and S_0=0 if $E_n > E_c$.

That the sticking of CO on Ru(0001) only decreases gradually and maintains a large value, also at high energies (not explainable by the soft-cube model) points to the fact that the molecule-surface interaction depends on more than just the few parameters in that model. A similar behavior has been seen for CO (molecular) sticking on e.g. Ni(111) [159] and Pt(111) [146]. Harris and Luntz showed in a molecular beam experiment investigating the sticking and scattering of CO on Pt(111), that the dependence of S_0 on energy and angle could be explained by a molecule-surface interaction, which was laterally and rotationally strongly corrugated [146]. Translational to rotational (E_{rot}) and normal to parallel energy ($E_{parallel}$) conversions caused substantial energy scrambling in the interaction. This also explained the observed scaling of S_0 with total rather than normal energy. We believe that a similar strong corrugation is present for CO/Ru(0001), as evident from comparing the sticking data for CO/Ru(0001) with CO/Pt(111).

How does this deep corrugated well affect dissociation. For CO on Pt(111), no dissociation occurred at kinetic energies ranging from 0.05 to 3.5 eV [146]. Since the barrier is calculated to be 2.9 eV [144], it is obvious from this, that translational activation is ineffective in promoting dissociation. A calculation by Billing showed that the translational threshold for dissociation of CO on Pt(111) is 8 eV [160]. Again, because of the deep corrugated molecular well, energy gets scrambled into many degrees of freedom from E_{trans} on the way in, to $E_{parallel}$ and E_{rot}, which probably have little coupling to the reaction coordinate. When a large fraction of energy is dumped out of the reactive coordinates (E_{trans} and E_{vib}) into other modes, it is hard to achieve dissociation. Besides, the deep well and the energy scrambling will also lead to more energy transfer to the surface, which further depletes energy from the reaction coordinate and inhibits dissociation. Also, Lee *et al*. showed that no dissociation of CO occurred on Ni(111) for kinetic energies up to 2 eV [145]. The calculated barrier, 1.4 eV [144], is substantially lower than the kinetic energy of the incoming molecule, and

again translational activation seems to be insufficient to promote dissociation. Lee *et al.* argued in terms of a barrier solely in the vibrational coordinate. But as discussed above, the explanation is probably more involved.

Now we can rationalize the behavior of the associatively desorbing CO molecules in the LAAD experiment. Despite, that the molecule is formed with a lot of energy at the transition state, the desorption is occurring with thermal translational energies. On its way out, the CO molecule loses its energy in the interaction with the strongly corrugated molecular well. The fact that energy scrambling occurs on the way in and inhibits dissociation is entirely consistent with our LAAD results via the principle of detailed balance. An incoming molecule with high energy, even above the barrier height, does not dissociate [114,115]. It is therefore unlikely that a molecule formed at the transition state, with energy equivalent to the barrier height, desorb containing all the energy. Whether the molecular well is approached from the gasphase (adsorption) or from the surface (after recombination of C and O), interaction with the well leads to energy scrambling, dissipation and finally trapping in the well. Desorption is only occurring because the surface temperature is above the desorption temperature for molecular CO. A simplified 1-dim PES for dissociative adsorption/ associative desorption is shown in Figure 45a illustrating the above discussion.
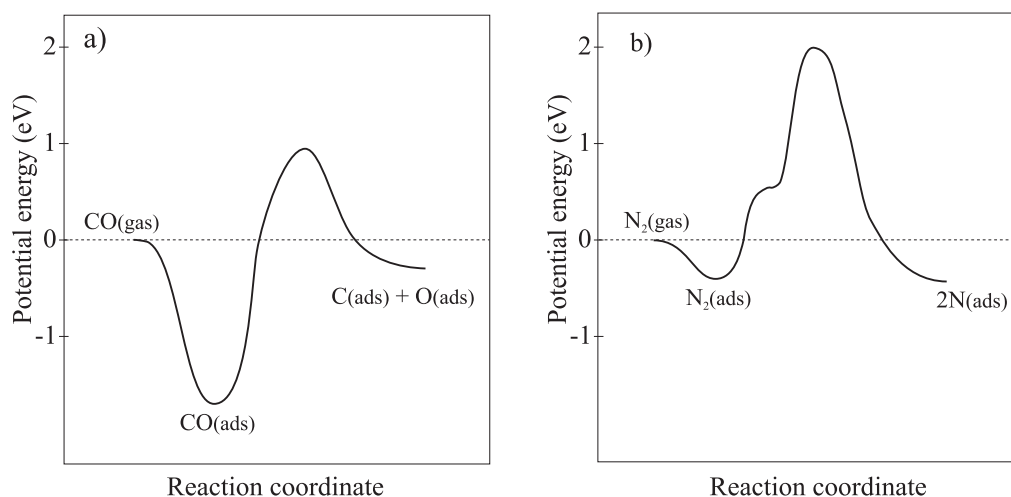
Figure 45. 1-dim PES for **a)** CO and **b)** N_2 interacting with Ru(0001). Reading from right to left describe the associative desorption. The origin is taken as the free CO + Ru(0001), free N_2 + Ru(0001) asymptote, respectively.

Let us now go back and compare with the N_2 LAAD. When two N-atoms recombine on the surface, a substantial barrier of ca 2 eV is surmounted. The minimum energy PES has been pictured in Figure 45b and shows after passing the transition state a very weak metastable molecular well [32] approximately 0.4 eV above zero (the free molecule in the gasphase). Next, a stable but weak molecular well with a binding energy of 0.44 eV [32] (see Figure 45b). Besides being weaker, the molecular well for the homonuclear N_2 is probably less orientationally corrugated than for the heteronuclear CO.

As the N_2 LAAD experiments showed, nothing, or at least a very small amount of energy is lost to the lattice. When N_2 recombines and desorbs none of the molecular wells seem to affect the translational energy of the desorbing molecule. To show that the weak molecular well not leads to large energy dissipation in N_2 adsorption, in contrast to CO/Ru(0001), some adsorption and scattering experiments for N_2/Ru(0001) will be discussed below.

Seets *et al* investigated the dynamics of N_2 molecular adsorption on Ru(0001) and showed that the molecular sticking at low translational energies proceeds via a physisorbed precursor, explained by a cube-model [161,162]. At higher energies they found evidence for an activated direct mechanism initially saturating at $S_0=0.12$ above translational energies of ~0.2 eV. Presumably the apparent barrier, not evident from DFT calculations of the minimum energy pathway, refers to the multi-dimensionality, i.e. collisions with different molecular orientations and/or impact parameters which do show a barrier. At higher translational energies, above 0.7 eV, S_0 decreases again [161,162], in agreement with direct sticking into the molecular well, where the fall off with energy again can be explained by a cube-model.

Papageorgopoulos *et al.* studied the scattering of N_2 from Ru(0001) and observed what is termed lobular scattering, i.e. a broad peak about the specular direction [138]. The experiments were done at $T_s=550$ K where no molecular adsorption is taking place. A strong interaction with the molecular well would show up, though, in terms of so-called trapping-desorption, where the molecule equilibrates on the surface in the molecular well and desorbs as a ~cosine distribution about the surface normal. This is not observed. Coupled with fact that Seets *et al* sees little trapping at high energy, the effect of the well for N_2 is not too big and there is thus no evidence for the molecular well leading to large energy dissipation in adsorption as for CO/Ru(0001). Also, translational activation in dissociative chemisorption is observed for N_2/Ru(0001) but not for CO/Ru(0001). To illustrate the differences between CO an N_2, the simplified 1-dim PES's can be compared in Figure 45b.

Certainly it is possible to imagine cases of associative desorption, where thermalization only occurs partly and the molecule loses a fraction of the energy available from the barrier. The angular distribution may contribute to the answer. Molecules desorbing directly are expected to have an angular distribution peaked sharply in the normal direction due to repulsion from the high barrier, whereas molecules interacting with the well, are losing part of their (normal) energy and will desorb with a broader angular distribution. In the limit of very long lifetime in the well, molecules would thermalize completely and are thus expected to desorb from the molecular well in a broad angular distribution (~cosine)$^{\text{¤}}$. It would furthermore be necessary to measure the internal state distribution to determine whether all degrees of freedom are thermalized due to the interaction with the molecular well on the surface.

$^{\text{¤}}$ Matsushima measured the angular distribution of N_2 during a TPD experiment to be ~$\cos^{7\pm3}\varphi$, where φ is the angle to the surface normal [163]. This is consistent with a high barrier. It should be noted that he deposited N on the surface using an ion gun and that the defects created this way could affect the measurement.

9.4 Conclusion

Laser assisted associative desorption of CO showed that even though the molecule is formed over a significant barrier the energy is dissipated when the molecule passes through the strong molecular well in the desorption process, leading to a desorption at ~thermal energies. This is in contrast to LAAD of N_2, which not showed significant thermalization. This was explained in terms of a much weaker well, not interacting significantly with the desorbing N_2 molecule.

10 Conclusion

This final chapter presents the concluding remarks on the technique of Laser Assisted Associative Desorption (LAAD), followed by general conclusions on the experimental results presented in this thesis as well as a danish summary.

10.1 Concluding remarks on LAAD

Several methods have now been developed to study the dynamics and kinetics of activated adsorption. Measurements of the dissociation barrier can be made directly via energy dependent molecular beam studies. If the barrier is only in the translational coordinate (early barrier) the experimental challenge is to obtain sufficient translational energies to achieve significant sticking to surmount the barrier and probe the PES in adsorption. If the barrier is late, i.e. mainly in the vibrational coordinate, we furthermore need to control the energy we put into the vibrational coordinate. One would have to do sticking experiments at different nozzle temperatures, varying the translational energy by e.g. changing mixing ratios of seed/carrier gas. This is necessary to determine the state-resolved sticking functions, which are needed to estimate the barrier. This was done successfully for H_2/Cu, where the barrier is only ~0.6 eV [14]. If the barrier is very high, say several eV as for N_2 on Ru(0001), this can be difficult.

Another adsorption-technique is the thermal high-pressure experiment. Kinetic measurements of thermal rates at high pressure measure the activation energy for dissociation. When barriers are high, only a very small fraction of the molecules in the thermal gas, the high-energy tail of the Maxwell-Boltzmann distribution, have sufficient energy to react. Although a high barrier reaction occurs with low probability many molecule-surface collisions are taking place due to the high pressure. Not nearly the same control over the various degrees is obtained as in molecular beam experiments and the insight into the dynamics of the reaction is therefore not as detailed. The thermal rates seem in some cases to be strongly influenced by the presence of lower barrier minority sites such as defects/steps. Dissociation occurs then predominantly at these sites. For N_2/Ru(0001) defects completely dominated the reaction [26]. On the other hand, it seems that high-energy molecular beams mainly probe the majority terrace sites [26,29].

Some of the problems in adsorption experiments for high barrier reactions are related to difficulties in supplying enough energy into the molecule to overcome the barrier. Alternatively, one can determine the barrier via associative desorption, measuring the energy of the desorbing molecules. Since this is essentially the time reversed scenario of dissociative adsorption, the results should be related by detailed balance.

In desorption experiments the excitation which causes desorption is the interaction between the adsorbate and the thermal heat bath of the substrate. Desorption is simply achieved by heating the surface. The desorbing molecules are then detected in the gas phase either by a QMS or by the use of state-resolved laser spectroscopic techniques. In beam experiments the angle of incidence and the translational energy can be well

controlled. Also vibrational energy is to some extent controllable. Desorption experiments using state-resolved detection techniques allows further insight to all molecular degrees of freedom, including the internal. We can take H_2/Cu as an example. As already mentioned, adsorption experiments demonstrated vibrational as well as translational activation in dissociative chemisorption [14]. Associative desorption experiments were in agreement with these findings and could be related via detailed balance [18]. Furthermore, the detailed quantum state-resolved desorption experiments revealed the effect of rotational energy. This was not obtainable through adsorption experiments, due to the lack of control over rotational energy of the molecules in the beam. But the role of molecular rotations in adsorption could be inferred from the desorption experiments via detailed balance [20,21,124].

It appears that desorption experiments provide a deeper insight to the dynamics of the reaction than molecular beam experiments. Different techniques have been used to study associative desorption. These will be briefly summarized and compared with LAAD below.

The "Permeation method" has been used extensively to study the H_2/Cu system [164,165]. A thin single-crystal is mounted on a tube and molecules (gas at high pressure) are dosed from the backside. They dissociate and diffuse through the crystal, recombine on the crystals vacuum side, desorb as molecules and can then be detected. This method is limited to high temperatures, where diffusion is significant, and also to systems that "allow" diffusion through the solid.

Another technique has recently been used to study associative desorption [71,166]. A surface is dosed continuously with atoms, which adsorb, recombine and desorb molecularly at sufficiently high surface temperatures. Alternatively molecules containing the desired species are used for dosing, like NH_3 in the study of N_2 associative desorption [31]. When the dosing is suddenly stopped, the equilibrium between adsorption and desorption is perturbed, and only desorption is occurring until the coverage reaches a new equilibrium value. When using atoms, dosing has to be stopped also to make sure that no molecules from Eley-Rideal abstractions and scattered non-dissociated molecules are detected. The disadvantage of this method is the rather low sensitivity. At surface temperatures above the desorption temperature, the coverage is expected to be low. When the dosing is shut off, the equilibrium coverage is even lower than when dosing is occurring. This results in molecules desorbing at a rather low rate because of the low coverage. Higher coverages can only be achieved at lower surface temperature. But this will again result in a small rate according to the Arrhenius formula. In the T-jump method, we desorb a relatively large amount of gas over a very short time of only 100 ns. The flux is therefore much higher. It should be noted that for N_2/Ru(0001) the results were probably influenced by defects [31].

Both alternative techniques need sophisticated state-resolved laser based detection methods to obtain TOF distributions, whereas detection following a T-jump in LAAD can also be done with only a mass spectrometer. For N_2/Ru(0001) it was even possible via LAAD, without state-resolved detection, to determine that associative desorbing N_2 were formed in high vibrational states.

An advantage of the two alternative methods is the well-defined temperature, whereas desorption in LAAD is occurring over a finite (but narrow) temperature range. For N_2/Ru(0001) exact knowledge of the temperature was not necessary, though. The only change with temperature, apart from the higher desorption yield, was a lower "vibrational resolution" in the TOF distribution. The overall energetics did not change significantly and determination of the barrier was not sensitive to exact knowledge of the temperature.

LAAD can be used to study a wide range of adsorbate coverages as demonstrated for N_2/Ru(0001). Furthermore, the surface temperature in LAAD can be varied simply, by changing the laser intensity. In both alternative techniques the coverage and temperature is coupled as discussed above and can therefore only be varied over a limited range.

For N_2/Ru(0001) the problems with defects in adsorption experiments did not seem to appear when using LAAD. There were two reasons. Diffusion to defects was limited due to the high diffusion barrier for N/Ru(0001) and the short time scale of the heating. Although the activation energy for desorption from terrace sites is higher, also the pre-exponential is higher. It was discussed that the rapid laser heating then favors desorption from the terrace sites.

As to LAAD of CO from Ru(0001). At first glance, the thermal desorbing CO could be seen as a limitation of LAAD, but one that is shared by all techniques. One has to remember that determination of barriers in a sticking experiment did not give any results either. The thermal desorbing CO was a consequence of the dynamics of the reaction. Even though the CO was formed over a high barrier the thermalized desorption was explained by an energy loss in the deep and corrugated molecular well.

The presence of a deep molecular well seems in general to inhibit translational activation of dissociation of diatomic molecules on metal surfaces. This is the case for CO on Pt(111), Ni(111) and Ru(0001), where the molecule-surface binding energy is on the order of 1.5 eV. In contrast, translational activation is observed for dissociation of CO on Cu(110) where the molecular well depth is only 0.5 eV [167]. Also e.g. N_2 on Ru(0001) [27,29], H_2 on Cu [17,18] and O_2 on W(110) [168] only have weak molecular binding and do indeed show translational activation of dissociative chemisorption. The dynamics may be more complicated and this criteria is by no means expected to be valid in all cases.

We found that if no dissociation occurs for incident translational energies above the barrier height, when there is a deep molecular well, then there is a possibility for strong thermalization in associative desorption as observed for CO/Ru(0001). For N_2/Ru(0001) translational activation is observed, and our LAAD experiments demonstrated that no significant interaction with the molecular well occurs in associative desorption. Another example is the LAAD measurements we have made on methane associative desorbing from Ru(0001). The reaction $CH_{3(ads)} + H_{(ads)} \rightarrow CH_{4(gas)}$ shows methane desorbing with hyper-thermal energies in full accord with the observed translational activation in dissociative chemisorption [169]. Also methane experiences only a very weak molecule-surface binding. These experiments will be discussed in detail elsewhere [108].

In conclusion, when applicable LAAD is a very effective technique to study the dynamics of high barrier gas-surface reactions. Including state-resolved detection would lead to a further improvement and is currently in progress [170].

10.2 Summary of the experimental results

Surface dynamics studies on well-defined metal single crystals have identified two fundamental classes of bond-breaking reactions at surfaces: Direct dissociation of the molecule upon impact, and indirect dissociation via an adsorbed molecular 'precursor' state. The molecular beam study of methanol decomposition on Pt(111) showed that both dissociation mechanisms can occur in parallel. A non-activated indirect channel existed alongside a direct channel with an activation barrier of ~0.5 eV. This occurred through a surface site dependence and modification of the surface allowed us to control one of the channels. The non-activated, precursor mediated channel occurred at minority defect sites, while the activated, direct channel occurred at the majority terrace sites.

In heterogeneous catalysis, where a surface is used as a catalyst, new chemical species are formed by reactions on a surface. The initial step is adsorption of the reactants on the surface. Chemical reactions on catalyst surfaces mostly occur under conditions of high adsorbate coverages. In some cases adsorption of one species can induce desorption of another pre-adsorbed species. This is a process, which has to be considered since removing one of the reactants is not desired.

Catalytic ammonia synthesis on a Ru-surface is believed to proceed via N_2 dissociation on a surface followed by hydrogenation of N atoms. As an alternative mechanism it was suggested that ammonia could be formed by adding H atoms, one by one, to a N_2 molecule adsorbed on Ru(0001) [53,54].
We attempted to produce ammonia by exposing a N_2 covered Ru(0001) surface to a D or H atom beam. We found instead, under our experimental conditions, that this was leading to prompt desorption of the N_2 molecules. A strong isotope effect was observed, where a D atom was found to be twice as effective as an H atom in displacing a N_2. We proposed that the mechanism for N_2 displacement is creation of a "thermal hot spot" by the incident atom accelerated in the atom/surface potential well. As well as phonons, there is a possibility of direct energy transfer between D(H) and N_2 leading to excitation of the N_2-Ru bond.

Because there is a very large barrier to N_2 dissociation on Ru, it is very difficult to build up large coverages of adsorbed N. In fact, there is now considerable disagreement as to the maximum coverage allowed on Ru surfaces. We reported a novel way to produce high coverage states of nitrogen atoms adsorbed on Ru(0001) using an atomic N beam for dosing. For low atom doses, well known low coverage states were produced, but for higher atom doses, several previously unknown higher coverage states were sequentially filled. These states exhibited well-defined temperature programmed desorption (TPD) peaks, which shifted to considerably lower temperatures with N coverage. The highest N coverage obtainable was almost 1 ML N/Ru. The large decrease in Ru-N bond strength with N coverage apparent in our results was in good agreement with density functional theory (DFT). A combination of

these calculations and our experiments indicated that the highest coverage states are in fact metastable, relative to associative desorption, stabilized only by the increased barrier between the gas phase and the adsorbed state.

An experimental technique which we termed Laser Assisted Associative Desorption (LAAD) has been presented in this thesis. LAAD provides great insight into the dynamics of associative desorption and its time reversed process, dissociative chemisorption. Other experimental techniques used for studying the kinetics and dynamics of activated dissociative chemisorption are often of quite limited utility when energy barriers are very high (>1 eV). A dynamical study of the interaction of N_2 with a Ru(0001) surface was presented, demonstrating the power of this LAAD technique to high barrier gas-surface reactions. It was shown that N_2 is preferentially desorbed into very high vibrational states and that the barriers, directly measured by LAAD, between gas phase N_2 and adsorbed N atoms increases from 2 eV to > 3 eV with increasing N coverage on the surface. These experimental results prompted new DFT calculations of the barriers, which were shown to be in excellent agreement with the experiments. It was shown that the application of detailed balance leads to prediction of dissociation probabilities in agreement with recent molecular beam experiments.

LAAD applied to associative desorption of CO from Ru(0001) showed that even though the molecule is formed over a significant barrier the energy is dissipated when the molecule passes through the strong molecular well in the desorption process, leading to a desorption at ~thermal energies.

Most UHV surface science studies of dissociative chemisorption on metal surfaces, i.e. molecular beam studies, generally study the dissociative chemisorption on the bare metal surface in the limit of zero surface coverage. However, for industrially relevant conditions, the coverage of dissociated species is often quite high. While it is well recognized that a high coverage of the dissociated species can reduce the number of available dissociation sites, the studies presented here pointed out that the presence of dissociated species on the surface can also strongly affect the height of the dissociation barrier at available sites. LAAD was proven to be a very effective technique to study the effects, changes in coverage had on the barrier.

10.3 Outlook

High barrier gas-surface reactions of dissociative adsorption are difficult to study experimentally with the more conventional techniques: Supersonic molecular beams and thermal high-pressure dosing. It is possible to overcome some of the problems by instead studying associative desorption, which is the time-reversed process of dissociative adsorption. The insight into the dynamics of the process seems to be more detailed than what is achievable from adsorption experiments. The technique of laser assisted associative desorption was presented in this thesis. It was shown that LAAD could be applied to study systems like N_2/Ru(0001) and CO/Ru(0001), but the technique is generally applicable. As long as it is possible to prepare a given surface with the desired adsorbates, LAAD can be used to measure translational energy distributions of associative desorbing molecules from which detailed information about the dynamics can be inferred. A wide range of coverages and effects of surface

temperatures can be studied with LAAD. Including state-resolved detection of the desorbing molecules will further improve the output of LAAD. Many adsorbate/ surface systems are waiting to be studied in the future.

10.4 Dansk sammenfatning (Danish summary)

Overfladefysik har i de seneste årtier udviklet sig til at være et selvstændigt forskningsområde, som generelt drejer det sig om de fysiske og kemiske egenskaber af overflader og vekselvirkningen mellem overflader og gasser eller elektromagnetisk stråling. Udover den fundamentale videnskabelige interesse er overfladefysik motiveret af en række anvendelser indenfor mikroelektronik, katalyse, overflade korrosion og tribologi. Denne afhandling er koncentreret omkring dynamikken af gas-overflade vekselvirkninger med speciel vægt på dissociativ adsorption og associativ desorption. Disse processer er fundamentale trin af kemiske gas-overflade reaktioner, tildels motiveret af betydningen indenfor heterogen katalyse.

Brydning af molekylebindinger ved metaloveflader kan ske via to grundlæggende mekanismer. Enten den direkte, hvor et molekyle dissocierer så snart det rammer metaloverfladen, eller en indirekte som foregår via en såkaldt molekylær pre-cursor hvor molekylet først adsorberer intakt på overfladen, termaliserer og derefter dissocierer ved termisk aktivering. Ved brug af molekylestråle teknikker kan man studere ved hvilken mekanisme molekylet dissocierer. Dette har vi undersøgt for metanol på en Pt(111) overflade og fundet at *begge* mekanismer kan foregå parallelt. En direkte proces, der foregår på de flade terasser og en pre-cursor proces, som foregår ved defekter.

Når et molekyle eller et atom adsorberer på en overflade kan den frigivne adsorptionsenergi resultere i desorption af andre adsorbater. Vi har vist, at N_2 molekyler adsorberet på Ru(0001) desorberer omgående når D eller H atomer adsorber. En isotop effekt blev observeret, hvor D atomerne viste sig at være dobbelt så effektive som H atomerne til at desorbere N_2 molekylerne. Dette blev forklaret ved en mekanisme, hvor en "termisk hot spot" blev dannet ved adsorption af hydrogen atomet. Desorption af N_2 skyldes således gitter-fononer. Det blev diskutteret at delvis eksitation af N_2-Ru bindingen også kan ske ved direkte energioverførsel mellem N_2 og det indkomne atom.

Der har været stor interesse for vekselvirkning mellem nitrogen og rutenium (Ru), tildels pga muligheden for at bruge rutenium som en effektiv katalysator til fremstilling af ammoniak. Det rate-begrænsende trin i ammoniak-syntesen er dissociation af N_2 på Ru overfladen. På Ru(0001) er der en meget høj dissociations barriere, som gør det svært at opbygge en høj N-dækning på overfladen. Vi har vist, at ved brug af N atom dosering kan man opbygge de velkendte lavdæknings tilstande af N/Ru(0001) såvel som nye højdæknings tilstande. Disse blev studeret ved bl.a. temperatur programeret desorption (TPD). Ved at sammenholde desorptions energier fra TPD med beregnede adsorptions energier fra literaturen blev det bestemt, at højdæknings tilstandene er metastabile, kun stabiliseret ved en øget barriere mellem gasfase N_2 og de adsorberede atomer.

Studiet af gas-overflade reaktioner er vanskelige når barrierer er meget høje. Det er ikke uden problemer at anvende teknikker som molekylestråler og højtryks dosering i studiet af dissociativ kemisorption. En eksperimentel metode kaldet Laser Assisteret Associativ Desorption (LAAD) blev præsenteret i denne afhandling. LAAD giver dyb indsigt i dynamikken af associativ desorption, som er den tidsomvendte proces af dissociativ adsorption. En række af de ting, som voldte adsorptions teknikkerne problemer, var elimineret ved brug af LAAD.

Vi har studeret associativ desorption af N_2 fra Ru(0001) ved brug af LAAD. Det blev vist, at N_2 desorberer i meget høje vibrationstilstande og at barrieren stiger kraftigt med nitrogendækningen. Disse resultater gav anledning til nye teoretiske beregninger, som viste sig at være i perfekt overenstemmelse med vores eksperimentelle resultater. Ved brug af detaljeret balance blev adsorptionssandsynligheder beregnet fra LAAD resultaterne. Disse viste sig at være i god overenstemmelse med de nyeste eksisterende molekylestråle data.

11 References

[1]   L. Diekhöner, D.A. Butler, A. Baurichter and A.C. Luntz,
        Parallel pathways in methanol decomposition on Pt(111).
        Surf. Sci. **409**: 384, (1998).
[2]   L. Diekhöner, A. Baurichter, H. Mortensen and A.C. Luntz,
        Observation of metastable atomic nitrogen adsorbed on Ru(0001).
        J. Chem. Phys. **112**: 2507, (2000).
[3]   L. Diekhöner, H. Mortensen, A. Baurichter and A.C. Luntz,
        Coverage dependence of activation barriers: Nitrogen on Ru(0001).
        J. Vac. Sci. Technol. A. **18**: in press, (2000).
[4]   L. Diekhöner, H. Mortensen, A. Baurichter, A.C. Luntz and B. Hammer,
        *Dynamics of high barrier surface reactions: Laser Assisted Associative
        Desorption of N_2 from Ru(0001).*
        Phys. Rev. Lett. **84**: 4906, (2000).
[5]   J.A. Barker and D.J. Auerbach,
        *Gas-surface interactions and dynamics; thermal energy atomic and molecular
        beam studies.*
        Surf. Sci. Rep. **4**(1-2): 1, (1985).
[6]   J.E. Lennard-Jones,
        Processes of adsorption and diffusion on solid surfaces.
        Trans. Faraday. Soc. **28**: 333, (1932).
[7]   C.T. Rettner, E.K. Schweizer, H. Stein and D.J. Auerbach,
        *Molecular-beam studies of the precursor-mediated dissociative chemisorption
        of nitrogen on W(100).*
        J. Vac. Sci. Technol., A. **7**: 1863, (1989).
[8]   C.T. Rettner, E.K. Schweizer and H. Stein,
        *Dynamics of the chemisorption of N_2 and molecular nitrogen on W(100):
        precursor-mediated and activated dissociation.*
        J. Chem. Phys. **93**: 1442, (1990).
[9]   D.C. Seets, M.C. Wheeler and C.B. Mullins,
        *Mechanism of the dissociative chemisorption of methane over Ir(110):
        trapping-mediated or direct?*
        Chem. Phys. Lett. **266**: 431, (1997).
[10]   D.C. Seets, M.C. Wheeler and C.B. Mullins,
        *Trapping-mediated and direct dissociative chemisorption of methane on
        Ir(110): A comparison of molecular beam and bulb experiments.*
        J. Chem. Phys. **107**: 3986, (1997).
[11]   D.C. Seets, C.T. Reeves, B.A. Ferguson, M.C. Wheeler and C.B. Mullins,
        *Dissociative chemisorption of methane on Ir(111): Evidence for direct and
        trapping-mediated mechanisms.*
        J. Chem. Phys. **107**: 10229, (1997).
[12]   H. Mortensen, L. Diekhöner, A. Baurichter, E. Jensen and A.C. Luntz,
        Dynamics of ammonia decomposition on Ru(0001).
        J. Chem. Phys. **submitted**, (2000).

[13]   D. Halstead and S. Holloway,
         The influence of potential energy surface topologies on the dissociation of molecular hydrogen.
         J. Chem. Phys. **93**: 2859, (1990).

[14]   C.T. Rettner, D.J. Auerbach and H.A. Michelsen,
         Role of vibrational and translational energy in the activated dissociative adsorption of molecular deuterium on Cu(111).
         Phys. Rev. Lett. **68**: 1164, (1992).

[15]   M. Hand and S. Holloway. *The scattering of H_2 and D_2 from Cu(100): vibrationally assisted dissociative adsorption.*
         Surf. Sci. **211-212**: 940, (1989).

[16]   L.B.F. Juurlink, P.R. McCabe, R.R. Smith, C.L. Dicologero and A.L. Utz,
         Eigenstate-resolved studies of gas-surface reactivity: CH_4 (v3) dissociation on Ni(100).
         Phys. Rev. Lett. **83**: 868, (1999).

[17]   M.J. Cardillo, M. Balooch and R.E. Stickney,
         Detailed balancing and quasi-equilibrium in the adsorption of hydrogen on copper.
         Surf. Sci. **50**: 263, (1975).

[18]   H.A. Michelsen and D.J. Auerbach,
         A critical examination of data on the dissociative adsorption and associative desorption of hydrogen at copper surfaces.
         J. Chem. Phys. **94**: 7502, (1991).

[19]   C.T. Rettner, E.K. Schweizer and C.B. Mullins,
         Desorption and trapping of argon at a hydrogen-saturated tungsten (2H-W(100)) surface and a test of the applicability of detailed balance to a nonequilibrium system.
         J. Chem. Phys. **90**: 3800, (1989).

[20]   H.A. Michelsen, C.T. Rettner and D.J. Auerbach,
         State-specific dynamics of molecular deuterium desorption from Cu(111): the role of molecular rotational motion in activated adsorption-desorption dynamics.
         Phys. Rev. Lett. **69**: 2678, (1992).

[21]   H.A. Michelsen, C.T. Rettner, D.J. Auerbach and R.N. Zare,
         Effect of rotation on the translational- and vibrational-energy dependencies of the dissociative adsorption of molecular deuterium on Cu(111).
         J. Chem. Phys. **98**: 8294, (1993).

[22]   M.J. Murphy and A. Hodgson,
         Adsorption and desorption dynamics of H_2 and D_2 on Cu(111): The role of surface temperature and evidence for corrugation of the dissociation barrier.
         J. Chem. Phys. **108**: 4199, (1998).

[23]   G.R. Darling and S. Holloway,
         Vibrational effects in the associative desorption of hydrogen.
         Surf. Sci. **268**: L305, (1992).

[24]   H. Shi, K. Jacobi and G. Ertl,
         Dissociative chemisorption of nitrogen on Ru(0001).
         J. Chem. Phys. **99**: 9248, (1993).

[25]   H. Dietrich, P. Geng, K. Jacobi and G. Ertl,
         Sticking coefficient for dissociative adsorption of N_2 on Ru single-crystal surfaces.
         J. Chem. Phys. **104**: 375, (1996).

[26]   S. Dahl, A. Logadottir, R.C. Egeberg, J.H. Larsen, I. Chorkendorff, E. Törnqvist and J.K. Nørskov,
         Role of steps in N_2 activation on Ru(0001).
         Phys. Rev. Lett. **83**: 1814, (1999).

[27]   L. Romm, G. Katz, R. Kosloff and M. Asscher,
         Dissociative Chemisorption of N_2 on Ru(001) Enhanced by Vibrational and Kinetic Energy: Molecular Beam Experiments and Quantum Mechanical Calculations.
         J. Phys. Chem. B. **101**: 2213, (1997).

[28]   A. Kleyn, *private communication,* (1999).

[29]   R.C. Egeberg, J.H. Larsen and I. Chorkendorff,
         Molecular beam study of N_2 dissociation on Ru(0001).
         private communication, (1999).

[30]   L. Diekhöner, H. Mortensen, A. Baurichter and A.C. Luntz, *Molecular beam studies of N_2/Ru*, unpublished. 1999.

[31]   M.J. Murphy, J.F. Skelly, A. Hodgson and B. Hammer,
         Inverted vibrational distributions for N2 recombination at Ru(001): Evidence for a metastable molecular chemisorption well.
         J. Chem. Phys. **110**: 6954, (1999).

[32]   J.J. Mortensen, Y. Morikawa, B. Hammer and J.K. Nørskov,
         Density functional calculations of N_2 adsorption and dissociation on a Ru(0001) surface.
         J. Catal. **169**: 85, (1997).

[33]   A.C. Luntz, M.D. Williams and D.S. Bethune,
         The sticking of molecular oxygen on a Pt(111) surface.
         J. Chem. Phys. **89**(7): 4381, (1988).

[34]   G. Scoles,
         Atomic and molecular beam methods. Vol. 1. 1988: Oxford Univ. Press.

[35]   J.C. Walling, *Tunable paramagnetic-ion solid-state lasers*, in *Topics in Applied Physics*, L.F. Mollenhauer and J.C. White, Editors. 1987, Springer-Verlag.

[36]   H. Mortensen, *Ph.D. Thesis*, *SDU-Odense Universitet*. to be published.

[37]   B.A. Sexton,
         Methanol decomposition on Pt(111).
         Surf. Sci. **102**: 271, (1981).

[38]   K.D. Gibson and L.H. Dubois,
         Step effects in the thermal decomposition of methanol on Pt(111).
         Surf. Sci. **233**: 59, (1990).

[39]   J.L. Davis and M.A. Barteau,
         Decarbonylation and decomposition pathways of alcohols on Pd(111).
         Surf. Sci. **187**: 387, (1987).

[40]   R.J. Levis, J. Zhicheng, N. Winograd, S. Akhter and J.M. White,
         Catal. Lett. **1**: 385, (1988).

[41]   D.M. Collins and W.E. Spicer,
         The adsorption of CO, O_2 and H2 on Pt(111).
         Surf. Sci. **69**: 85, (1977).

[42] H. Steininger, S. Lehwald and H. Ibach,
      On the adsorption of CO on Pt(111).
      Surf. Sci. **123**: 264, (1982).

[43] D.A. King and M.G. Wells,
      Reaction mechanism in chemisorption kinetics. Nitrogen on the {100} plane of tungsten.
      Proc. Roy. Soc. London, Ser. A. **339**(1617): 245, (1974).

[44] J. Harris, *Mechanical energy transfer in particle-surface collisions*, in *Dynamics of Gas-Surface Interactions*, C.T. Rettner and M.N.R. Ashfold, Editors. 1991, The Royal Society of Chemistry: London. p. 1.

[45] J.L. Gland,
      Molecular and atomic adsorption of oxygen on the Pt(111) and Pt(S)-12(111) x (111) surfaces.
      Surf. Sci. **93**: 487, (1980).

[46] H.P. Bonzel, A.M. Franken and G. Pirug,
      The segregation and oxidation of silicon on Pt(111), or: The question of the "Platinum Oxide".
      Surf. Sci. **104**: 625, (1981).

[47] S. Akhter, C.M. Greenlief, W.-H. Chen and J.M. White,
      A SIMS study of the influence of low levels of silicon and calcium on the adsorption properties of O_2 on Pt(111).
      Appl. Surf. Sci. **25**: 154, (1986).

[48] A.C. Luntz and P. Kratzer,
      D_2 dissociative adsorption on and associative desorption from Si(100): dynamic consequences of an ab initio potential energy surface.
      J. Chem. Phys. **104**: 3075, (1996).

[49] S.R. Tennison, in *Catalytic Ammonia Synthesis*, J.R. Jennings, Editor. 1991, Plenum: New York. p. 303.

[50] S. Dahl, P.A. Taylor, E. Törnqvist and I. Chorkendorff,
      The synthesis of ammonia over a ruthenium single crystal.
      J. Catal. **178**(2): 679, (1998).

[51] T.H. Rod, B. Hammer and J.K. Nørskov,
      Nitrogen adsorption and hydrogenation on a $MoFe_6S_9$ complex.
      Phys. Rev. Lett. **82**: 4054, (1999).

[52] B. Fastrup,
      On the interaction of N_2 and H_2 with Ru catalyst surfaces.
      Catal. Lett. **48**: 111, (1997).

[53] J.K. Nørskov, *private communication*, (1998).

[54] T.H. Rod, A. Logadottir and J.K. Nørskov,
      Ammonia synthesis at low temperature.
      J. Chem. Phys. **112**: 5343, (2000).

[55] W.J. Mitchell, J. Xie, T.A. Jachimowski and W.H. Weinberg,
      Carbon Monoxide Hydrogenation on the Ru(001) Surface at Low Temperature Using Gas-Phase Atomic Hydrogen: Spectroscopic Evidence for the Carbonyl Insertion Mechanism on a Transition Metal Surface.
      J. Am. Chem. Soc. **117**(9): 2606, (1995).

[56] C. Åkerlund, I. Zoric, B. Kasemo, A. Cupolillo, F. Buatier de Mongeot and M. Rocca,
Dissociation of O_2 chemisorbed on Ag (110) and Pt(111) induced by energetic Xe atoms.
Chem. Phys. Lett. **270**: 157, (1997).

[57] C. Åkerlund, I. Zoric and B. Kasemo,
Collision induced desorption and dissociation of O_2 on Pt(111).
J. Chem. Phys. **109**: 737, (1998).

[58] L. Romm, Y. Zeiri and M. Asscher,
Collision induced desorption of N_2 from Ru(001).
J. Chem. Phys. **108**: 8605, (1998).

[59] C.T. Rettner and J. Lee,
Dynamic displacement of O_2 from Pt(111): a new desorption mechanism.
J. Chem. Phys. **101**: 10185, (1994).

[60] M.C. Wheeler, D.C. Seets and C.B. Mullins,
Angular dependence of the dynamic displacement of O_2 from Pt(111) by atomic oxygen.
J. Chem. Phys. **107**: 1672, (1997).

[61] C.T. Rettner and D.J. Auerbach,
Dynamics of the displacement of CO from Cu(111) by H atoms incident from the gas phase.
J. Chem. Phys. **105**: 8842, (1996).

[62] G.A. Kimmel, K.P. Stevenson and B.D. Kay.
Adsorption driven displacement of N_2 from Pt(111).
Abstract from 46'th AVS International Symposium. 1999. Seattle, WA, USA.

[63] H. Mortensen, *Adsorption and desorption of molecules from metal surfaces - extracting the details*, Master thesis, *Fysisk Institut, SDU-Odense Universitet.* 1998.

[64] H. Shi and K. Jacobi,
Evidence for physisorbed N_2 in the monolayer on Ru(001) at 40 K.
Surf. Sci. **278**: 281, (1992).

[65] P. Feulner and D. Menzel,
Unusual coverage dependence of a sticking coefficient: N_2/Ru(001).
Phys. Rev. B: **25**: 4295, (1982).

[66] A.B. Anton, N.R. Avery, B.H. Toby and W.H. Weinberg,
The chemisorption of nitrogen on the (001) surface of ruthenium.
J. Electron Spectrosc. Relat. Phenom. **29**: 181, (1983).

[67] M. Lindroos, H. Pfnür, P. Feulner and D. Menzel,
A study of the adsorption sites of hydrogen on Ru(001) at saturation coverage by electron reflection.
Surf. Sci. **180**: 237, (1987).

[68] J.K. Nørskov and B.I. Lundqvist,
Correlation between sticking probability and adsorbate-induced electron structure.
Surf. Sci. **89**: 251, (1979).

[69] B. Hellsing, B.I. Lundqvist and M. Persson,
Electronic damping mechanism for vibrations, rotations and translations of adsorbates on metal surfaces.
Surf. Sci. **126**: 147, (1983).

[70]   B. Hammer,
        Bond activation at mono-atomic steps: NO dissociation at corrugated Ru(0001).
        Phys. Rev. Lett. **83**: 3681, (1999).
[71]   A. Hodgson,
        State resolved desorption measurements as a probe of surface reactions.
        Prog. Surf. Sci. **63**: 1, (2000).
[72]   P.A. Redhead,
        Vacuum. **12**: 203, (1962).
[73]   C. Stampfl and M. Scheffler,
        Theoretical study of O adlayers on Ru(0001).
        Phys. Rev. B: **54**: 2868, (1996).
[74]   M. Lindroos, H. Pfnür, G. Held and D. Menzel,
        Adsorbate induced reconstruction by strong chemisorption: Ru(001)p(2x2)-O.
        Surf. Sci. **222**: 451, (1989).
[75]   S. Schwegmann, A.P. Seitsonen, H. Dietrich, H. Bludau, H. Over, K. Jacobi and G. Ertl,
        The adsorption of atomic nitrogen on Ru(0001): geometry and energetics.
        Chem. Phys. Lett. **264**: 680, (1997).
[76]   J. Trost, T. Zambelli, J. Wintterlin and G. Ertl,
        Adsorbate-adsorbate interactions from statistical analysis of STM images: N/Ru(0001).
        Phys. Rev. B: **54**: 17850, (1996).
[77]   C. Stampfl, S. Schwegmann, H. Over, M. Scheffler and G. Ertl,
        Structure and stability of a high-coverage (1x1) oxygen phase on Ru(0001).
        Phys. Rev. Lett. **77**: 3371, (1996).
[78]   M.C. Wheeler, D.C. Seets and C.B. Mullins,
        Kinetics and dynamics of the initial dissociative chemisorption of oxygen on Ru(001).
        J. Chem. Phys. **105**: 1572, (1996).
[79]   H. Pfnür, G. Held, M. Lindroos and D. Menzel,
        Oxygen induced reconstruction of a close-packed surface: a LEED IV study on Ru(001)-p(2x1)O.
        Surf. Sci. **220**: 43, (1989).
[80]   K.L. Kostov, M. Gsell, P. Jakob, T. Moritz, W. Widdra and D. Menzel,
        Observation of a novel high density 3O(2x2) structure on Ru(001).
        Surf. Sci. **394**: L138, (1997).
[81]   H. Dietrich, K. Jacobi and G. Ertl,
        Coverage, lateral order, and vibrations of atomic nitrogen on Ru(0001).
        J. Chem. Phys. **105**: 8944, (1996).
[82]   H. Rauscher, K.L. Kostov and D. Menzel,
        Adsorption and decomposition of hydrazine on Ru(001).
        Chem. Phys. **177**: 473, (1993).
[83]   K. Jacobi,
        Nitrogen on ruthenium single-crystal surfaces.
        Phys. Stat. Sol. (a). **177**: 37, (2000).
[84]   A. Logadottir and J.K. Nørskov, *private communication*, (1999).
[85]   R.A. Young, R.L. Sharpless and R. Stringham,
        Catalyzed Dissociation of N_2 in Microwave Discharges. I.
        J. Chem. Phys. **40**: 117, (1964).

[86]   S.N. Foner and R.L. Hudson,
        Mass spectrometric studies of metastable nitrogen atoms and molecules in active nitrogen.
        J. Chem. Phys. **37**: 1662, (1962).

[87]   K.R. Lykke and B.D. Kay,
        Two-photon spectroscopy of molecular nitrogen: multiphoton ionization, laser-induced fluorescence, and direct absorption via the a" $^1\sum_g^+$ state.
        J. Chem. Phys. **95**: 2252, (1991).

[88]   M. Schick, J. Wie, W.J. Mitchell and W.H. Weinberg,
        Interaction of gas-phase atomic deuterium with the Ru(001)-p(1x2)-O surface: kinetics of hydroxyl and water formation.
        J. Chem. Phys. **104**: 7713, (1996).

[89]   H. Pfnür, P. Feulner and D. Menzel,
        The influence of absorbate interactions on kinetics and equilibrium for CO on Ru(001). II. Desorption kinetics and equilibrium.
        J. Chem. Phys. **79**: 4613, (1983).

[90]   T. Zambelli, J. Trost, J. Wintterlin and G. Ertl,
        Diffusion and atomic hopping of N atoms on Ru(0001) studied by scanning tunneling microscopy.
        Phys. Rev. Lett. **76**: 795, (1996).

[91]   W. Tsai and W.H. Weinberg,
        Steady-state decomposition of ammonia on the Ru(001) surface.
        J. Phys. Chem. **91**: 5302, (1987).

[92]   P. Jakob, M. Stichler and D. Menzel,
        The adsorption of NO on Ru(001) and on O(2x1)/Ru(001) revisited.
        Surf. Sci. **370**: L185, (1997).

[93]   P. He and K. Jacobi,
        Vibrational analysis of the 1x1-O overlayer on Ru(0001).
        Phys. Rev. B: **55**: 4751, (1997).

[94]   B. Hammer, L.B. Hansen and J.K. Nørskov,
        Improved adsorption energetics within density function theory using revised PBE functionals.
        Phys. Rev. **B59**: 7413, (1999).

[95]   J.H. Larsen, *Reactivity of pure and modified surfaces*, PhD thesis. 1998, Technical University of Denmark: Lyngby, Denmark.

[96]   A. Böttcher and H. Niehus,
        Formation of subsurface oxygen at Ru(0001).
        J. Chem. Phys. **110**: 3186, (1999).

[97]   J.J. Mortensen, B. Hammer and J.K. Nørskov,
        A theoretical study of adsorbate-adsorbate interactions on Ru(0001).
        Surf. Sci. **414**: 315, (1998).

[98]   C. Nagl, R. Schuster, S. Renisch and G. Ertl,
        Regular mixing in a two-dimensional lattice system: the coadsorption of N and O on Ru(0001).
        Phys. Rev. Lett. **81**: 3483, (1998).

[99]   C.J. Hagedorn, M.J. Weiss and W.H. Weinberg,
        Ammonia decomposition on Ru(001) using gas-phase atomic hydrogen.
        J. Vac. Sci. Technol., A. **16**: 984, (1998).

[100] L. Danielson, M.J. Dresser, E.E. Donaldson and D.R. Sandstrom,
Effects of an electron beam on adsorption and desorption of ammonia on Ru(0001).
Surf. Sci. **71**: 615, (1978).

[101] J.M. Hicks, *Laser heating and time-resolved measurements of transient temperature changes on surfaces*, in *Laser Spectroscopy and Photochemistry on Metal Surfaces*, H.-L. Dai and W. Ho, Editors. 1995, World Scientific. p. 589.

[102] S.M. George, *Laser-induced thermal desorption*, in *Investigations of Surfaces and Interfaces - part A*, B.W. Rossiter and R.C. Baetzold, Editors. 1993, John Wiley & Sons. p. 453.

[103] A.A. Deckert, J.L. Brand, M.V. Arene and S.M. George,
Surface diffusion of carbon monoxide on Ru(0001) studied using laser-induced thermal desorption.
Surf. Sci. **208**: 441, (1989).

[104] J.H. Bechtel,
Heating of solid targets with laser pulses.
J. Appl. Phys. **46**: 1585, (1975).

[105] J.F. Ready,
Effects of high-power laser radiation.
1971, New York: Academic Press.

[106] S. Nettesheim and R. Zenobi,
Pulsed laser heating of surfaces: nanosecond timescale temperature measurement using black body radiation.
Chem. Phys. Lett. **255**: 39, (1996).

[107] A.M. Prokhorov, V.I. Konov, I. Ursu and I.N. Mihailescu,
Laser heating of metals.
. The Adam Hilger series on optics and optoelectronics. 1990, Bristol: Hilger.

[108] H. Mortensen, L. Diekhöner, A. Baurichter and A.C. Luntz,
Dynamics of CH_4 associative desorption.
In preparation.

[109] J. Frohn, J. Reynolds and T. Engel,
Surface morphology changes upon laser heating of Pt(111).
Surf. Sci. **320**: 93, (1994).

[110] G. Hoogers, D.C. Papageorgopoulos and D.A. King,
Strain-induced disordering of metal surfaces: rapid laser heating of Rh{111} and Rh{332}.
Surf. Sci. **310**: 147, (1994).

[111] H.-J. Ernst, F. Charra and L. Douilard,
Interband electronic excitation-assisted atomic-scale restructuring of metal surfaces by nanosecond pulsed laser light.
Science. **279**: 679, (1998).

[112] S.R. Brueck and D.J. Ehrlich,
Stimulated surface-plasme-wave scattering and growth of a periodic structure in laser-photodeposited metal films.
Phys. Rev. Lett. **48**: 1678, (1982).

[113] B. Poelsema and G. Comsa, eds. *Scattering of thermal energy atoms from disordered surfaces*.
Springer tracts in modern physics. Vol. 115. 1989, Springer-Verlag.

[114] S. Kneitz, J. Gemeinhardt, H. Koschel, G. Held and H.-P. Steinrück,
Energy and temperature dependent sticking coefficients of CO on ultrathin copper layers on Ru(0001).
Surf. Sci. **433-435**: 27, (1999).

[115] S. Kneitz, J. Gemeinhardt and H.-P. Steinrück,
A molecular beam study of the adsorption dynamics of CO on Ru(0001), Cu(111) and pseudomorphic Cu monolayer on Ru(0001).
Surf. Sci. **440**: 307, (1999).

[116] H. Pfnür and D. Menzel,
The influence of adsorbate interactions on kinetics and equilibrium for CO on Ru(001). I. Adsorption kinetics.
J. Chem. Phys. **79**(5): 2400, (1983).

[117] K.-H. Allers, H. Pfnür, P. Feulner and D. Menzel,
Angular and velocity distributions of CO desorbed from adsorption layers on Ni(100) and Pt(111): examples of non-activated desorption.
Surf. Sci. **291**: 167, (1993).

[118] G. Wedler and H. Ruhmann,
Laser induced thermal desorption of CO from Fe(110) surfaces.
Surf. Sci. **121**: 464, (1982).

[119] T.J. Chuang,
Laser-induced molecular processes on surfaces.
Surf. Sci. **178**: 763, (1986).

[120] D. Burgess, R. Viswanathan, I. Hussla, P.C. Stair and E. Weitz,
Pulsed laser induced thermal desorption of CO from copper surfaces.
J. Chem. Phys. **79**: 5200, (1983).

[121] K. Jacobi, H. Dietrich and G. Ertl,
Nitrogen chemistry on ruthenium single-crystal surfaces.
Appl. Surf. Sci. **121**: 558, (1997).

[122] J. Frohn, R. Reynolds and T. Engel,
Surface morphology changes upon laser heating of Pt(111).
Surf. Sci. **320**: 93, (1994).

[123] H.-J. Ernst, F. Charra and L. Douillard,
Interband electronic excitation-assisted restructuring of metal surfaces by nanosecond pulsed laser light.
Science. **279**: 679, (1998).

[124] C.T. Rettner, H.A. Michelsen and D.J. Auerbach,
Quantum-state-specific dynamics of the dissociative adsorption and associative desorption of H_2 at a Cu(111) surface.
J. Chem. Phys. **102**: 4625, (1995).

[125] M.R. Hand and S. Holloway,
A theoretical study of the dissociation of H_2/Cu.
Journal of Chemical Physics. **91**: 7209, (1989).

[126] A.C. Luntz and D.S. Bethune,
Activation of methane dissociation on a Pt(111) surface.
J. Chem. Phys. **90**: 1274, (1989).

[127] H.A. Michelsen, C.T. Rettner and D.J. Auerbach,
On the influence of surface temperature on adsorption and desorption in the D_2/Cu(111) system.
Surf. Sci. **272**: 65, (1992).

[128] A.T. Pasteur, S.J. Dixon-Warren, Q. Ge and D.A. King,
Dynamics of hydrogen dissociation on Pt{100}: steering, screening and thermal roughening effects.
J. Chem. Phys. **106**: 8896, (1997).

[129] M. Mavrikakis, B. Hammer and J.K. Nørskov,
Effect of Strain on the Reactivity of Metal Surfaces.
Phys. Rev. Lett. **81**: 2819, (1998).

[130] A.C. Luntz and J. Harris,
Methane dissociation on metals: a quantum dynamics model.
Surf. Sci. **258**: 397, (1991).

[131] A.C. Luntz,
A simple model for associative desorption and dissociative chemisortion.
Submitted. (2000).

[132] R.B. Levine, *Information theory approach to reaction dynamics*, in *Ann. Rev. Phys. Chem.*, B.S. Rabinovitch, J.M. Schur, and H.L. Strauss, Editors. 1978.

[133] R.B. Levine,
Chemical dynamics via molecular beam and laser techniques.
1982, New York: Oxford University Press.

[134] T. Zambelli, J. Wintterlin, J. Trost and G. Ertl,
Identification of the "active sites" of a surface-catalyzed reaction.
Science. **273**(5282): 1688, (1996).

[135] B. Hammer, *private communication*, (2000).

[136] B. Hammer and J.K. Nørskov, *Theory of adsorption and surface reactions*, in *Chemisorption and Reactivity on Supported Clusters and Thin Films*, R.M. Lambert and G. Pacchioni, Editors. 1997, Kluwer Academic Press. p. 285.

[137] M. Asscher, *Private communication*, (2000).

[138] D.C. Papageorgopoulos, B. Berenbak, M. Verwoest, B. Riedmüller, S. Stolte and A.W. Kleyn,
A molecular beam study of the scattering and chemisorption dynamics of N_2 on Ru(0001).
Chem. Phys. Lett. **305**: 401, (1999).

[139] C.T. Rettner, D.J. Auerbach and H.A. Michelsen,
Observation of direct vibrational excitation in collisions of molecular hydrogen and molecular deuterium with a Cu(111) surface.
Phys. Rev. Lett. **68**: 2547, (1992).

[140] L. Romm, O. Citri, R. Kosloff and M. Asscher,
A remarkable heavy atom isotope effect in the dissociative chemisorption of nitrogen on Ru(001).
J. Chem. Phys. **112**: 8221, (2000).

[141] R. Kosloff, *private communication*, (1999).

[142] R.D. Kelley and D.W. Goodman. *The methanation reaction.* in *Chem. Phys. Solid Surf. Heterog. Catal.* 1982: Elsevier, Amsterdam, Netherlands.

[143] R.D. Kelley and D.W. Goodman,
Catalytic methanation over single-crystal nickel and ruthenium: reaction kinetics on different crystal planes and the correlation of surface carbide concentration with reaction rate.
Surf. Sci. **123**: L743, (1982).

[144] Y. Morikawa, J.J. Mortensen, B. Hammer and J.K. Nørskov,
CO adsorption and dissociation on Pt(111) and Ni(111) surfaces.
Surf. Sci. **386**: 67, (1997).

[145] M.B. Lee, J.D. Beckerle, S.L. Tang and S.T. Ceyer,
Lack of translational energy activation of the dissociative chemisorption of carbon monoxide on Ni(111).
J. Chem. Phys. **87**: 723, (1987).

[146] J. Harris and A.C. Luntz,
Sticking and scattering in the molecular chemisorption regime: CO on Pt(111).
J. Chem. Phys. **91**: 6421, (1989).

[147] M. Kiskinova, G. Pirug and H.P. Bonzel,
Coadsorption of potassium and CO on Pt(111).
Surf. Sci. **133**: 321, (1983).

[148] F.M. Hoffmann,
The kinetics of CO dissociation on Ru(001): Time-resolved vibrational spectroscopy at elevated pressures.
J. Chem. Phys. **90**: 2816, (1988).

[149] E. Shincho, C. Egawa, S. Naito and K. Tamaru,
The behavior of CO adsorbed on Ru(1,1,10) and Ru(001); the dissociation of CO at the step sites of the Ru(1,1,10) surface.
Surf. Sci. **149**: 1, (1985).

[150] E. Shincho, C. Egawa, S. Naito and K. Tamaru,
The behavior of carbon species produced by CO dispropotionation on Ru(1,1,10) and Ru(001) surfaces.
Surf. Sci. **155**: 153, (1985).

[151] L.L. Lauderback and W.N. Delgas,
CO dissociation and C-D interaction on Ru(001).
J. Catalysis. **105**: 55, (1987).

[152] J.C. Fuggle, E. Umbach, P. Feulner and D. Menzel,
Electron induced dissociation of carbon monoxide on Ru(001). A study by thermal desorption and electron spectroscopies.
Surf. Sci. **64**: 69, (1977).

[153] T.E. Madey, H.A. Engelhardt and D. Menzel,
Adsorption of oxygen and oxidation of CO on the Ru(001) surface.
Surf. Sci. **48**: 304, (1975).

[154] K.L. Kostov, H. Rauscher and D. Menzel,
Adsorption of carbon monoxide on oxygen-covered Ru(001).
Surf. Sci. **278**: 62, (1992).

[155] P. Feulner and D. Menzel,
The adsorption of hydrogen on Ru(001): adsorption states, dipole moments and kinetics of adsorption and desorption.
Surf. Sci. **154**: 465, (1985).

[156] M.-C. Wu, Q. Xu and D.W. Goodman,
Investigations of Graphitic Overlayers Formed from Methane Decomposition on Ru(0001) and Ru(11$\bar{2}$0) Catalysts with Scanning Tunneling Microscopy and High-Resolution Electron Energy Loss Spectroscopy.
J. Phys. Chem. **98**: 5104, (1994).

[157] J. Hrbek,
Carbonacous overlayers on Ru(0001).
J. Vac. Sci. Technol. A. **4**: 86, (1986).

[158] H. Pfnür, P. Feulner, H.A. Engelhardt and D. Menzel,
*An example of "fast" desorption: anomalously high pre-exponentials for CO
desorption from Ru (001).*
Chem. Phys. Lett. **59**: 481, (1978).

[159] S.L. Tang, M.B. Lee, J.D. Beckerle, M.A. Hines and S.T. Ceyer,
*Effect of translational energy on chemisorption: evidence for a precursor to
molecular chemisorption.*
J. Chem. Phys. **82**: 2826, (1985).

[160] G.D. Billing,
Inelastic scattering and chemisorption of CO on a Pt(111) surface.
Chem. Phys. **86**: 349, (1984).

[161] D.C. Seets, M.C. Wheeler and C.B. Mullins,
Dynamics of molecular chemisorption of N_2 on the Ru(001) surface.
J. Vac. Sci. Technol., A. **14**: 1566, (1996).

[162] D.C. Seets, M.C. Wheeler and C.B. Mullins,
*Kinetics and dynamics of nitrogen adsorption on Ru(001): evidence for direct
molecular chemisorption.*
Chem. Phys. Lett. **257**: 280, (1996).

[163] T. Matsushima,
*Angular distribution of the combinative desorption of nitrogen atoms on
Ru(0001) surfaces.*
Surf. Sci. Lett. **197**: L287, (1988).

[164] G. Comsa and R. David,
Dynamical parameters of desorbing molecules.
Surf. Sci. Rep. **5**(4): 145, (1985).

[165] H.A. Michelsen, C.T. Rettner and D.J. Auerbach, *The adsorption of hydrogen
at copper surfaces: a model system for the study of activated adsorption*, in
Surface reactions, R.J. Madix, Editor. 1993. p. 185.

[166] M.J. Murphy and A. Hodgson,
Internal state distributions for D_2 recombinative desorption from Ag(111).
Surf. Sci. **368**: 55, (1996).

[167] B.E. Hayden and D.C. Godfrey,
*Molecular beam scattering of CO from Cu(110): The effect of incident
translational energy.*
J. Elec. Spec. and Related Phenomena. **45**: 351, (1987).

[168] C.T. Rettner, L.A. DeLouise and D.J. Auerbach,
*Effect of incidence kinetic energy and surface coverage on the dissociative
chemisorption of oxygen on W(110).*
J. Chem. Phys. **85**: 1131, (1986).

[169] J.H. Larsen, P.M. Holmblad and I. Chorkendorff,
Dissociative sticking of CH_4 on Ru(0001).
J. Chem. Phys. **110**: 2637, (1999).

[170] V.V. Petrunin, A. Baurichter, E. Jensen, H. Mortensen, L. Diekhöner and A.C.
Luntz, (2000).